Multibody Syst Dyn (2014) 32:445–509
DOI 10.1007/s11044-013-9387-2

Energetic consistency conditions for standard impacts

Part II: Poisson-type inequality impact laws

Christoph Glocker

Received: 19 February 2013 / Accepted: 28 June 2013 / Published online: 27 July 2013

Abstract The paper presents a full account of Poisson's impact law in inequality form. Based on an entirely new setting for the decompression phase, impact laws for unilateral and bilateral geometric and kinematic constraints and various friction elements are introduced and equipped with an impact coefficient in the sense of Poisson's impulse ratio. Energetic consistency is proven for small and similar impact coefficients via the condition number of the Delassus operator. Energetic consistency is generally proven for frictionless systems, as well as for systems containing one single frictional contact. A counter-example is developed, which demonstrates a possible energy increase for Poisson impacts in the presence of more than one frictional contact.

Keywords Impact · Collision · Friction · Energy · Poisson · Coulomb

1 Introduction

In Part I of this contribution [27], the standard Newtonian impact laws that are commonly applied in nonsmooth dynamics have been analyzed for energetic consistency. These impact laws are designed for frictional multicontact problems as well as for sprag clutches and bilateral constraints, to be used within a general multibody framework. They have proven to provide reasonable results for many applications. However, the discouraging observation has been made that Newton's kinematic restitution law immediately causes serious energetic inconsistencies when sprag clutches and contact constraints are equipped with different restitution coefficients in a coupled problem, which was demonstrated by a slide-push mechanism. Even worse, the much more common frictional contact shares this unnatural behavior, because it can be regarded as a combination of a contact constraint and a friction element, which itself is composed of the aforementioned sprag clutches. As the impact coefficient for the friction element is normally zero, any choice of a nonzero restitution coefficient in the associated contact constraint may immediately produce the said energetic

C. Glocker (✉)
IMES—Center of Mechanics, ETH Zurich, CLA J23.1, 8092 Zurich, Switzerland
e-mail: glocker@imes.mavt.ethz.ch

inconsistency, which was first observed by Kane in [28]. Because of this deficiency, we feel an urgent need for at least one alternative approach to frictional multiimpacts, which we try to satisfy by Poisson's impact law in inequality form.

Poisson's law is the second classical approach to impacts. It defines the restitution coefficient as the ratio of the impulsive forces from compression and decompression. The first inequality formulation for frictional Poisson impacts is found in [22]. There are, however, several deficiencies in that contribution: Only one-dimensional friction has been considered. The decompression phase for the friction element has been formulated heuristically, which has led to an awkward definition of the tangential restitution coefficient, together with another impact parameter without any clear mechanical meaning. Due to the lack of mathematical structure, the decompression phase in [22] cannot be generalized to two-dimensional friction, and any attempt to analyze the energetic properties of this impact model is cumbersome. Finally, there is the well-known flaw in the energy proof in [22], which makes it impossible to say anything about the energetic consistency for nonequal impact coefficients. As an inevitable consequence, Poisson's impact law in inequality form needs to be substantially revised, which we are trying to do in the paper at hand. Our aim is to present here a full account on this problem, in which the basic philosophy is still the same as in the original publication: to split the multiimpact event in two common phases and to successively treat each of them by an algebraic inequality problem. The compression phase has been left unchanged, with the only difference that it is now treated by normal cone inclusion instead of linear complementarity, in order to access spatial friction. For the rest of the paper, the following changes and additions have been performed:

- an entirely new and different setup of the decompression phase, together with a mathematically consistent representation based on algebraic set operations and normal cone inclusions
- extension of Poisson's impact law to the following impact elements, which all are equipped with a restitution coefficient: kinematic unilateral constraints, geometric and kinematic bilateral constraints, isotropic and orthotropic Coulomb friction elements, and any friction element following the proposed normal cone approach as, e.g., Coulomb–Contensou friction (not treated here)
- two sufficient conditions for energetic consistency in relation to similar and small impact coefficients, derived from the condition number of the Delassus operator
- energetic consistency proof for general frictionless finite-dimensional Lagrangian systems, containing an arbitrary number of unilateral and bilateral kinematic and geometric constraints
- energetic consistency proof for general finite-dimensional Lagrangian systems with *one* frictional contact, the latter being set up by one geometric unilateral constraint and one arbitrary Coulomb friction element following the proposed structure
- general proof on the equivalence of Poisson's and Newton's impact laws in inequality form, if all impact coefficients are equal to each other
- one and the first counterexample that demonstrates a possible energy increase for Poisson impacts in the presence of more than one frictional contact

Poisson impacts in inequality form are *much more* involved than Newtonian impacts. This is caused by the nature of the impulse approach, requiring the impact to be split into two phases, which both have to be processed within a suitable mathematical framework. Important parts of the contribution at hand have been taken from the master thesis [51] of the author's former student Fritz Stöckli. This comprises in particular the proofs in Sects. 5–7 and the example in Sect. 10, which were in large parts independently developed by him.

The literature about impacts is voluminous. The subject is fundamental, rooting back to the very beginning of mechanics, and the sources for impacts are diverse, and not at all limited to collisions. We do not even try to present an exhaustive literature overview, but we restrict ourselves to the topics that are relevant for the multibody community. We therefore have evaluated all contributions on impacts from this journal since its foundation, which roughly coincides with the first attempt in 1995 to extend Poisson's impact law to multicontacts within an inequality framework. Only some contributions from other sources are taken into account in the following literature survey, to give a reasonably coherent picture of the today's state of the art.

Energy preserving integration in discrete mechanics In this branch of computational mechanics, the concept of discrete derivatives is used to develop energy preserving numerical schemes from variational or energetic principles. The resulting difference equations are used to compute the velocity increments in a time step, and are therefore able to treat impulsive motion as well, as demonstrated in [35] for a completely elastic collision. A similar approach is taken in [21] to numerically process an oblique frictionless impact of a flexible bar against a rigid wall. Typical for contributions from this area is that the impact laws are never explicitly addressed. They somehow come along with the chosen discretization and are treated as such. An extension toward multicontact configurations with friction seems hardly possible, as the contact and impact laws are too camouflaged by this approach. In contrast, several energy preserving integrators under inequality impact laws have been developed in [37], together with consistent integration routines for partially elastic impacts with and without friction. These integrators are also based on discrete derivatives, but the full inequality framework including the specific impact laws has been taken into account in the governing variational principles.

Impacts and bilateral constraints Bilateral constraints cannot impact by themselves, but they can react on impacts by impulsive forces and have therefore to be taken into account in impact theory. Noteworthy is in particular the contribution [8], which provides a comprehensive theoretical study on how frictionless impacts are affected by the addition of bilateral constraints, and how this entire problem has to be dealt with the Lagrangian multiplier and the minimal coordinates approach. Another situation in which impulsive behavior occurs is the sudden application of bilateral constraints on a system, in order to instantaneously block an existing joint, or to model dynamic mass capture and the like. Such types are treated in [12, 30, 33], all within an equality framework. A more sophisticated approach for such constraint addition or deletion would in the author's opinion be a Coulomb-type impact element, in which the "normal force" is replaced by an impulsive control to turn the constraint on (and off) as needed [25]. Various types of switches can indeed be realized within an inequality framework.

Completely inelastic impacts No publications were found on *frictionless one-point collisions*, which is the most trivial case in impact theory. Within the example of human walking with crutches, *one-point collisions with friction* are treated in [19] by case distinction, i.e., by writing down the impact equations for each of the various friction phases. *Multicontact with spike constraints* is the standard model for human and robotic walking; see [3–5, 40, 56] for gait generation, optimal trajectory planning, and walking simulation. Although tangential impulsive forces are present in these contributions, the main difficulties of Coulomb friction are avoided by the assumption of unconditional stick after the impact. The impact problem is then solved within the framework of equalities, without explicitly checking the sign restriction of the normal impulsive forces. *Multicontact with friction* is treated in [20, 41] by

a full inequality approach within a time-stepping and discrete dynamics framework, respectively. Again, the impact laws are not explicitly addressed, as they come along with chosen discretization scheme. It is therefore expected that completely inelastic impacts have been implemented.

Newtonian impacts Newtonian impacts are understood as collisions in which a kinematic restitution coefficient is used to resolve the normal direction of the impact. In [50], a *frictionless one-point collisions* is formulated within a multibody system approach for the optimization of a circuit breaker by using equalities. *One-point collisions with friction* are extensively treated in [13]. The impact is formulated within a general multibody framework and processed with Routh's method without *and* with bisection of the collision time. The latter can be regarded as an impact sub-sequencing technique, in which the various friction phases are explicitly processed, and which resolves some (but not all) of the energetic inconsistencies observed in the original example of Kane. In [17], this approach is generalized to spatial friction by using Keller's method. *Frictionless multicontacts* are treated in [11] within the Appellian classification of impulsive constraints. The presence of additional bilateral constraints is explicitly taken into account, and the overall problem is stated in the framework of equalities. For the animation of articulated bodies, a multiconstraint approach is presented in [32]. Collisions are treated by a kind of Newtonian impact law, which is by words related to linear complementarity. In [42], an interesting approach to multiimpacts is presented by relating them to penalization methods. The problem is treated within the full inequality framework, and the frictionless collisions are characterized by an extended impact law that allows for nonlocal interactions. A model for *multicontacts with friction* within the idea of complementarity is developed in [7, 18, 49]. It uses inner and outer friction cones together with a maximum dissipation principle to compute the post-impact velocities. In [9], frictional multiimpacts are exploited by a generalized Newtonian impact law, involving non-diagonal restitution matrices and extending the classical setting to, e.g., far distance effects as in Newton's cradle.

Poisson impacts Poisson impacts require a bisection of the impact event into at least two phases, the compression and decompression phase. The end of the impact is classically determined by the impulse ratio condition on the normal impulsive force of a contact, also called the kinetic restitution coefficient. No publications were found on *frictionless one-point collisions*, which is trivial and well understood today. There is, however, a number of publications about *one-point collisions with friction*. In [14, 34], planar frictional impacts within a multibody system are processed with Routh's method. This approach is generalized to spatial one-point collisions with isotropic friction in [17, 57], in which Keller's method is used to resolve the various friction phases. *Frictionless multicontacts* are treated in [31] by processing the compression and decompression phase within an equality framework. The sign restrictions on the relative velocities and the impulsive forces are met by a trial and error method. Coulomb friction is taken into account in the impact-free motion, but not mentioned for the impacts. The original paper on *multicontacts with friction* within Poisson's impact law is [22]. There are only a few derivatives of this setting, as in [10] with an extension to impulsive contact moments, and in [43–45] with a modified tangential decompression phase which roots back to [6].

Impacts in the sense of Stronge In this class, Stronge's energetic coefficient of restitution [52, 53] is used to determine the end of the decompression phase by an energy ratio condition on the normal direction of a contact. No publications were found on *frictionless*

one-point collisions. It is well known today that Newton's, Poisson's, and Stronge's restitution coefficients agree with each other for this case. *One-point collisions with friction* are extensively treated in [14, 16] by Routh's method for a planar frictional contact within a multibody framework. In [14], it has been shown that Poisson's impact law is always energetically consistent for a single planar contact, and that there is a one-to-one correspondence between Poisson's and Stronge's restitution coefficient. These findings have further been discussed in [15, 55]. An extension of the above to spatial contacts is found in [17, 58], in which the collision is resolved by Keller's method and applied to the three-dimensional Painlevé problem in [58]. There is only one contribution [36], in which the idea of an energetic restitution coefficient is applied to *frictionless multicontacts*. The authors decompose the overall kinetic energy of the system into a portion that can be affected by the impact, and another portion which remains unaffected, to apply then the energetic restitution law on the former. Although dealing with more than one constraint, this approach has rather to be attributed to single collisions, as one and the same restitution coefficient is used for all of the involved contacts. Within such a situation, it can be shown that the three different concepts for restitution lead at the end to the very same results. Finally, no publications were found on *multicontacts with friction* within Stronge's approach.

The literature overview reveals the various aspects of impacts in theory and applications, but also the pressing need for multiimpact laws other than the Newtonian. We therefore strive to develop a setting for Poisson impacts, which is general enough to cover at least some of the issues related to constraint activation and switching, in addition to the frictional collision problem. The paper is organized as follows: In Sect. 2, some basic algebraic operations on sets are reviewed, as they are needed to properly set up our model of the decompression phase for Poisson impacts. The latter is introduced in Sect. 3, together with a short review of Newtonian impacts, which naturally lead for the completely inelastic case to the Poisson compression phase. In Sect. 4, the entire collection of impact elements from [27] is adapted to our setting of Poisson impacts, by strictly following the theoretical framework developed so far. Each impact element is discussed separately, and in particular their decompression phases are explained in detail. Energetic consistency is addressed in Sects. 5–8 for various impact configurations. In Sect. 5, energetic consistency is achieved for sufficiently small or similar impact coefficients within arbitrary combinations of impact elements, whereas unconditional consistency is proven for frictionless systems and systems with only one frictional contact in Sects. 6 and 7. In Sect. 8, equivalence of Poisson and Newtonian impacts [27] is proven under kinematic pre-impact consistency and equal impact coefficients. Section 9 contains three examples which are the slide-push mechanism from [27], Kane's frictional impact of a double pendulum, and Newton's cradle with three balls. They are presented in full detail to support the preceding energy proofs, and to demonstrate that Poisson impacts can reproduce to a certain extent far-distance effects, as nondiagonal Newtonian restitution matrices. Finally, an example is presented in Sect. 10, in which an increase in the kinetic energy is observed for Poisson impacts. Required are one frictional contact and at least one additional impact element, together with the assumption of a common compression and decompression phase.

2 Basic algebraic set operations

In this section, some basic operations on sets are reviewed. The following material is entirely taken from [47, 48], and later used to set up the compression and decompression phase of Poisson impacts.

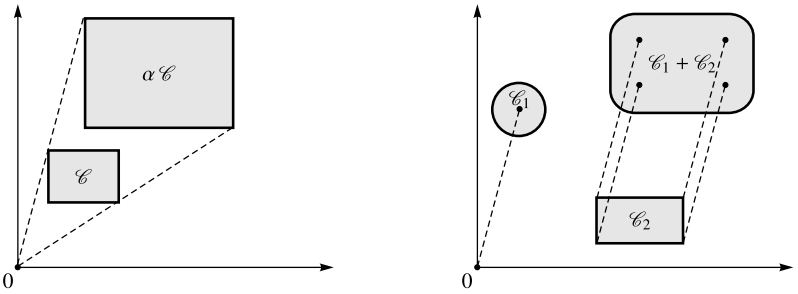

Fig. 1 Scalar multiplication and addition of convex sets as illustrated in [23]

Let $\mathscr{C}$ be a (not necessarily convex) subset of $\mathbb{R}^n$ and $\alpha \in \mathbb{R}$. The scalar multiple $\alpha\mathscr{C}$ of $\mathscr{C}$ is defined as

$$\alpha\mathscr{C} := \{\alpha\mathbf{x} \mid \mathbf{x} \in \mathscr{C}\}. \tag{1}$$

Geometrically, the set $\alpha\mathscr{C}$ is obtained by upscaling or downscaling $\mathscr{C}$ and has therefore the same shape as $\mathscr{C}$; see left part of Fig. 1. Scalar multiplication preserves convexity, i.e. $\alpha\mathscr{C}$ is convex if $\mathscr{C}$ is. Furthermore, note that $\alpha\mathscr{C} = \{0\}$ for $\alpha = 0$, even if $\mathscr{C}$ is unbounded as, e.g., $\mathscr{C} = \mathbb{R}^+_0$.

Addition of sets is performed in the sense of the Minkowski sum. Let $\mathscr{C}_1$ and $\mathscr{C}_2$ be subsets of $\mathbb{R}^n$. Then

$$\mathscr{C}_1 + \mathscr{C}_2 := \{\mathbf{x}_1 + \mathbf{x}_2 \mid \mathbf{x}_1 \in \mathscr{C}_1,\ \mathbf{x}_2 \in \mathscr{C}_2\}. \tag{2}$$

Again, convexity is preserved by this operation as shown in [47]: For $\mathscr{C}_1$ and $\mathscr{C}_2$ being convex, there sum also is. Addition of a disk $\mathscr{C}_1$ and a rectangle $\mathscr{C}_2$ is shown in the right part of Fig. 1. Each element of the disk $\mathscr{C}_1$ has to be added to every element of the rectangle $\mathscr{C}_2$ to give the sum $\mathscr{C}_1 + \mathscr{C}_2$.

There is a number of algebraic laws that can directly be derived from (1) and (2). The following list is again taken from [47]:

$$\mathscr{C}_1 + \mathscr{C}_2 = \mathscr{C}_2 + \mathscr{C}_1, \tag{3}$$

$$(\mathscr{C}_1 + \mathscr{C}_2) + \mathscr{C}_3 = \mathscr{C}_1 + (\mathscr{C}_2 + \mathscr{C}_3), \tag{4}$$

$$\alpha_1(\alpha_2\mathscr{C}) = (\alpha_1\alpha_2)\mathscr{C}, \tag{5}$$

$$\alpha(\mathscr{C}_1 + \mathscr{C}_2) = \alpha\mathscr{C}_1 + \alpha\mathscr{C}_2. \tag{6}$$

Convexity is not required for the sets in (3)–(6), but apparently preserved.

Another important operation that stringently requires convexity is the following distribution law: Let $\mathscr{C}$ be a *convex* set and let $\alpha_1 \geq 0$, $\alpha_2 \geq 0$. Then

$$(\alpha_1 + \alpha_2)\mathscr{C} = \alpha_1\mathscr{C} + \alpha_2\mathscr{C}. \tag{7}$$

This implies among others that $2\mathscr{C} = \mathscr{C} + \mathscr{C}$ if $\mathscr{C}$ is convex, and that the convex set $\mathscr{D} = \alpha_1\mathscr{C} + \alpha_2\mathscr{C}$ has the same shape as the convex set $\mathscr{C}$.

We will further need the concept of recession cones from [47]. A vector $\mathbf{y} \neq 0$ is called a *direction of recession* of the convex set $\mathscr{C}$ if

$$\mathbf{x} + \alpha\mathbf{y} \in \mathscr{C} \quad \text{for every } \mathbf{x} \in \mathscr{C} \text{ and for every } \alpha \geq 0. \tag{8}$$

Condition (8) means that a half-line $\{\alpha\mathbf{y} \mid \alpha \geq 0\}$ with direction $\mathbf{y}$ does not leave the set $\mathscr{C}$ when attached to any of its points $\mathbf{x}$, provided that $\mathbf{y}$ is a direction of recession of $\mathscr{C}$. These half-lines characterize therefore the directions in which the set $\mathscr{C}$ is unbounded. The union of all such half-lines is called the *recession cone* of $\mathscr{C}$ and denoted by $0^+\mathscr{C}$. By using the notion of lim sup for multifunctions, the recession cone of $\mathscr{C}$ is defined in [48] as

$$0^+\mathscr{C} := \limsup_{\alpha\to 0^+}(\alpha\mathscr{C}) = \left\{\mathbf{y} \mid \exists \mathbf{x}^k \in \mathscr{C},\ \alpha_k \to 0^+,\ \text{with } \alpha_k\mathbf{x}^k \to \mathbf{y}\right\}. \tag{9}$$

A simple consequence on (8) is the property

$$\mathscr{C} = \mathscr{C} + 0^+\mathscr{C}, \tag{10}$$

which can also be seen from (7) by setting $\alpha_1 = 1$ and taking the limit in the sense of (9) for $\alpha_2 \to 0^+$. The recession cone $0^+\mathscr{C}$ of a convex set $\mathscr{C}$ is a convex cone containing the origin. If the convex set $\mathscr{C}$ is bounded, the recession cone reduces to the single element $0^+\mathscr{C} = \{0\}$. Only unbounded convex sets *may* have nontrivial recession cones.

As a final example on nontrivial recession cones (9) and *positive* scaling (1), consider closed convex cones, i.e., *closed* convex sets $\mathscr{K}$ for which $\alpha\mathbf{x} \in \mathscr{K}$ whenever $\mathbf{x} \in \mathscr{K}$ and $\alpha > 0$. It immediately follows from this definition that

$$0^+\mathscr{K} = \mathscr{K} \quad \text{and} \quad \alpha\mathscr{K} = \mathscr{K} \quad \text{for } \alpha > 0. \tag{11}$$

The simplest special case of the above is $\mathscr{K} = \mathbb{R}$, for which $0^+\mathbb{R} = \mathbb{R}$ and $\alpha\mathbb{R} = \mathbb{R}$ apparently applies. Another example is $\mathscr{K} = \mathbb{R}_0^-$, for which we get $0^+\mathbb{R}_0^- = \mathbb{R}_0^-$ and $\alpha\mathbb{R}_0^- = \mathbb{R}_0^-$ for $\alpha > 0$. Nontrivial recession cones will be of interest for Poisson's impact law only in these two situations, which will be met again in Sect. 4.1.

3 The standard impact problem for inequality impact laws of Poisson type

In this section, we set up the impact problem for impact laws of Poisson type. The concept of Poisson impacts requires the impact event to be decomposed into two subevents, which we call the *phase of compression* and the *phase of decompression*. We define the phase of compression to be a completely inelastic Newtonian impact, i.e., a Newtonian impact processed with all restitution coefficients ε_i equal to zero. The phase of decompression is classically terminated by an impulse ratio condition on the impact contacts, which has been extended for a first time to inequality systems in [22]. Although (one-dimensional) friction has been considered in [22], the formulation of the decompression phase is too artificial to be extended to spatial configuration when the tangential restitution coefficients are chosen unequal to zero. We therefore develop in this section an alternative, much more structured setting for the decompression phase, which can be applied to all the impact elements introduced in [27].

3.1 Newtonian impacts revisited

In a first step, we recapitulate the standard impact problem for inequality impact laws of Newton type as it has been presented in [27]. The impact for such an event is completely determined by the conditions

$$\mathbf{M}\left(\mathbf{u}^+ - \mathbf{u}^-\right) = \sum_{i=1}^{n} \mathbf{W}_i \mathbf{\Lambda}_i, \tag{12}$$

$$\boldsymbol{\gamma}_i = \mathbf{W}_i^{\mathrm{T}}\mathbf{u}, \tag{13}$$

$$\boldsymbol{\xi}_i = \boldsymbol{\gamma}_i^+ + \varepsilon_i \boldsymbol{\gamma}_i^-, \tag{14}$$

$$\boldsymbol{\xi}_i \in \mathscr{N}_{\mathscr{C}_i}(-\boldsymbol{\Lambda}_i). \tag{15}$$

Assumed in (12)–(15) is an autonomous Lagrangian system in local coordinates $\mathbf{q} \in \mathbb{R}^f$ with mass matrix $\mathbf{M}(\mathbf{q})$ and n impact elements. The generalized velocities are denoted by $\mathbf{u} := \dot{\mathbf{q}}$, where $\mathbf{u}^+$ and $\mathbf{u}^-$ are their post and preimpact values. The right-hand side of the impact equation (12) consists of the n generalized impulsive forces $\mathbf{R}_i := \mathbf{W}_i \boldsymbol{\Lambda}_i$, where $\mathbf{W}_i = (\mathbf{w}_{1i}, \ldots, \mathbf{w}_{m(i)i})$ and $\boldsymbol{\Lambda}_i = (\Lambda_{1i}, \ldots, \Lambda_{m(i)i})^{\mathrm{T}}$ are composed for each impact element i of $m(i)$ linearly independent generalized force directions $\mathbf{w}_{ji}(\mathbf{q})$ and $m(i)$ scalar impulsive forces Λ_{ji}, respectively. Associated with each direction $\mathbf{w}_{ji}(\mathbf{q})$ is a local velocity component $\gamma_{ji} = \mathbf{w}_{ji}^{\mathrm{T}}\mathbf{u}$. These are typically the normal and tangential relative velocities that are met in frictional collision problems. For each impact element, these velocity components may be gathered in a vector $\boldsymbol{\gamma}_i = (\gamma_{1i}, \ldots, \gamma_{m(i)i})^{\mathrm{T}}$, which then leads to Eq. (13).

Furthermore, each impact element i is equipped with a Newtonian restitution coefficient ε_i, which relates the post and preimpact relative velocities $\boldsymbol{\gamma}^+$ and $\boldsymbol{\gamma}^-$ according to (14). The entities $\boldsymbol{\xi}_i = (\xi_{1i}, \ldots, \xi_{m(i)i})^{\mathrm{T}}$ are just auxiliary variables, used to make the associated impact laws (15) more compact. The impact laws themselves are formulated as normal cone inclusions, where $\mathscr{C}_i \subset \mathbb{R}^{m(i)}$ denotes the convex set associated with the impact element i, and $\mathscr{N}_{\mathscr{C}_i}(-\boldsymbol{\Lambda}_i)$ is the normal cone $\mathscr{N}_{(\cdot)}(\cdot)$ of the set $\mathscr{C}_i$ evaluated at the point $-\boldsymbol{\Lambda}_i$. Inclusion (15) implies that the impulsive forces $-\boldsymbol{\Lambda}_i$ are restricted to the sets $\mathscr{C}_i$, i.e., $-\boldsymbol{\Lambda}_i \in \mathscr{C}_i$. The sets $\mathscr{C}_i$ can therefore be interpreted as the reservoirs of negative impulsive forces that are provided by the individual impact elements i.

In addition to convexity, each of the sets $\mathscr{C}_i$ has been assumed in [27] to contain the 0-element,

$$0 \in \mathscr{C}_i. \tag{16}$$

By this property and by the definition of the normal cone, one is able to derive from (15) the inequality

$$\boldsymbol{\xi}_i^{\mathrm{T}} \boldsymbol{\Lambda}_i \leq 0. \tag{17}$$

In other words, the inequality (17) holds for each pair $(\boldsymbol{\xi}_i, \boldsymbol{\Lambda}_i)$ fulfilling the inclusion (15), if 0 is contained in $\mathscr{C}_i$ as one of its elements. The inequality (17) has been used in the energy proofs of Newton's impact law and will be met in a similar context for Poisson impacts.

3.2 The reservoirs of impulsive forces for compression and decompression

We now set up the mathematical structure for Poisson's impact law by defining the reservoirs of impulsive forces for compression and decompression, and by introducing Poisson's restitution coefficient. This structure will strictly be followed in all of the subsequent sections of the paper. The basic idea is to split in a well-defined way the sets $\mathscr{C}_i$ of Newton's impact law (15) into two sets $\mathscr{C}_i^{(-)}$ and $\mathscr{C}_i^{(+)}$, from which the first one is used for the impulsive forces during compression, and the second one for the impulsive forces during decompression in Poisson's law. In this way, kinetic consistency is intrinsically anchored in the resulting impact law by assuring that the overall impulsive force $-(\boldsymbol{\Lambda}_i^{(-)} + \boldsymbol{\Lambda}_i^{(+)})$ as well as the impulsive forces $-\boldsymbol{\Lambda}_i^{(-)}$, $-\boldsymbol{\Lambda}_i^{(+)}$ of the two subevents never leave the sets $\mathscr{C}_i$ and $\mathscr{C}_i^{(-)}$, $\mathscr{C}_i^{(+)}$ designed for them.

By applying (7) with $\alpha_1 := \alpha$ and $\alpha_2 := (1 - \alpha)$ on the individual sets $\mathscr{C}_i$ in Newton's impact law (15), we may write them each in the form

$$\mathscr{C}_i = \alpha_i \mathscr{C}_i + (1 - \alpha_i)\mathscr{C}_i \quad \text{with } 0 < \alpha_i < 1. \tag{18}$$

We introduce now the reservoirs of impulsive forces for compression $\mathscr{C}_i^{(-)}$ and decompression $\mathscr{C}_i^{(+)}$ for Poisson's impact law as scaled versions of the original set $\mathscr{C}_i$ by setting

$$\mathscr{C}_i^{(-)} := \alpha_i \mathscr{C}_i, \qquad \mathscr{C}_i^{(+)} := (1-\alpha_i)\mathscr{C}_i. \tag{19}$$

This enables us to rewrite Eq. (18) as

$$\mathscr{C}_i = \mathscr{C}_i^{(-)} + \mathscr{C}_i^{(+)}. \tag{20}$$

Note that $\mathscr{C}_i^{(-)}$ and $\mathscr{C}_i^{(+)}$ have by (19) the same shape as $\mathscr{C}_i$. Also, note that strict inequalities on the bounds of α_i have been used in (18), in contrast to (7) where weak inequalities are allowed. This stronger restriction is motivated by physical reasons that are later explained in detail for the individual impact elements. Roughly speaking, a reduction of either one of the sets $\mathscr{C}_i^{(-)}$ and $\mathscr{C}_i^{(+)}$ to just the null element, as it would happen in (19) for $\alpha_i = 0$ or $\alpha_i = 1$, would be too restrictive for certain impact elements. However, we will need the limits $\alpha_i = 0$ and $\alpha_i = 1$ to properly formulate the sets $\mathscr{C}_i^{(-)}$ and $\mathscr{C}_i^{(+)}$ for Coulomb friction under any and all circumstances, even under degenerated ones, but also for deriving certain conditions under which Newton's and Poisson's laws are equivalent. It will turn out that the best object from the physical point of view for these cases is the recession cone of $\mathscr{C}_i$, i.e., the set $0^+\mathscr{C}_i$ that is obtained by taking the limit for $\alpha_i \to 0^+$ and $(1-\alpha_i) \to 0^+$ in the sense of (9). We therefore extend now (18) to weak inequalities by *defining*

$$\mathscr{C}_i^{(-)} := 0^+\mathscr{C}_i \quad \text{for } \alpha_i = 0, \qquad \mathscr{C}_i^{(+)} := 0^+\mathscr{C}_i \quad \text{for } \alpha_i = 1. \tag{21}$$

Note that (20) still holds for these two cases in the form $\mathscr{C}_i = \mathscr{C}_i + 0^+\mathscr{C}_i$, which can be seen from (10).

In our extension of Poisson's impact law to arbitrary convex reservoirs of impulsive forces, an auxiliary set $\mathscr{D}_i$ with the same shape as $\mathscr{C}_i$ is needed,

$$\mathscr{D}_i := \kappa_i \mathscr{C}_i \quad \text{with } \kappa_i > 0. \tag{22}$$

This set is introduced, together with Poisson's coefficient of restitution ϵ_i, such that the relation

$$\mathscr{C}_i^{(+)} = \mathscr{D}_i + \epsilon_i \mathscr{C}_i^{(-)} \quad \text{with } \epsilon_i > 0 \tag{23}$$

holds true. The restrictions on κ_i and ϵ_i in Eqs. (22) and (23) are again formulated as strong inequalities. Their extension to weak inequalities has again to be understood in the sense of (9), i.e.,

$$\mathscr{D}_i := 0^+\mathscr{C}_i \quad \text{for } \kappa_i = 0 \tag{24}$$

and

$$\mathscr{C}_i^{(+)} = \mathscr{D}_i + 0^+\mathscr{C}_i^{(-)} \quad \text{for } \epsilon_i = 0. \tag{25}$$

By our setting of Poisson impacts, there is already a first restriction on the Poisson restitution coefficient, namely $\epsilon_i \geq 0$ by (23) and (25). This restriction is a consequence on the chosen framework of convexity, in particular on Eq. (7), which ensures distributivity. The definition of the various sets in (19) and (22), as well as the way in which Poisson's coefficient of restitution is introduced in (23) is not mandatory, and other approaches might work as well. We have chosen this setting, because it yields Poisson's law for frictionless impacts as in its original unilateral formulation [22], and because it can additionally cover certain types of

Coulomb friction *with* tangential restitution, i.e., Poisson type impact elements, which have never been introduced so far.

In a last step, we can now determine the value of κ_i in (22) by putting (22) and (19) into (23). This gives

$$(1-\alpha_i)\mathscr{C}_i = \kappa_i \mathscr{C}_i + \epsilon_i \alpha_i \mathscr{C}_i, \tag{26}$$

and by the rules (3)–(6) and (7) the desired value of κ_i,

$$\kappa_i = 1 - (1+\epsilon_i)\alpha_i. \tag{27}$$

Together with the inequality $\kappa_i \geq 0$, one finally obtains $\mathscr{D}_i$ in (22) as

$$\mathscr{D}_i = \big(1-(1+\epsilon_i)\alpha_i\big)\mathscr{C}_i \quad \text{with } 1-(1+\epsilon_i)\alpha_i \geq 0. \tag{28}$$

In order to set up all three sets $\mathscr{C}_i^{(-)}$, $\mathscr{C}_i^{(+)}$, and $\mathscr{D}_i$, only two parameters are needed. These are the Poisson restitution coefficient ϵ_i which has to be provided anyway, and a value for α_i that will explicitly be needed only for the case of Coulomb type friction elements. For all the other impact elements discussed in Sect. 4, the particular value of α_i is insignificant, although they strictly follow the setup provided so far.

3.3 The Poisson impact law

In the classical setting of single contact collisions, Poisson's impact law splits the collision event into a phase of compression and a succeeding phase of decompression. The compression phase is figuratively understood as the phase in which the contacting bodies are increasingly deformed by the normal contact forces whilst their normal relative velocity is reduced until standstill. During this process, the entire portion of the kinetic energy which is accessible by the contact forces, is used to achieve the deformed state of the bodies at the end of compression.

The idea of a common phase of compression can in general not be transferred to multi-contact situations. A well-known counterexample is Newton's cradle, in which the impulse transfer takes place sequentially from the first to the last ball. Nevertheless, there are many situations for which the model of a common phase of compression has shown to produce reasonable results. In order to extend the phase of compression to standard impact problems as in (12)–(15), we follow the idea of maximum possible energy reduction within the admissible sets of impulsive forces as described above. In other words, we define the end of compression as the velocities $\mathbf{u}^\circ$ obtained by minimizing the associated kinetic energy $T^\circ = \frac{1}{2}\mathbf{u}^{\circ\mathrm{T}}\mathbf{M}\mathbf{u}^\circ$ under the impulsive force restrictions $-\boldsymbol{\Lambda}_i^{(-)} \in \mathscr{C}_i^{(-)}$ in the impact equation for compression, $\mathbf{M}(\mathbf{u}^\circ - \mathbf{u}^-) = \sum_i \mathbf{W}_i \boldsymbol{\Lambda}_i^{(-)}$. It turns out that the optimality conditions for this minimization problem are precisely the equations for a completely inelastic Newtonian impact, i.e., (12)–(15) with all $\varepsilon_i = 0$, as shown in the Appendix of this paper. After having adjusted for this case the notation in (12)–(15), we obtain

$$\mathbf{M}\big(\mathbf{u}^\circ - \mathbf{u}^-\big) = \sum_{i=1}^{n} \mathbf{W}_i \boldsymbol{\Lambda}_i^{(-)}, \tag{29}$$

$$\boldsymbol{\gamma}_i = \mathbf{W}_i^{\mathrm{T}}\mathbf{u}, \tag{30}$$

$$\boldsymbol{\xi}_i^\circ = \boldsymbol{\gamma}_i^\circ, \tag{31}$$

$$\boldsymbol{\xi}_i^\circ \in \mathscr{N}_{\mathscr{C}_i^{(-)}}\big(-\boldsymbol{\Lambda}_i^{(-)}\big) \tag{32}$$

as the conditions that define the compression phase. Note that (29)–(32) can only be interpreted as the maximum dissipation conditions of the said minimization problem if all the sets $\mathscr{C}_i^{(-)}$ are *constant* subsets of $\mathbb{R}^{m(i)}$. The latter does *not* apply for Coulomb type friction, for which the reservoirs of tangential impulsive forces $\mathscr{C}_i^{(-)}$ depend on the values of the associated normal impulsive forces $\Lambda_k^{(-)}$, leading to sets $\mathscr{C}_i^{(-)}(\Lambda_k^{(-)})$ in (32) of a priori unknown size. In this case, (29)–(32) can at best be understood as the solution of a so-called quasi-optimization problem. Nevertheless, the definition of Poisson's compression phase as a completely inelastic Newtonian impact is not affected by the above. It still carries certain maximality properties related to dissipation and provides a clean link to Newtonian impacts. This definition has already been used in [24] for frictionless unilateral constraints, and is still in accordance with the approach presented in [22].

The phase of decompression is the second and final phase in Poisson impact models. It succeeds the phase of compression and is initiated with the generalized velocities $\mathbf{u}^\circ$ at the end of compression. The decompression phase is classically understood as the impact phase in which the deformations gained during compression are partly released and reconverted into kinetic energy. For the normal direction of an impact contact, this dissipative behavior is achieved by taking only a fraction $\epsilon_i \Lambda_i^{(-)}$ of the compression impulse $\Lambda_i^{(-)}$ to let it act as the decompression impulse $\Lambda^{(+)}$. The parameter ϵ_i to specify this fraction is called the Poisson restitution coefficient. In other words, the impulsive force for decompression $\Lambda_i^{(+)}$ in Poisson's impact law is determined such that the auxiliary variable $\Delta_i := \Lambda_i^{(+)} - \epsilon_i \Lambda_i^{(-)}$ becomes equal to zero. We now adopt this concept and extend it to arbitrary impact elements within an inequality approach by defining Poisson's decompression phase as

$$\mathbf{M}\big(\mathbf{u}^+ - \mathbf{u}^\circ\big) = \sum_{i=1}^{n} \mathbf{W}_i \boldsymbol{\Lambda}_i^{(+)}, \tag{33}$$

$$\boldsymbol{\gamma}_i = \mathbf{W}_i^{\mathrm{T}} \mathbf{u}, \tag{34}$$

$$\boldsymbol{\Delta}_i = \boldsymbol{\Lambda}_i^{(+)} - \epsilon_i \boldsymbol{\Lambda}_i^{(-)}, \tag{35}$$

$$\boldsymbol{\gamma}_i^+ \in \mathscr{N}_{\mathscr{D}_i}(-\boldsymbol{\Delta}_i), \tag{36}$$

where $\mathbf{u}^+$ are the Poisson post-impact generalized velocities with which the impact terminates. The auxiliary variable $\boldsymbol{\Delta}_i$ appears now in (35) in vectorial form. In contrast to the classical Poisson impact law, $\boldsymbol{\Delta}_i$ is not set equal to zero, but related to the post-impact relative velocities $\boldsymbol{\gamma}_i^+$ by the inequality impact law (36). This impact law is formulated as a normal cone inclusion, involving the auxiliary set $\mathscr{D}_i$ as specified in (28). In Sect. 4, we will explicitly state these sets for each individual impact element, and we will discuss the particular physical meaning of the associated impact laws (36). We further will explain why $\boldsymbol{\Delta}_i$ cannot simply be set equal to zero for the contacts in a multi-impact problem, as it is classically done for single collisions.

Note also that property (16) applies for each of the sets $\mathscr{C}_i^{(-)}$, $\mathscr{C}_i^{(+)}$, and $\mathscr{D}_i$. This is ensured by their special construction according to (19) and (28), and yields

$$0 \in \mathscr{C}_i^{(-)}, \qquad 0 \in \mathscr{C}_i^{(+)}, \qquad 0 \in \mathscr{D}_i. \tag{37}$$

Together with the two normal cone inclusions (32) and (36), one obtains from (37) the inequalities

$$\boldsymbol{\xi}_i^{\circ\mathrm{T}} \boldsymbol{\Lambda}_i^{(-)} \leq 0, \qquad \boldsymbol{\gamma}_i^{+\mathrm{T}} \boldsymbol{\Delta}_i \leq 0 \tag{38}$$

in the same way as (17) has been deduced from (16) and (15). These inequalities will be met again in the energy proofs for Poisson impacts. Another consequence of (37) on the above sets is that

$$\mathscr{D}_i \subseteq \mathscr{C}_i^{(+)} \quad \text{and} \quad \epsilon_i \mathscr{C}_i^{(-)} \subseteq \mathscr{C}_i^{(+)} \tag{39}$$

for $\epsilon_i \geq 0$, which can directly be seen from (23) and (25).

In a final step, we formulate the compression and decompression phase as a standard normal cone inclusion problem that can be processed by an inequality solver. We set $\mathbf{W} := (\mathbf{W}_1, \ldots, \mathbf{W}_n)$, $\boldsymbol{\Lambda}^{(-)} := (\boldsymbol{\Lambda}_1^{(-)\mathrm{T}}, \ldots, \boldsymbol{\Lambda}_n^{(-)\mathrm{T}})^{\mathrm{T}}$, $\boldsymbol{\Lambda}^{(+)} := (\boldsymbol{\Lambda}_1^{(+)\mathrm{T}}, \ldots, \boldsymbol{\Lambda}_n^{(+)\mathrm{T}})^{\mathrm{T}}$, $\boldsymbol{\Delta} := (\boldsymbol{\Delta}_1^{\mathrm{T}}, \ldots, \boldsymbol{\Delta}_n^{\mathrm{T}})^{\mathrm{T}}$, $\boldsymbol{\gamma} := (\boldsymbol{\gamma}_1^{\mathrm{T}}, \ldots, \boldsymbol{\gamma}_n^{\mathrm{T}})^{\mathrm{T}}$, $\boldsymbol{\xi} := (\boldsymbol{\xi}_1^{\mathrm{T}}, \ldots, \boldsymbol{\xi}_n^{\mathrm{T}})^{\mathrm{T}}$, and $\boldsymbol{\epsilon} := \operatorname{diag}(\epsilon_i \mathbf{I}_i)$ with $\mathbf{I}_i$ the $m(i) \times m(i)$ identity matrix, and rewrite (29)–(31) and (33)–(35) as

$$\mathbf{M}\big(\mathbf{u}^{\circ} - \mathbf{u}^{-}\big) = \mathbf{W}\boldsymbol{\Lambda}^{(-)}, \qquad \mathbf{M}\big(\mathbf{u}^{+} - \mathbf{u}^{\circ}\big) = \mathbf{W}\boldsymbol{\Lambda}^{(+)}, \tag{40}$$

$$\boldsymbol{\gamma} = \mathbf{W}^{\mathrm{T}}\mathbf{u}, \qquad \boldsymbol{\gamma} = \mathbf{W}^{\mathrm{T}}\mathbf{u}, \tag{41}$$

$$\boldsymbol{\xi}^{\circ} = \boldsymbol{\gamma}^{\circ}, \qquad \boldsymbol{\Delta} = \boldsymbol{\Lambda}^{(+)} - \boldsymbol{\epsilon}\boldsymbol{\Lambda}^{(-)}. \tag{42}$$

By taking in (41) the differences $\boldsymbol{\gamma}^{\circ} - \boldsymbol{\gamma}^{-} = \mathbf{W}^{\mathrm{T}}(\mathbf{u}^{\circ} - \mathbf{u}^{-})$ and $\boldsymbol{\gamma}^{+} - \boldsymbol{\gamma}^{\circ} = \mathbf{W}^{\mathrm{T}}(\mathbf{u}^{+} - \mathbf{u}^{\circ})$, and eliminating the terms $(\mathbf{u}^{\circ} - \mathbf{u}^{-})$ and $(\mathbf{u}^{+} - \mathbf{u}^{\circ})$ with the help of (40), one obtains

$$\boldsymbol{\gamma}^{\circ} - \boldsymbol{\gamma}^{-} = \mathbf{G}\boldsymbol{\Lambda}^{(-)}, \qquad \boldsymbol{\gamma}^{+} - \boldsymbol{\gamma}^{\circ} = \mathbf{G}\boldsymbol{\Lambda}^{(+)}, \tag{43}$$

with $\mathbf{G}$ being the symmetric and positive semidefinite Delassus operator defined by

$$\mathbf{G} = \mathbf{W}^{\mathrm{T}}\mathbf{M}^{-1}\mathbf{W}. \tag{44}$$

By using (42), we now eliminate $\boldsymbol{\gamma}^{\circ}$ from the first equation and $\boldsymbol{\Lambda}^{(+)}$ from the second equation in (43). This gives

$$\boldsymbol{\xi}^{\circ} = \boldsymbol{\gamma}^{\circ} = \mathbf{G}\boldsymbol{\Lambda}^{(-)} + \boldsymbol{\gamma}^{-}, \qquad \boldsymbol{\gamma}^{+} = \mathbf{G}\boldsymbol{\Delta} + \big(\mathbf{G}\boldsymbol{\epsilon}\boldsymbol{\Lambda}^{(-)} + \boldsymbol{\gamma}^{\circ}\big), \tag{45}$$

which is the desired formulation. To solve the impact, one first calculates the preimpact relative velocities from (41) as $\boldsymbol{\gamma}^{-} = \mathbf{W}^{\mathrm{T}}\mathbf{u}^{-}$. With this result, the first equation in (45) together with the impact laws (32) is processed to give the relative velocities after compression and the compression impulsive forces $(\boldsymbol{\gamma}^{\circ}, \boldsymbol{\Lambda}^{(-)})$. By using these values, the right equation in (45) together with the impact laws (36) can be solved, either analytically by case distinction or numerically by an inequality solver, to compute the relative velocities after decompression and the auxiliary variables $(\boldsymbol{\gamma}^{+}, \boldsymbol{\Delta})$. From $\boldsymbol{\Delta}$, the decompression impulsive forces $\boldsymbol{\Lambda}^{(+)}$ are then obtained by the second equation in (42). The compression and decompression impulsive forces $\boldsymbol{\Lambda}^{(-)}$ and $\boldsymbol{\Lambda}^{(+)}$ are finally put into (40), to compute the generalized velocities $\mathbf{u}^{\circ}$ at the end of compression and $\mathbf{u}^{+}$ at the end of the impact.

Already for a small number of impact elements, say three or four, an analytical solution via case distinction becomes cumbersome and nearly impractical because of the combinatorial nature of inclusion problems, and the impact has to be treated numerically. One approach is to formulate (45) together with (32), (36) as a linear complementarity problem, and to apply one of the standard solvers as, e.g., Lemke's algorithm. This approach, however, is limited to planar problems. For the general setting, proximal point formulations processed with Gauss–Seidel iterations have become the method of choice, which include as special cases some formerly developed algorithms as Moreau's cycling through the contacts, Panagiotopoulos' alternating processing of a normal and tangential convex optimization problem, and the augmented Lagrangian approach as introduced to mechanics by Alart and Cournier. For an extensive overview about available algorithms, we refer to [1].

4 Impact elements

In this section, we study in detail the physical meaning of the decompression impact law (36) for various impact elements. The impact law for compression (32) will not be discussed, as it agrees with the special case $\varepsilon_i = 0$ of a Newtonian impact. The latter has extensively been treated in [27], and everything said about this case keeps its meaning here for the compression phase. However, we do provide for each impact element the graph of the compression impact law, together with the associated graph for expansion, to graphically display how these two are related with each other.

The section is divided into two subsections, in which two different types of impulsive force reservoirs $\mathscr{C}_i$ are considered. The first subsection is devoted to sets $\mathscr{C}_i$ for which the choice of $\alpha_i \in [0, 1]$ in (19) and (21) is immaterial. In the second subsection, sets $\mathscr{C}_i$ of Coulomb type are assumed, and the associated values of α_i are determined.

4.1 Closed convex cones

We first consider impact elements whose impulsive force reservoirs $\mathscr{C}_i$ are closed convex cones $\mathscr{C}_i = \mathscr{K}_i$. In this case, we have by (11) that $0^+\mathscr{C}_i = \mathscr{C}_i$ and $\alpha_i\mathscr{C}_i = \mathscr{C}_i$ for $\alpha_i > 0$, such that the impulsive force reservoirs for compression and decompression in (19), (21) become

$$\mathscr{C}_i^{(-)} = \mathscr{C}_i, \qquad \mathscr{C}_i^{(+)} = \mathscr{C}_i \tag{46}$$

for $0 \le \alpha_i \le 1$. In the same way, we determine the auxiliary set $\mathscr{D}_i$ from (22), (24) to be

$$\mathscr{D}_i = \mathscr{C}_i \tag{47}$$

for any $\kappa_i \ge 0$. Note that the three sets in (46) and (47) do not explicitly depend on α_i, which means that the particular value of $\alpha_i \in [0, 1]$ to obtain these sets is insignificant. As a consequence, the inequality $(1 + \epsilon_i)\alpha_i \le 1$ in (28) does *not* impose an additional restriction on the Poisson restitution coefficient $\epsilon_i \ge 0$, as α_i can always be chosen small enough to allow for arbitrarily high values of ϵ_i.

4.1.1 Geometric unilateral constraints

Only the essentials of the geometric unilateral constraint in its capacity as an impact element are presented here. Additional comments and a detailed discussion of the kinematic and kinetic properties can be found in [27]. A geometric unilateral constraint is represented by a weak inequality on its gap function, $g_i(\mathbf{q}) \ge 0$. Strict inequality indicates separation, whereas equality corresponds to contact. The gap function can be formulated such that $\gamma_i = \dot{g}_i$ is the normal contact relative velocity with $\gamma_i = \mathbf{w}_i^{\mathrm{T}}\mathbf{u}$ and $\mathbf{w}_i^{\mathrm{T}} = \partial g_i/\partial \mathbf{q}$. For a closed gap $g_i(\mathbf{q}) = 0$, the pre and post-impact kinematic consistency conditions are $\gamma_i^- \le 0$ and $\gamma_i^+ \ge 0$. The geometric unilateral constraint is a one-dimensional impact element, $m(i) = 1$. The impulsive force Λ_i associated with this impact element should act as a compressive magnitude $\Lambda_i \ge 0$ but not pull on the contact, which leads by $-\Lambda_i \in \mathscr{C}_i$ to the impulsive force reservoir

$$\mathscr{C}_i = \mathbb{R}_0^-, \tag{48}$$

as already stated in [27] for Newtonian impacts. The set $\mathbb{R}_0^-$ in (48) is a closed convex cone. Equations (46) and (47) therefore apply, and the impulsive force reservoirs needed for Poisson impacts are identified as

$$\mathscr{C}_i^{(-)} = \mathbb{R}_0^-, \qquad \mathscr{C}_i^{(+)} = \mathbb{R}_0^-, \qquad \mathscr{D}_i = \mathbb{R}_0^-. \tag{49}$$

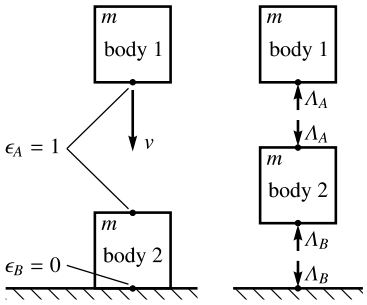

Fig. 2 A configuration for which Poisson's decompression law is required in inequality form to prevent body 2 from penetrating the ground during decompression. This is achieved by allowing for impulsive decompression forces $\Lambda_B^{(+)} > \epsilon_B \Lambda_B^{(-)}$ in contact B as indicated in the second line of (52)

With this result, the impact law (36) for decompression is recognized to be a normal cone inclusion on the set $\mathscr{D}_i = \mathbb{R}_0^-$, which can likewise be stated in terms of the unilateral primitive Upr or by the standard inequality-complementarity conditions; see [27]. We therefore have at least three equivalent formulations for this impact law, which are

$$\gamma_i^+ \in \mathscr{N}_{\mathbb{R}_0^-}(-\Lambda_i) \quad \text{or} \quad -\Lambda_i \in \mathrm{Upr}\left(\gamma_i^+\right) \quad \text{or} \quad \gamma_i^+ \geq 0, \quad \Lambda_i \geq 0, \quad \gamma_i^+ \Lambda_i = 0. \tag{50}$$

The most explicit form of this impact law is obtained by substituting back the auxiliary variable Λ_i from (35),

$$\Lambda_i = \Lambda_i^{(+)} - \epsilon_i \Lambda_i^{(-)}, \tag{51}$$

and a subsequent evaluation of the inequality-complementarity conditions in (50). The latter yields by case distinction the two conditions

$$\begin{aligned} \Lambda_i^{(+)} = \epsilon_i \Lambda_i^{(-)} \quad &\Rightarrow \quad \gamma_i^+ \geq 0, \\ \Lambda_i^{(+)} > \epsilon_i \Lambda_i^{(-)} \quad &\Rightarrow \quad \gamma_i^+ = 0, \end{aligned} \tag{52}$$

which is again a full representation of the decompression impact law (36) for this particular impact element.

The formulation (50) of Poisson's decompression impact law for the geometric unilateral constraint is in full accordance with the original version [22], in which it has been introduced by using the inequality-complementarity conditions. It provides nonnegative impulsive forces for both the compression and decompression phase: For compression, consider (32) together with (49), i.e., $-\Lambda_i^{(-)} \in \mathscr{C}_i^{(-)} = \mathbb{R}_0^-$. For decompression, it is directly seen from (52), i.e. $\Lambda_i^{(+)} \geq \epsilon_i \Lambda_i^{(-)}$ together with $\epsilon_i \geq 0$. In contrast to Newton's impact law [27], Poisson's law is always kinematically consistent for the geometric unilateral constraint. In other words, it always terminates by (52) with an admissible post-impact relative velocity $\gamma_i^+ \geq 0$, independent of the sign of the preimpact relative velocity γ_i^-.

The first line in (52) shows the impulse ratio condition in Poisson's impact law as classically used for single contact problems within an equality approach. It is kept in our setting in precisely the same way, but only *as long as post-impact penetration* $\gamma_i^+ < 0$ *can be avoided.* In the case that the original Poisson decompression impulsive force $\Lambda_i^{(+)} = \epsilon_i \Lambda_i^{(-)}$ is too small to provide kinematically admissible post-impact relative velocities $\gamma_i^+ \geq 0$, the second line in (52) takes over and increases $\Lambda_i^{(+)}$ to a value that at least $\gamma_i^+ = 0$ is reached. This situation is not pathological as one might probably think, but very common in multicontact problems: Consider two bodies with mass m each, as displayed in Fig. 2. Body 2 rests on the ground, whereas body 1 is dropped to hit body 2 with velocity v. The preimpact relative velocities in the contacts A and B are therefore $\gamma_A^- = -v$ and $\gamma_B^- = 0$. One may

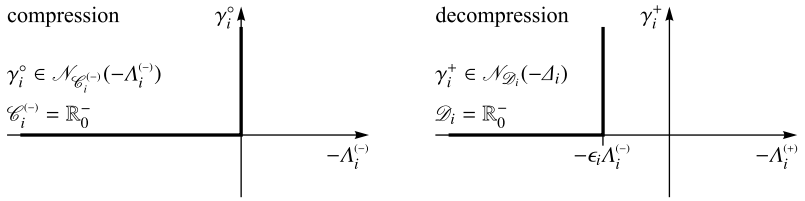

Fig. 3 Unilateral geometric and kinematic constraints: The graphs of the impact law for compression (32) and decompression (36) in the $(-\Lambda_i^{(-)}, \gamma_i^\circ)$ and $(-\Lambda_i^{(+)}, \gamma_i^+)$ planes, where $\xi_i^\circ = \gamma_i^\circ$ and $\Delta_i = \Lambda_i^{(+)} - \epsilon_i \Lambda_i^{(-)}$ according to (31) and (35), respectively

verify that compression terminates with $\gamma_A^\circ = \gamma_B^\circ = 0$, and that the compression impulsive forces are $\Lambda_A^{(-)} = \Lambda_B^{(-)} = mv$. We now assume different Poisson restitution coefficients for the contacts, namely $\epsilon_A = 1$ and $\epsilon_B = 0$. If we would now process this multicontact problem by *only* the first line in (52), the decompression impulsive forces would be $\Lambda_A^{(+)} = mv$ and $\Lambda_B^{(+)} = 0$, meaning that the reaction with the ground would be missing. We would therefore obtain as post-impact relative velocities $\gamma_A^+ = 2v > 0$ and $\gamma_B^+ = -v < 0$, the latter violating the post-impact kinematic consistency condition $\gamma_B^+ \geq 0$. If, however, the example is processed with the *full* impact law (52), then it turns out that its first line applies to contact A, and its second line to contact B. The result is $\gamma_A^+ = v > 0$, $\gamma_B^+ = 0$ and $\Lambda_A^{(+)} = \Lambda_B^{(+)} = mv$, as we expect it to be.

Figure 3 shows the graphs of the impact law for compression (32) and decompression (36) in the $(-\Lambda_i^{(-)}, \gamma_i^\circ)$ and $(-\Lambda_i^{(+)}, \gamma_i^+)$ planes. The graph for compression has already been presented within the framework of Newtonian impacts in [27], whereas the graph for decompression is drawn according to (52). Compared with each other, we see that both graphs have the same shape, and that the graph for decompression in this exposition is shifted by the value $\epsilon_i \Lambda_i^{(-)}$ to the left.

4.1.2 Kinematic unilateral constraints

The kinematic unilateral constraint is a linear inequality constraint on velocity level of the form $\gamma_i = \mathbf{w}_i^{\mathrm{T}}\mathbf{u} \geq 0$. It permits motion without any resistance in one direction but blocks in the other direction. The pre and post-impact kinematic consistency conditions are therefore $\gamma_i^- \geq 0$ and $\gamma_i^+ \geq 0$. The technical realization of a kinematic unilateral constraint is a sprag clutch. The dimension of this impact element is $m(i) = 1$. Kinematic unilateral constraints can not impact by themselves, but they can react on impacts with unbounded forces in the blocked direction, $\Lambda_i \geq 0$, see [27]. The impulsive force reservoir is therefore identical with the one for the geometric unilateral constraint, namely $\mathscr{C}_i = \mathbb{R}_0^-$ as displayed in (48). As a consequence, the resulting impact law is the very same as for the geometric unilateral constraint, and Eqs. (49)–(52) as well as Fig. 3 apply without any changes. Also, note that the impact terminates by (52) always with an admissible post-impact relative velocity $\gamma_i^+ \geq 0$, no matter what the sign of the preimpact relative velocity γ_i^- has been.

The physical interpretation of the first line in (52) for the kinematic unilateral constraint is straightforward: If the sprag clutch has been loaded during compression with $\Lambda_i^{(-)} > 0$, then the decompression impulse $\epsilon_i \Lambda_i^{(-)}$ allows the relative velocity in the sprag clutch to jump to post-impact values γ_i^+ greater than zero and, therefore, to an instantaneous motion in the unconstrained direction. The second line of (52) has to be interpreted in a similar way as for the geometric unilateral constraint: If the decompression impulse $\Lambda_i^{(+)}$ obtained from

the first line is—for any reason—not strong enough to prevent the sprag clutch from moving in its blocked direction, it will be increased until at least a standstill $\gamma_i^+ = 0$ in the clutch at the end of the impact is attained.

It has been shown in Sect. 6 of [27] that already the most elementary combination of one unilateral geometric and one unilateral kinematic constraint may lead to an energy increase when Newton's impact law is applied. This is in striking contrast to Poisson's impact law, under which the very same system behaves well, as it will be demonstrated in Sect. 9.1. We will prove in Sect. 6 energetic consistency for even an arbitrary arrangement of unilateral and bilateral geometric and kinematic constraints under the common restrictions on the restitution coefficients ϵ_i, and we will revisit in Sect. 9.1 the slide-push mechanism from [27] to demonstrate how unilateral geometric and kinematic constraints interact under Poisson's law.

4.1.3 Geometric bilateral constraints

Geometric bilateral constraints are equality constraints of the form $g_i(\mathbf{q}) = 0$. They can be transformed to velocity level by differentiation, which yields with $\dot{g}_i = \gamma_i$ and $\mathbf{w}_i^{\mathrm{T}} = \partial g_i / \partial \mathbf{q}$ the constraint velocity $\gamma_i = \mathbf{w}_i^{\mathrm{T}} \mathbf{u}$. In order to keep the system on the constraint manifold, one sets $g_i(\mathbf{q}_0) = 0$ at a specific time instant t_0 and makes sure that this value of g_i will never be left, by demanding $\gamma_i = 0$ for all times t. The condition $\gamma_i = 0$ has to apply in particular for the pre and post-impact constraint velocities, which reveals the kinematic consistency conditions for the impact as $\gamma_i^- = 0$ and $\gamma_i^+ = 0$. The dimension of this impact element is again $m(i) = 1$. As sprag clutches, geometric bilateral constraints cannot impact by themselves, but react on impacts. Forces in geometric bilateral constraints are assumed to be of any size and, if necessary, even of impulsive nature Λ_i. In particular, there is no sign restriction on these forces, such that the impulsive force reservoir can be identified as

$$\mathscr{C}_i = \mathbb{R}. \tag{53}$$

The real numbers constitute a closed convex cone, and Eqs. (46) and (47) therefore apply. As a result, we obtain for the three impulsive force reservoirs

$$\mathscr{C}_i^{(-)} = \mathbb{R}, \qquad \mathscr{C}_i^{(+)} = \mathbb{R}, \qquad \mathscr{D}_i = \mathbb{R}. \tag{54}$$

The decompression impact law (36) is now a normal cone inclusion on the set of real numbers $\mathscr{D}_i = \mathbb{R}$, i.e., a set without boundary points. The auxiliary variable $-\Delta_i \in \mathbb{R}$ is therefore always from the interior of $\mathbb{R}$, for which the normal cone reduces to just the null element. This gives by (36) the only value $\gamma_i^+ = 0$ for the post-impact constraint velocity, which in addition fulfills the kinematic consistency condition. We therefore may write the decompression impact law by either one of the following two equivalent conditions:

$$\gamma_i^+ \in \mathscr{N}_{\mathbb{R}}(-\Delta_i) \quad \text{or} \quad -\Delta_i \in \mathbb{R}, \quad \gamma_i^+ = 0. \tag{55}$$

After substituting back the auxiliary variable Δ_i from (35),

$$\Delta_i = \Lambda_i^{(+)} - \epsilon_i \Lambda_i^{(-)}, \tag{56}$$

the right representation of the decompression impact law in (55) may equivalently be expressed in terms of $\Lambda_i^{(+)}$ and γ_i^+, which yields

$$\Lambda_i^{(+)} \in \mathbb{R}, \quad \gamma_i^+ = 0. \tag{57}$$

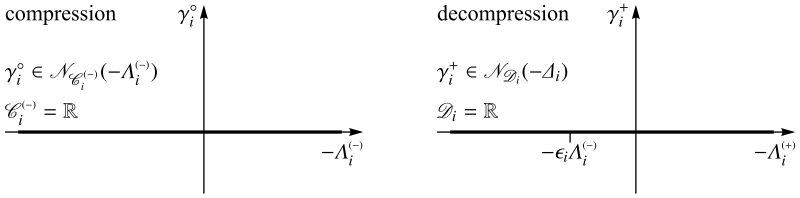

Fig. 4 Bilateral geometric and kinematic constraints: The graphs of the impact laws for compression (32) and decompression (36) in the $(-\Lambda_i^{(-)}, \gamma_i^\circ)$ and $(-\Lambda_i^{(+)}, \gamma_i^+)$ planes, where $\xi_i^\circ = \gamma_i^\circ$ and $\Delta_i = \Lambda_i^{(+)} - \epsilon_i \Lambda_i^{(-)}$ according to (31) and (35), respectively

Apparently, there are no restrictions on the decompression impulsive force $\Lambda_i^{(+)}$, and the impact terminates with the only admissible post-impact constraint velocity $\gamma_i^+ = 0$, as it should be.

Figure 4 shows on the left the graph of the Poisson impact law for compression (32) in the $(-\Lambda_i^{(-)}, \gamma_i^\circ)$ plane, which has already been presented in [27]. On the right, the graph for decompression is depicted in the $(-\Lambda_i^{(+)}, \gamma_i^+)$ plane according to (36) or, more explicitly, to (57). As already for the unilateral constraints in Fig. 3, both graphs have again the same shape, and the graph for decompression is shifted by the value $\epsilon_i \Lambda_i^{(-)}$ to the left. This shift can not be detected in the figure, because the graph is mapped onto itself, but can be traced from (56), which actually reads $-\Lambda_i^{(+)} \in \mathbb{R} - \epsilon_i \Lambda_i^{(-)}$ when $-\Delta_i \in \mathbb{R}$ from (55) is taken into account.

4.1.4 Kinematic bilateral constraints

We consider kinematic bilateral constraints of the form $\gamma_i = \mathbf{w}_i^{\mathrm{T}}\mathbf{u} = 0$, as already assumed in [27]. They impose equality constraints on velocity level upon the system, which are mechanically realized by the accompanying constraint forces. The latter are not restricted to any size and may even be of impulsive nature Λ_i, because kinematic bilateral constraints may react on impacts, although they can not impact by themselves. The reservoir for the impulsive forces $-\Lambda_i$ is therefore again $\mathscr{C}_i = \mathbb{R}$, just as in (53) for the geometric bilateral constraints. As a consequence, all the conclusions (54)–(57) apply without any modification for the kinematic bilateral constraint, including even the graphs in Fig. 4. The kinematic consistency conditions derived from the constraint $\gamma_i = 0$ are in the case of an impact apparently $\gamma_i^- = 0$ and $\gamma_i^+ = 0$. Kinematic post-impact consistency is guaranteed by the impact law (57), because it always terminates with $\gamma_i^+ = 0$.

4.2 Coulomb type sets

Coulomb friction elements i are usually used together with geometric unilateral constraints k to model the load dependent resistance in the tangential direction of contact problems. One of the main characteristics of Coulomb friction is that the size of the friction force reservoirs linearly depends on the applied normal loads. In order to extend this concept to impacts, we define an impulsive force reservoir $\mathscr{C}_i$ to be of Coulomb type, if it consists of a given shape $\mathscr{A}_i$ which scales in the sense of (1) with the impulsive normal force $\Lambda_k \geq 0$ of the associated geometric unilateral constraint, i.e.,

$$\mathscr{C}_i(\Lambda_k) = \Lambda_k \mathscr{A}_i. \tag{58}$$

We assume the convex set $\mathscr{A}_i$ to be *bounded*, which is sufficient for our later applications, but which *excludes* spike constraints. As a consequence, we have ${}^0\mathscr{A}_i = \{0\}$, and also ${}^0\mathscr{C}_i = \{0\}$ whenever Λ_k is finite. Based on the definition (58), we now develop a setting for Coulomb type impact laws which is in perfect agreement with Sect. 3.2. In particular, we determine the values for α_i and κ_i, and the three sets $\mathscr{C}_i^{(-)}$, $\mathscr{C}_i^{(+)}$, and $\mathscr{D}_i$ in terms of the known shapes $\mathscr{A}_i$. In the succeeding subsections, these results will be applied to specific bounded sets $\mathscr{A}_i$, to reveal Poisson's impact laws for certain one- and two-dimensional Coulomb type elements.

The overall impulsive force Λ_k of the associated unilateral geometric constraint, set up by its contribution to compression $\Lambda_k^{(-)}$ and decompression $\Lambda_k^{(+)}$, is

$$\Lambda_k = \Lambda_k^{(-)} + \Lambda_k^{(+)}. \tag{59}$$

By putting this expression into (58), we obtain for the overall Coulomb type reservoir

$$\mathscr{C}_i = \Lambda_k^{(-)}\mathscr{A}_i + \Lambda_k^{(+)}\mathscr{A}_i. \tag{60}$$

Our model of the frictional Poisson impact now is to claim that the Coulomb type force restriction $-\Lambda_i \in \mathscr{C}_i = \Lambda_k \mathscr{A}_i$ applies not only for the entire impact event, but separately for both the compression and decompression phase. In other words, we want to have $-\Lambda_i^{(-)} \in \Lambda_k^{(-)}\mathscr{A}_i$ and $-\Lambda_i^{(+)} \in \Lambda_k^{(+)}\mathscr{A}_i$, which enables us to identify the sets $\mathscr{C}_i^{(-)}$ and $\mathscr{C}_i^{(+)}$ with the help of (60) and (20) as

$$\mathscr{C}_i^{(-)} = \Lambda_k^{(-)}\mathscr{A}_i, \qquad \mathscr{C}_i^{(+)} = \Lambda_k^{(+)}\mathscr{A}_i. \tag{61}$$

The next step is to determine the value of α_i in (19). This can be accomplished by taking the first equation in (19) and substituting $\mathscr{C}_i^{(-)}$ from (61) and $\mathscr{C}_i$ from (58). Alternatively, one could take the second equation in (19) together with $\mathscr{C}_i^{(+)}$ from (61) and again $\mathscr{C}_i$ from (58). The results for both approaches are

$$\Lambda_k^{(-)}\mathscr{A}_i = \alpha_i \Lambda_k \mathscr{A}_i, \qquad \Lambda_k^{(+)}\mathscr{A}_i = (1-\alpha_i)\Lambda_k \mathscr{A}_i, \tag{62}$$

from which we identify

$$\Lambda_k^{(-)} = \alpha_i \Lambda_k, \qquad \Lambda_k^{(+)} = (1-\alpha_i)\Lambda_k \tag{63}$$

as a solution. We have presented both equations, because we want to show explicitly the following: Due to the exceptional cases in the compression and decompression impact laws for the unilateral geometric constraints, it might happen that either $\Lambda_k^{(-)} = 0$ or $\Lambda_k^{(+)} = 0$, although $\Lambda_k > 0$. This requires in (63) either $\alpha_i = 0$ or $\alpha_i = 1$, which now justifies our former choice of weak inequalities on α_i instead of the strong inequalities in (18).

The auxiliary set $\mathscr{D}_i$ in (28), needed for the decompression impact law (36), has still to be determined. With the help of (58), the first equation in (63), and (59), we get

$$\begin{aligned}
\mathscr{D}_i &= \big(1-(1+\epsilon_i)\alpha_i\big)\mathscr{C}_i \\
&\overset{(58)}{=} \big(1-(1+\epsilon_i)\alpha_i\big)\Lambda_k\mathscr{A}_i \\
&\overset{(63)}{=} \big(\Lambda_k - (1+\epsilon_i)\Lambda_k^{(-)}\big)\mathscr{A}_i \\
&\overset{(59)}{=} \big(\Lambda_k^{(-)} + \Lambda_k^{(+)} - (1+\epsilon_i)\Lambda_k^{(-)}\big)\mathscr{A}_i,
\end{aligned} \tag{64}$$

which finally gives

$$\mathscr{D}_i = \left(\Lambda_k^{(+)} - \epsilon_i \Lambda_k^{(-)}\right)\mathscr{A}_i. \tag{65}$$

We further have to ensure the inequality on the right in (28), which is by (27) the same as to guarantee that $\kappa_i \geq 0$. With $\mathscr{D}_i$ according to (22) and $\mathscr{C}_i$ according to (58), we get

$$\mathscr{D}_i = \kappa_i \mathscr{C}_i = \kappa_i \Lambda_k \mathscr{A}_i. \tag{66}$$

By comparing this expression with (65), the term $\kappa_i \Lambda_k$ is identified to be

$$\kappa_i \Lambda_k = \Lambda_k^{(+)} - \epsilon_i \Lambda_k^{(-)}. \tag{67}$$

Since $\Lambda_k \geq 0$, we conclude that

$$\Lambda_k^{(+)} \geq \epsilon_i \Lambda_k^{(-)} \tag{68}$$

is sufficient for the inequality $\kappa_i \geq 0$ to hold. We further know by $\Delta_k \geq 0$ in (50) or, more explicitly, by (52) that

$$\Lambda_k^{(+)} \geq \epsilon_k \Lambda_k^{(-)} \tag{69}$$

always applies for the geometric unilateral constraint. We can therefore guarantee for the inequality (68) to hold, if we choose the tangential impact coefficient ϵ_i to be not larger than the impact coefficient ϵ_k of the associated geometric unilateral constraint,

$$\epsilon_i \leq \epsilon_k. \tag{70}$$

This condition is an additional restriction on the tangential impact coefficient $\epsilon_i \geq 0$, which ensures that $\kappa_i \geq 0$, and that the set $\mathscr{D}_i$ determined in (65) fully meets the structure set up in Sect. 3.2.

4.2.1 Kinematic step constraints of Coulomb type

The kinematic step constraint of Coulomb type is a one-dimensional impact element ($m(i) = 1$), which is used to model frictional effects in planar collisions. It acts on the tangential relative velocity $\gamma_i = \mathbf{w}_i^{\mathrm{T}}\mathbf{u}$ by the tangential impulsive force Λ_i. We call this impact element a kinematic step constraint, because it can be formulated on the velocity level by set-valued sign functions ,which form upward steps in the velocity-impulse planes. The impulsive force reservoir of this impact element has been assumed in [27] to be

$$\mathscr{C}_i(\Lambda_k) = \Lambda_k \mu_i [-1, 1], \tag{71}$$

where μ_i is the coefficient of friction. As required for (58), the set $\mathscr{C}_i$ depends linearly on the impulsive normal force $\Lambda_k \geq 0$ of the associated geometric unilateral constraint. We may therefore identify from (71) the shape $\mathscr{A}_i$ in (58) as

$$\mathscr{A}_i = \mu_i [-1, 1], \tag{72}$$

which is a bounded convex set. As a consequence, Eqs. (61) and (65) apply in the form

$$\mathscr{C}_i^{(-)} = \Lambda_k^{(-)} \mu_i [-1, 1], \qquad \mathscr{C}_i^{(+)} = \Lambda_k^{(+)} \mu_i [-1, 1], \qquad \mathscr{D}_i = \left(\Lambda_k^{(+)} - \epsilon_i \Lambda_k^{(-)}\right)\mu_i [-1, 1] \tag{73}$$

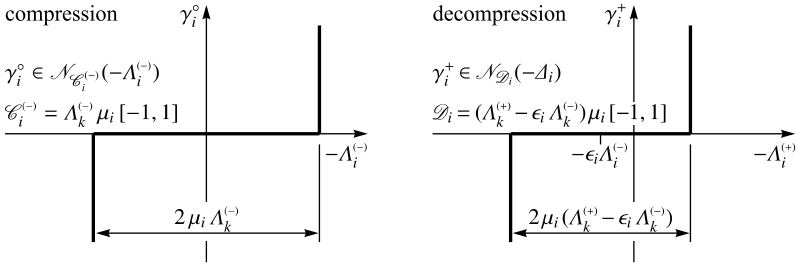

Fig. 5 Kinematic step constraint of Coulomb type: The graphs of the impact laws for compression (32) and decompression (36) in the $(-\Lambda_i^{(-)}, \gamma_i^\circ)$ and $(-\Lambda_i^{(+)}, \gamma_i^+)$ planes, where $\xi_i^\circ = \gamma_i^\circ$ and $\Delta_i = \Lambda_i^{(+)} - \epsilon_i\Lambda_i^{(-)}$ according to (31) and (35), respectively

for the three force reservoirs, and the restitution coefficient ϵ_i has to meet the inequality (70). With $\mathscr{D}_i$ from (73), the impact law for decompression (36) takes the form

$$\gamma_i^+ \in \mathcal{N}_{\mathscr{D}_i}(-\Delta_i). \tag{74}$$

By evaluating this normal cone inclusion, one obtains for the three cases that $-\Delta_i$ is either in the interior of $\mathscr{D}_i$ or at one of its boundary points the three conditions

$$\begin{aligned} |\Delta_i| < \mu_i\big(\Lambda_k^{(+)} - \epsilon_i\Lambda_k^{(-)}\big) \quad &\Rightarrow \quad \gamma_i^+ = 0, \\ \Delta_i = -\mu_i\big(\Lambda_k^{(+)} - \epsilon_i\Lambda_k^{(-)}\big) \quad &\Rightarrow \quad \gamma_i^+ \geq 0, \\ \Delta_i = +\mu_i\big(\Lambda_k^{(+)} - \epsilon_i\Lambda_k^{(-)}\big) \quad &\Rightarrow \quad \gamma_i^+ \leq 0, \end{aligned} \tag{75}$$

which fully characterize the impact law. Again, the auxiliary variable Δ_i is according to (35),

$$\Delta_i = \Lambda_i^{(+)} - \epsilon_i\Lambda_i^{(-)} \tag{76}$$

and is responsible for the shift of the associated graph, as for the former impact elements.

The graphs of the compression and decompression impact law in the $(-\Lambda_i^{(-)}, \gamma_i^\circ)$ and $(-\Lambda_i^{(+)}, \gamma_i^+)$ planes are depicted in Fig. 5. Both characteristics are shaped like an inverted set-valued sign function, which is typical for dry friction effects. The impact law for compression coincides again with a completely inelastic Newtonian impact, as discussed in [27]. The impulsive force for compression $\Lambda_i^{(-)}$ is restricted to values $-\mu_i\Lambda_k^{(-)} \leq \Lambda_i^{(-)} \leq +\mu_i\Lambda_k^{(-)}$. If $\Lambda_i^{(-)}$ is in the interior of this interval, compression terminates with stick $\gamma_i^\circ = 0$. Otherwise, sliding may take place in the one ($\gamma_i^\circ \geq 0$) or the other ($\gamma_i^\circ \leq 0$) direction. The graph for compression is horizontally centered at the origin, and its width is $2\mu_i\Lambda_k^{(-)}$, according to the size of the impulsive force reservoir $\mathscr{C}_i^{(-)}$ in (73).

The shape of an inverted set-valued sign function is fully characterized by three parameters. These are the width of its graph, and its horizontal and vertical shift. The most general implementation of a decompression law for one-dimensional friction would therefore require three impact parameters, if it is based on such a shape. However, vertical shifts have not been considered for all the previous impact elements, and our whole theoretical setting is indeed not designed to carry them. Therefore, only two parameters are remaining, and they are responsible for the horizontal shift and stretch of the decompression graph. The latter is depicted for the impact law (75), (76) in the right part of Fig. 5. One observes that this graph is centered at the value $-\epsilon_i\Lambda_i^{(-)}$, which corresponds to a horizontal shift to the left

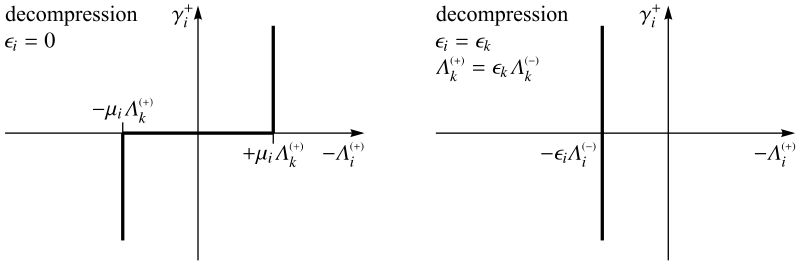

Fig. 6 Special cases for decompression: Completely inelastic frictional behavior is obtained for $\epsilon_i = 0$, as depicted on the *left*. Poisson's impact law can be observed in the right graph, where $\epsilon_i = \epsilon_k$ and $\Lambda_k^{(+)} = \epsilon_k \Lambda_k^{(-)}$ is required for the associated unilateral geometric constraint

for $\Lambda_i^{(-)} > 0$, and to the right for $\Lambda_i^{(-)} < 0$. According to the set $\mathscr{D}_i$, the width of the graph is $2\mu_i(\Lambda_k^{(+)} - \epsilon_i \Lambda_k^{(-)})$. It depends on another parameter, which is the friction coefficient μ_i. However, the friction coefficient μ_i must not be seen as an independent parameter that can freely be chosen to adjust the width for decompression, because the same μ_i is required for compression by the construction of our sets in (73). What we actually propose in our impact law (75) is therefore a one-parameter family of signum-shaped curves, in which the tangential restitution coefficient ϵ_i as the only adjustable parameter simultaneously affects both the shift and the stretch. Already because of this restriction, we can*not* expect our decompression law for frictional collisions to cover the overall variety of post-impact states that have been derived in academic examples and measured in experiments. Only a subset of them will be reproducible by (75).

In the following, we will shortly analyze how the tangential restitution coefficient ϵ_i affects the shape of the decompression graph. As a first special case, we set $\epsilon_i = 0$ in (75) and (76) to get

$$\begin{aligned} \left|\Lambda_i^{(+)}\right| < \mu_i \Lambda_k^{(+)} \quad &\Rightarrow \quad \gamma_i^+ = 0, \\ \Lambda_i^{(+)} = -\mu_i \Lambda_k^{(+)} \quad &\Rightarrow \quad \gamma_i^+ \geq 0, \\ \Lambda_i^{(+)} = +\mu_i \Lambda_k^{(+)} \quad &\Rightarrow \quad \gamma_i^+ \leq 0. \end{aligned} \tag{77}$$

These are precisely the conditions that one would empirically employ for pure Coulomb type friction, and they work pretty much in the same way as for compression: The impulsive force for decompression $\Lambda_i^{(+)}$ is restricted to values $-\mu_i \Lambda_k^{(+)} \leq \Lambda_i^{(+)} \leq +\mu_i \Lambda_k^{(+)}$. If $\Lambda_i^{(+)}$ is in the interior of this interval, decompression terminates with stick $\gamma_i^+ = 0$. Otherwise, sliding may take place in the one ($\gamma_i^+ \geq 0$) or the other ($\gamma_i^+ \leq 0$) direction. The graph for this case is depicted in the left part of Fig. 6. It is not horizontally shifted but centered at the origin, and its width is $2\mu_i \Lambda_k^{(+)}$, according to the size of the impulsive force reservoir $\mathscr{D}_i = \mathscr{C}_i^{(+)}$ in (73). In accordance with the terminology used for collisions, we may call this a *completely inelastic tangential behavior*.

As a second special case, we assume that ϵ_i is such that $\Lambda_k^{(+)} = \epsilon_i \Lambda_k^{(-)}$. This leads by (75) to $\Delta_i = 0$ as the only possible value, and to unrestricted velocities $\gamma_i^+ \gtrless 0$ as a consequence. With $\Delta_i = 0$ and Δ_i according to (76), we therefore obtain

$$\Lambda_i^{(+)} = \epsilon_i \Lambda_i^{(-)}, \quad \gamma_i^+ \in \mathbb{R}, \tag{78}$$

which is Poisson's impact law in its purest classical equality form. Note that there is no restriction, in particular no *sign* restriction on the velocity γ_i^+, as post-impact tangential

motion in both directions is kinematically admissible. The graph of the impact law (78) is shown in the right part of Fig. 6. It consists of one straight vertical line without any stick region, which is again horizontally shifted by the value $\epsilon_i \Lambda_i^{(-)}$. Finally, note that the equality $\Lambda_k^{(+)} = \epsilon_i \Lambda_k^{(-)}$ as required for (78) *only* applies if $\epsilon_i = \epsilon_k$ and $\Lambda_k^{(+)} = \epsilon_k \Lambda_k^{(-)}$, i.e., if the tangential and the normal restitution coefficients are chosen to be equal to each other, *and* if the associated geometric unilateral constraint operates in its regular regime according to the first line in (52). This can be deduced from the inequalities $\Lambda_k^{(+)} \geq \epsilon_k \Lambda_k^{(-)}$ in (52) and $\epsilon_i \leq \epsilon_k$ in (70).

Let us finally summarize how the shape of the decompression graph is deformed when the tangential restitution coefficient ϵ_i is increased from 0 to its maximal value ϵ_k *and* the associated geometric unilateral constraint operates according to $\Lambda_k^{(+)} = \epsilon_k \Lambda_k^{(-)}$: For $\epsilon_i = 0$, the decompression graph is the one depicted in the left of Fig. 6. By raising the value of ϵ_i, the center of the graph $\epsilon_i \Lambda_i^{(-)}$ is increasingly shifted in the horizontal direction, while its width $2\mu_i \Lambda_k^{(-)}(\epsilon_k - \epsilon_i)$ continuously decreases, until the configuration in the right part of Fig. 6 is reached for $\epsilon_i = \epsilon_k$. We note that the width of the decompression graph $2\mu_i \Lambda_k^{(-)}(\epsilon_k - \epsilon_i)$ is always smaller than or equal to the with for compression $2\mu_i \Lambda_k^{(-)}$, as long as $\epsilon_k \leq 1$ and $\epsilon_k, \epsilon_i \geq 0$. We further note that the maximal shift of the decompression graph under the common restrictions on the impact parameters is equal to $\Lambda_i^{(-)}$, which is obtained for $\epsilon_i = \epsilon_k = 1$. In this case, the impulsive forces for compression and decompression are by (78) equal to each other, $\Lambda_i^{(+)} = \Lambda_i^{(-)}$.

The compression phase as published in the original article [22] is identical with our approach here, i.e., its graph coincides with the one from the left of Fig. 5. The decompression phase in [22] proposes a two-parameter model, which allows to adjust the shift and the width of the decompression graph independently by the two parameters ε_T and ν. For the values $\varepsilon_T = \nu = 0$, the same completely inelastic frictional behavior is obtained as in (77) or equivalently, in the graph from the left of Fig. 6. It is, however, impossible to generally relate the two parameters ε_T and ν from [22] to the tangential restitution coefficient ϵ_i in (75), as the approach to develop the decompression impact law has been different in [22]: At this time, the impact law has been stated intuitively by taking into account some physical aspects, but without a theoretical umbrella as the one proposed in Sect. 3.2. The mathematical consistency of our new and improved version will us allow in Sect. 5 to draw conclusions that would never have been possible within the original setting.

4.2.2 Isotropic Coulomb-type friction

Isotropic Coulomb-type friction is the simplest two-dimensional extension ($m(i) = 2$) of the Coulomb-type kinematic step constraint. Together with the geometric unilateral constraint, it is used to model spatial contact situations. We denote by $\boldsymbol{\gamma}_i = (\gamma_{1i}, \gamma_{2i})^{\mathrm{T}}$ the two components of the tangential relative velocities $\gamma_{1i} = \mathbf{w}_{1i}^{\mathrm{T}}\mathbf{u}$, $\gamma_{2i} = \mathbf{w}_{2i}^{\mathrm{T}}\mathbf{u}$ in the contact plane, and by $\boldsymbol{\Lambda}_i = (\Lambda_{1i}, \Lambda_{2i})^{\mathrm{T}}$ the corresponding tangential impulsive forces. The friction coefficient is again denoted by μ_i, and the associated impulsive normal force by Λ_k. The impulsive force reservoir $\mathscr{C}_i(\Lambda_k)$ for this impact element has been introduced in [27] as

$$\mathscr{C}_i(\Lambda_k) = \left\{ \boldsymbol{\Gamma}_i \in \mathbb{R}^2 \mid \|\boldsymbol{\Gamma}_i\| \leq \mu_i \Lambda_k \right\} \tag{79}$$

and consists of a circular disk with radius $\mu_i \Lambda_k$. With the help of the set

$$\mathscr{B}_{\mu_i} := \left\{ \boldsymbol{\Xi}_i \in \mathbb{R}^2 \mid \|\boldsymbol{\Xi}_i\| \leq \mu_i \right\}, \tag{80}$$

which constitutes another disk with radius μ_i, the impulsive force reservoir $\mathscr{C}_i$ in (79) can be rewritten as

$$\mathscr{C}_i(\Lambda_k) = \Lambda_k \mathscr{B}_{\mu_i}. \tag{81}$$

This enables us to identify the shape $\mathscr{A}_i$ in (58) as $\mathscr{A}_i = \mathscr{B}_{\mu_i}$, and with it the three sets in (61) and (65) as

$$\mathscr{C}_i^{(-)} = \Lambda_k^{(-)} \mathscr{B}_{\mu_i}, \qquad \mathscr{C}_i^{(+)} = \Lambda_k^{(+)} \mathscr{B}_{\mu_i}, \qquad \mathscr{D}_i = \left(\Lambda_k^{(+)} - \epsilon_i \Lambda_k^{(-)}\right) \mathscr{B}_{\mu_i}. \tag{82}$$

With $\mathscr{D}_i$ from (82), we obtain the impact law (36) for decompression as

$$\boldsymbol{\gamma}_i^+ \in \mathscr{N}_{\mathscr{D}_i}(-\boldsymbol{\Delta}_i), \tag{83}$$

where $\boldsymbol{\Delta}_i$ according to (35), i.e.,

$$\boldsymbol{\Delta}_i = \boldsymbol{\Lambda}_i^{(+)} - \epsilon_i \boldsymbol{\Lambda}_i^{(-)}. \tag{84}$$

In contrast to the scalar impact laws from the previous sections, a full vectorial representation is needed here to express that the two tangential directions in the contact plane are not independent from each other.

The normal cone inclusion (83) can be brought by case distinction to a more explicit form. For interior points $\boldsymbol{\Delta}_i$ of the set $\mathscr{D}_i$, the normal cone reduces to the single element $\{0\}$, and decompression terminates with stick $\boldsymbol{\gamma}_i^+ = 0$. If $-\boldsymbol{\Delta}_i$ is at the boundary of $\mathscr{D}_i$, the normal cone provides a half-line orthogonal to the boundary of $\mathscr{D}_i$ at the point $-\boldsymbol{\Delta}_i$, which specifies the admissible set of post-impact velocities $\boldsymbol{\gamma}_i^+$. Both cases together can be stated as

$$\begin{aligned} \|\boldsymbol{\Delta}_i\| < \mu_i\left(\Lambda_k^{(+)} - \epsilon_i \Lambda_k^{(-)}\right) \quad &\Rightarrow \quad \boldsymbol{\gamma}_i^+ = 0, \\ \|\boldsymbol{\Delta}_i\| = \mu_i\left(\Lambda_k^{(+)} - \epsilon_i \Lambda_k^{(-)}\right) \quad &\Rightarrow \quad \boldsymbol{\gamma}_i^+ = \kappa_i \mathbf{e}_i(\boldsymbol{\Delta}_i), \quad \kappa_i \geq 0, \end{aligned} \tag{85}$$

where $\mathbf{e}_i(\boldsymbol{\Delta}_i)$ in the second line represents the aforementioned half-line and constitutes the slip direction. It can be expressed as

$$\mathbf{e}_i(\boldsymbol{\Delta}_i) := -\frac{\boldsymbol{\Delta}_i}{\|\boldsymbol{\Delta}_i\|}, \tag{86}$$

which is a direct consequence on the circular shape (82) of the set $\mathscr{D}_i$.

Figure 7 shows a graphical representation of the normal cone inclusions for compression and decompression. Displayed are the circular force reservoirs together with their associated slip directions. For elements from the interior of the force reservoirs, the normal cone is simply $\{0\}$, and the corresponding impact phase terminates with stick. For boundary points, sliding may take place in the direction as indicated. The circular force reservoir for compression is centered at the origin in the $(-\Lambda_{1i}^{(-)}, -\Lambda_{2i}^{(-)})$ plane. As a consequence, the velocity $\boldsymbol{\gamma}_i^\circ$ has precisely the same direction as the impulsive force $-\boldsymbol{\Lambda}_i^{(-)}$ when sliding takes place. The circular force reservoir for decompression is *not* centered at the origin in the $(-\Lambda_{1i}^{(+)}, -\Lambda_{2i}^{(+)})$ plane, but shifted by the value $\epsilon_i \boldsymbol{\Lambda}_i^{(-)}$ according to (84). In contrast to compression, the velocity $\boldsymbol{\gamma}_i^+$ and the impulsive force $-\boldsymbol{\Lambda}_i^{(+)}$ are no longer collinear for sliding, but only for the special case that $\boldsymbol{\Lambda}_i^{(+)}$ has the *same* direction as $\epsilon_i \boldsymbol{\Lambda}_i^{(-)}$. In this direction, the isotropic Coulomb type impact element behaves precisely in the same way as its one-dimensional counterpart, i.e., the kinematic step constraint from Sect. 4.2.1.

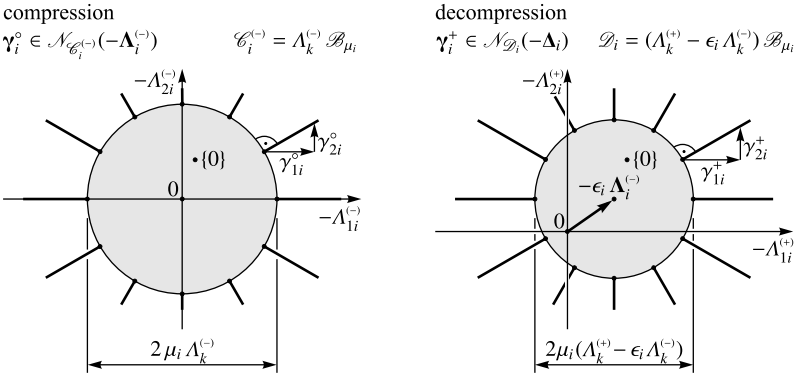

Fig. 7 Isotropic Coulomb-type friction: The graphs of the impact laws for compression (32) and decompression (36) displayed as normal cone inclusions, where $\boldsymbol{\xi}_i^\circ = \boldsymbol{\gamma}_i^\circ$ and $\boldsymbol{\Delta}_i = \boldsymbol{\Lambda}_i^{(+)} - \epsilon_i\,\boldsymbol{\Lambda}_i^{(-)}$ according to (31) and (35), respectively

Let us finally show how the impact law simplifies for the two special cases discussed at the end of Sect. 4.2.1. We first assume that the tangential restitution coefficient is equal to zero, $\epsilon_i = 0$. Together with $\boldsymbol{\Delta}_i = \boldsymbol{\Lambda}_i^{(+)}$ from (84), we obtain for the impact law (85)

$$\begin{aligned} \left\| \boldsymbol{\Lambda}_i^{(+)} \right\| < \mu_i\,\Lambda_k^{(+)} \quad &\Rightarrow \quad \boldsymbol{\gamma}_i^+ = 0, \\ \left\| \boldsymbol{\Lambda}_i^{(+)} \right\| = \mu_i\,\Lambda_k^{(+)} \quad &\Rightarrow \quad \boldsymbol{\gamma}_i^+ = \kappa_i\,\mathbf{e}_i(\boldsymbol{\Lambda}_i^{(+)}), \quad \kappa_i \geq 0, \end{aligned} \tag{87}$$

and the slip direction (86)

$$\mathbf{e}_i\left(\boldsymbol{\Lambda}_i^{(+)}\right) = -\frac{\boldsymbol{\Lambda}_i^{(+)}}{\|\boldsymbol{\Lambda}_i^{(+)}\|}. \tag{88}$$

The impact law shows now the typical Coulomb type structure and is in full analogy with the compression phase: The force reservoir with radius $\mu_i\,\Lambda_k^{(+)}$ is now centered at the origin in the $(-\Lambda_{1i}^{(+)}, -\Lambda_{2i}^{(+)})$ plane, and the velocity $\boldsymbol{\gamma}_i^+$ and the impulsive force $-\boldsymbol{\Lambda}_i^{(+)}$ have the same direction for sliding.

For the second special case, we assume that the associated geometric unilateral constraint operates in its regular regime $\Lambda_k^{(+)} = \epsilon_k\,\Lambda_k^{(-)}$, and that the normal and tangential restitution coefficients are equal, $\epsilon_i = \epsilon_k$. With these two assumptions, we obtain $\Lambda_k^{(+)} - \epsilon_i\,\Lambda_k^{(-)} = 0$, and the set $\mathscr{D}_i$ in (82) reduces to $\mathscr{D}_i = \{0\}$. The only possible value for $-\boldsymbol{\Delta}_i \in \mathscr{D}_i$ is therefore $\boldsymbol{\Delta}_i = 0$. With $\mathscr{N}_{\{0\}}(0) = \mathbb{R}^2$ in (83) and $\boldsymbol{\Delta}_i$ according to (84), the impact law for this case can now be stated as

$$\boldsymbol{\Lambda}_i^{(+)} = \epsilon_i\,\boldsymbol{\Lambda}_i^{(-)}, \quad \boldsymbol{\gamma}_i^+ \in \mathbb{R}^2. \tag{89}$$

This is the generalization of (78) to the two-dimensional case, in which we observe Poisson's impulse hypothesis in vectorial form, together with unrestricted post-impact velocities.

4.2.3 Orthotropic Coulomb-type friction

A model for orthotropic Coulomb type friction ($m(i) = 2$) with Newtonian restitution has been introduced in [27], which we now put in the framework of Poisson impacts. As for all the previous impact elements, only the decompression phase will be discussed. The compression phase coincides again with the case that the Newtonian restitution coefficient is

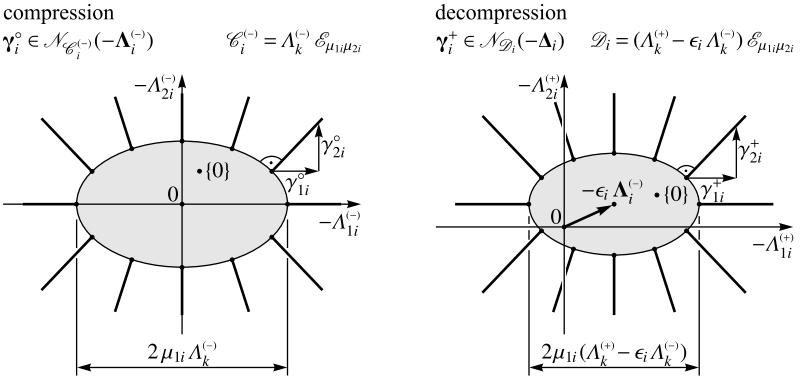

Fig. 8 Orthotropic Coulomb-type friction: The graphs of the impact laws for compression (32) and decompression (36) displayed as normal cone inclusions, where $\boldsymbol{\xi}_i^\circ = \boldsymbol{\gamma}_i^\circ$ and $\boldsymbol{\Delta}_i = \boldsymbol{\Lambda}_i^{(+)} - \epsilon_i\boldsymbol{\Lambda}_i^{(-)}$ according to (31) and (35), respectively

set equal to zero in [27]. For the reservoir of tangential impulsive forces, an elliptical set $\mathscr{C}_i(\Lambda_k)$ has been assumed in [27], with its semiaxes proportional to two different friction coefficients μ_{1i}, μ_{2i},

$$\mathscr{C}_i(\Lambda_k) = \left\{ \boldsymbol{\Gamma}_i \in \mathbb{R}^2 \;\middle|\; \frac{\Gamma_{1i}^2}{(\mu_{1i}\Lambda_k)^2} + \frac{\Gamma_{2i}^2}{(\mu_{2i}\Lambda_k)^2} \le 1 \right\}. \tag{90}$$

With $\boldsymbol{\Gamma}_i = \Lambda_k\,\boldsymbol{\Xi}_i$, this set is rewritten as a standard ellipse

$$\mathscr{E}_{\mu_{1i}\mu_{2i}} := \left\{ \boldsymbol{\Xi}_i \in \mathbb{R}^2 \;\middle|\; \frac{\Xi_{1i}^2}{\mu_{1i}^2} + \frac{\Xi_{2i}^2}{\mu_{2i}^2} \le 1 \right\}, \tag{91}$$

which enables us to state (90) as $\mathscr{C}_i(\Lambda_k) = \Lambda_k\mathscr{E}_{\mu_{1i}\mu_{2i}}$ and to identify the shape $\mathscr{A}_i$ in (58) as $\mathscr{A}_i = \mathscr{E}_{\mu_{1i}\mu_{2i}}$. The three sets in (61) and (65) therefore become

$$\mathscr{C}_i^{(-)} = \Lambda_k^{(-)}\mathscr{E}_{\mu_{1i}\mu_{2i}}, \qquad \mathscr{C}_i^{(+)} = \Lambda_k^{(+)}\mathscr{E}_{\mu_{1i}\mu_{2i}}, \qquad \mathscr{D}_i = \big(\Lambda_k^{(+)} - \epsilon_i\Lambda_k^{(-)}\big)\mathscr{E}_{\mu_{1i}\mu_{2i}}, \tag{92}$$

and the impact law for decompression (36) with $\boldsymbol{\Delta}_i$ according to (35) is

$$\boldsymbol{\gamma}_i^+ \in \mathcal{N}_{\mathscr{D}_i}(-\boldsymbol{\Delta}_i) \quad \text{with } \boldsymbol{\Delta}_i = \boldsymbol{\Lambda}_i^{(+)} - \epsilon_i\boldsymbol{\Lambda}_i^{(-)}. \tag{93}$$

The graph of this normal cone inclusion is depicted in the right part of Fig. 8, together with the graph for compression on the left. They both can be read in the same way as the graphs in Fig. 7.

In order to obtain a more explicit formulation of the impact law (93), we set $\boldsymbol{\Sigma}_i := (\Lambda_k^{(+)} - \epsilon_i\Lambda_k^{(-)})\,\boldsymbol{\Xi}_i$ in (91) and address $\mathscr{D}_i$ in (92) by the level set of the function

$$f(\boldsymbol{\Sigma}_i) := \frac{\Sigma_{1i}^2}{\mu_{1i}^2} + \frac{\Sigma_{2i}^2}{\mu_{2i}^2} - \big(\Lambda_k^{(+)} - \epsilon_i\Lambda_k^{(-)}\big)^2. \tag{94}$$

With $-\boldsymbol{\Delta}_i \in \mathscr{D}_i$ if and only if $f(-\boldsymbol{\Delta}_i) \le 0$, the impact law (93) can now be written as

$$\begin{aligned} f(-\boldsymbol{\Delta}_i) < 0 \quad &\Rightarrow \quad \boldsymbol{\gamma}_i^+ = 0, \\ f(-\boldsymbol{\Delta}_i) = 0 \quad &\Rightarrow \quad \boldsymbol{\gamma}_i^+ = \kappa_i\mathbf{e}_i(\boldsymbol{\Delta}_i), \quad \kappa_i \ge 0. \end{aligned} \tag{95}$$

As already in (86), the entity $\mathbf{e}_i(\boldsymbol{\Delta}_i)$ denotes the slip direction associated with the boundary points of $\mathscr{D}_i$. It can be determined from the differential of f,

$$\frac{\partial f}{\partial \boldsymbol{\Sigma}_i} = 2\left(\frac{\Sigma_{1i}}{\mu_{1i}^2}, \frac{\Sigma_{2i}}{\mu_{2i}^2}\right), \tag{96}$$

and subsequent normalization,

$$\mathbf{e}_i^{\mathrm{T}}(\boldsymbol{\Delta}_i) := \left(\frac{\partial f}{\partial \boldsymbol{\Sigma}_i} \Big/ \left\| \frac{\partial f}{\partial \boldsymbol{\Sigma}_i} \right\|\right)(-\boldsymbol{\Delta}_i). \tag{97}$$

The two special cases $\epsilon_i = 0$ and $\epsilon_i = \epsilon_k$ together with $\Lambda_k^{(+)} = \epsilon_k \Lambda_k^{(-)}$ can be derived from (93)–(97) as for the isotropic case with correlating results. For equal friction coefficients $\mu_{1i} = \mu_{2i} =: \mu_i$, the elliptical shapes in Fig. 8 become circular, and the resulting impact law is the same as in Sect. 4.2.2.

5 Energetic consistency conditions for arbitrary combinations of impact elements

In this section, we study the energetic consistency of Poisson impacts according to (29)–(32) and (33)–(36) for autonomous Lagrangian systems under an arbitrary arrangement of impact elements. We present a number of sufficient conditions under which the kinetic energy does not increase at the impact. The kinetic energy of an autonomous, i.e., not explicitly time-dependent mechanical system, may be written as a purely quadratic form

$$T = \frac{1}{2}\mathbf{u}^{\mathrm{T}}\mathbf{M}\mathbf{u}, \tag{98}$$

where $\mathbf{M}(\mathbf{q})$ is the symmetric and positive definite mass matrix and $\mathbf{u}$ the generalized velocities. As already pointed out in [27], the positions $\mathbf{q}$ are assumed to be constant during the impact and henceforth no longer addressed.

We denote the kinetic energy before the impact by T^-, at the end of compression by T°, and after the impact by T^+. In order to bring the overall energy difference $T^+ - T^-$ into a suitable form, some preliminary work is needed, which follows precisely the original article [22], but can also be found in [23, 46]. From (98), we get

$$\begin{aligned}
T^\circ - T^- &= \tfrac{1}{2}\mathbf{u}^{\circ\mathrm{T}}\mathbf{M}\mathbf{u}^\circ - \tfrac{1}{2}\mathbf{u}^{-\mathrm{T}}\mathbf{M}\mathbf{u}^- & T^+ - T^\circ &= \tfrac{1}{2}\mathbf{u}^{+\mathrm{T}}\mathbf{M}\mathbf{u}^+ - \tfrac{1}{2}\mathbf{u}^{\circ\mathrm{T}}\mathbf{M}\mathbf{u}^\circ \\
&= \tfrac{1}{2}(\mathbf{u}^\circ + \mathbf{u}^-)^{\mathrm{T}}\mathbf{M}(\mathbf{u}^\circ - \mathbf{u}^-) & &= \tfrac{1}{2}(\mathbf{u}^+ + \mathbf{u}^\circ)^{\mathrm{T}}\mathbf{M}(\mathbf{u}^+ - \mathbf{u}^\circ) \\
&\overset{(40)}{=} \tfrac{1}{2}(\mathbf{u}^\circ + \mathbf{u}^-)^{\mathrm{T}}\mathbf{W}\boldsymbol{\Lambda}^{(-)} & &\overset{(40)}{=} \tfrac{1}{2}(\mathbf{u}^+ + \mathbf{u}^\circ)^{\mathrm{T}}\mathbf{W}\boldsymbol{\Lambda}^{(+)} \\
&\overset{(41)}{=} \tfrac{1}{2}\boldsymbol{\Lambda}^{(-)\mathrm{T}}(\boldsymbol{\gamma}^\circ + \boldsymbol{\gamma}^-) & &\overset{(41)}{=} \tfrac{1}{2}\boldsymbol{\Lambda}^{(+)\mathrm{T}}(\boldsymbol{\gamma}^+ + \boldsymbol{\gamma}^\circ) \\
&=: W^{(-)} & &=: W^{(+)}
\end{aligned} \tag{99}$$

where the left column refers to compression, and the right column to decompression. In the last two lines of (99), the energy differences are recognized as the associated work $W^{(-)}$ and $W^{(+)}$ done by the individual impact elements, which will be used from now on. With the help of (43), the relative velocities $\boldsymbol{\gamma}^-$ are now eliminated from the left column, and $\boldsymbol{\gamma}^\circ$ in the same way from the right column,

$$W^{(-)} = -\frac{1}{2}\boldsymbol{\Lambda}^{(-)\mathrm{T}}\mathbf{G}\boldsymbol{\Lambda}^{(-)} + \boldsymbol{\Lambda}^{(-)\mathrm{T}}\boldsymbol{\gamma}^\circ, \qquad W^{(+)} = -\frac{1}{2}\boldsymbol{\Lambda}^{(+)\mathrm{T}}\mathbf{G}\boldsymbol{\Lambda}^{(+)} + \boldsymbol{\Lambda}^{(+)\mathrm{T}}\boldsymbol{\gamma}^+. \tag{100}$$

The overall energy difference or, equivalently, the overall impact work therefore becomes

$$W := W^{(-)} + W^{(+)} = -\frac{1}{2}\boldsymbol{\Lambda}^{(-)^{\mathrm{T}}}\mathbf{G}\boldsymbol{\Lambda}^{(-)} - \frac{1}{2}\boldsymbol{\Lambda}^{(+)^{\mathrm{T}}}\mathbf{G}\boldsymbol{\Lambda}^{(+)} + \boldsymbol{\Lambda}^{(-)^{\mathrm{T}}}\boldsymbol{\gamma}^{\circ} + \boldsymbol{\Lambda}^{(+)^{\mathrm{T}}}\boldsymbol{\gamma}^{+}. \tag{101}$$

In a further step, $\boldsymbol{\Lambda}^{(+)}$ is eliminated by $\boldsymbol{\Delta} = \boldsymbol{\Lambda}^{(+)} - \boldsymbol{\epsilon}\,\boldsymbol{\Lambda}^{(-)}$ according to (42), which yields for the second summand in (101)

$$\frac{1}{2}\boldsymbol{\Lambda}^{(+)^{\mathrm{T}}}\mathbf{G}\boldsymbol{\Lambda}^{(+)} \overset{(42)}{=} \frac{1}{2}\boldsymbol{\Delta}^{\mathrm{T}}\mathbf{G}\boldsymbol{\Delta} + \frac{1}{2}\boldsymbol{\Lambda}^{(-)^{\mathrm{T}}}\boldsymbol{\epsilon}\mathbf{G}\boldsymbol{\epsilon}\boldsymbol{\Lambda}^{(-)} + \boldsymbol{\Lambda}^{(-)^{\mathrm{T}}}\boldsymbol{\epsilon}\mathbf{G}\boldsymbol{\Delta}, \tag{102}$$

and for the last summand together with $\boldsymbol{\gamma}^{+} - \boldsymbol{\gamma}^{\circ} = \mathbf{G}\boldsymbol{\Lambda}^{(+)}$ from (43)

$$\begin{aligned}
\boldsymbol{\Lambda}^{(+)^{\mathrm{T}}}\boldsymbol{\gamma}^{+} &\overset{(42)}{=} \boldsymbol{\Delta}^{\mathrm{T}}\boldsymbol{\gamma}^{+} + \boldsymbol{\Lambda}^{(-)^{\mathrm{T}}}\boldsymbol{\epsilon}\boldsymbol{\gamma}^{+} \\
&\overset{(43)}{=} \boldsymbol{\Delta}^{\mathrm{T}}\boldsymbol{\gamma}^{+} + \boldsymbol{\Lambda}^{(-)^{\mathrm{T}}}\boldsymbol{\epsilon}(\boldsymbol{\gamma}^{\circ} + \mathbf{G}\boldsymbol{\Lambda}^{(+)}) \\
&\overset{(42)}{=} \boldsymbol{\Delta}^{\mathrm{T}}\boldsymbol{\gamma}^{+} + \boldsymbol{\Lambda}^{(-)^{\mathrm{T}}}\boldsymbol{\epsilon}\boldsymbol{\gamma}^{\circ} + \boldsymbol{\Lambda}^{(-)^{\mathrm{T}}}\boldsymbol{\epsilon}\mathbf{G}\boldsymbol{\Delta} + \boldsymbol{\Lambda}^{(-)^{\mathrm{T}}}\boldsymbol{\epsilon}\mathbf{G}\boldsymbol{\epsilon}\boldsymbol{\Lambda}^{(-)}.
\end{aligned} \tag{103}$$

Together with (102) and (103), the impact work (101) becomes

$$W = -\frac{1}{2}\boldsymbol{\Lambda}^{(-)^{\mathrm{T}}}\mathbf{G}\boldsymbol{\Lambda}^{(-)} - \frac{1}{2}\boldsymbol{\Delta}^{\mathrm{T}}\mathbf{G}\boldsymbol{\Delta} + \frac{1}{2}\boldsymbol{\Lambda}^{(-)^{\mathrm{T}}}\boldsymbol{\epsilon}\mathbf{G}\boldsymbol{\epsilon}\boldsymbol{\Lambda}^{(-)} + \boldsymbol{\Lambda}^{(-)^{\mathrm{T}}}\boldsymbol{\gamma}^{\circ} + \boldsymbol{\Delta}^{\mathrm{T}}\boldsymbol{\gamma}^{+} + \boldsymbol{\Lambda}^{(-)^{\mathrm{T}}}\boldsymbol{\epsilon}\boldsymbol{\gamma}^{\circ}, \tag{104}$$

and can finally be stated as

$$W = -\frac{1}{2}\boldsymbol{\Delta}^{\mathrm{T}}\mathbf{G}\boldsymbol{\Delta} - \frac{1}{2}\boldsymbol{\Lambda}^{(-)^{\mathrm{T}}}(\mathbf{G} - \boldsymbol{\epsilon}\mathbf{G}\boldsymbol{\epsilon})\boldsymbol{\Lambda}^{(-)} + \boldsymbol{\Delta}^{\mathrm{T}}\boldsymbol{\gamma}^{+} + \boldsymbol{\Lambda}^{(-)^{\mathrm{T}}}(\mathbf{I} + \boldsymbol{\epsilon})\boldsymbol{\gamma}^{\circ}. \tag{105}$$

Except of the notation, (104) is precisely the same expression as in Eq. (43) of the original article [22], and can also be found in [23, 46]. Note, however, that only geometric unilateral constraints and one-dimensional Coulomb type friction elements have been treated in these publications, whereas the entire collection of impact elements from Sect. 4 is covered here.

5.1 Isolated impact elements

Before studying the fully coupled problem, we want to quickly analyze the case that the individual impact elements are *completely isolated* and *independent* from each other, which means among others that the off-diagonal terms in the Delassus operator $\mathbf{G}$ are equal to zero, $\mathbf{G}_{ik} = \mathbf{W}_i^{\mathrm{T}}\mathbf{M}^{-1}\mathbf{W}_k = 0$ $(i \neq k)$. Under the assumption that each individual impact element behaves dissipatively, i.e., does not lead to an increase in its associated impact work W_i, certain restrictions on the impact parameters ϵ_i can be derived, such as the classical choice of $\epsilon_i \leq 1$ for the geometric unilateral constraint. The impact work

$$W = \sum_{i=1}^{n} W_i \tag{106}$$

can therefore be written by (105) for the individual impact elements as

$$W_i = -\frac{1}{2}\boldsymbol{\Delta}_i^{\mathrm{T}}\mathbf{G}_{ii}\boldsymbol{\Delta}_i - \frac{1}{2}\big(1 - \epsilon_i^2\big)\boldsymbol{\Lambda}_i^{(-)^{\mathrm{T}}}\mathbf{G}_{ii}\boldsymbol{\Lambda}_i^{(-)} + \boldsymbol{\Delta}_i^{\mathrm{T}}\boldsymbol{\gamma}_i^{+} + (1 + \epsilon_i)\boldsymbol{\Lambda}_i^{(-)^{\mathrm{T}}}\boldsymbol{\gamma}_i^{\circ}, \tag{107}$$

Table 1 Restrictions on the impact coefficients from kinetic and isolated energetic consistency. The index k denotes the geometric unilateral constraint associated with the friction element i

Unilateral constraints	Bilateral constraints	Coulomb type friction
$0 \leq \epsilon_i \leq 1$	$0 \leq \epsilon_i \leq 1$	$0 \leq \epsilon_i \leq \epsilon_k$

where $\mathbf{G}_{ii} = \mathbf{W}_i^{\mathrm{T}} \mathbf{M}^{-1} \mathbf{W}_i$ are the symmetric and positive definite diagonal entries of $\mathbf{G}$. By this property, we immediately have $\boldsymbol{\Delta}_i^{\mathrm{T}} \mathbf{G}_{ii} \boldsymbol{\Delta}_i \geq 0$ and $\boldsymbol{\Lambda}_i^{(-)^{\mathrm{T}}} \mathbf{G}_{ii} \boldsymbol{\Lambda}_i^{(-)} \geq 0$. Furthermore, it holds by (38) that $\boldsymbol{\Delta}_i^{\mathrm{T}} \boldsymbol{\gamma}_i^{+} \leq 0$ and $\boldsymbol{\Lambda}_i^{(-)^{\mathrm{T}}} \boldsymbol{\gamma}_i^{\circ} \leq 0$, where we have used $\boldsymbol{\xi}_i^{\circ} = \boldsymbol{\gamma}_i^{\circ}$ from (31). A sufficient condition on the full expression (107) to be less than or equal to zero is therefore to restrict the impact coefficient ϵ_i to values

$$|\epsilon_i| \leq 1, \tag{108}$$

to keep $(1 - \epsilon_i^2)$ nonnegative. Although this restriction provides energetic consistency for isolated impact elements, it does in general *not* ensure dissipativity for coupled systems. A counterexample will be presented in Sect. 10. For certain applications, it may even be necessary to disrespect the inequality (108), and to enforce an energy gain locally at certain impact elements to reach a desired post-impact state. That such an approach may be reasonable, also from the mechanical point of view, will be discussed in context with Newton's cradle in Sect. 9.3. Nevertheless, we will take the restriction (108) as a basis to derive energetic consistency conditions for coupled systems, which is done in the next section. When finally combining the bounds on ϵ_i from (108) with the kinetic restrictions $\epsilon_i \geq 0$ from Sect. 3.2 and $\epsilon_i \leq \epsilon_k$ for the Coulomb type elements in Sect. 4.2, one obtains the values summarized in Table 1.

5.2 Fully coupled systems

Energetic consistency of the individual impact elements as studied in the last section may get lost when the impact elements are coupled among each other by the off-diagonal terms in the Delassus matrix. In order to address this case, we keep the restrictions $-1 \leq \epsilon_i \leq 1$ from (108) and derive additional conditions on ϵ_i to ensure energetic consistency also for fully coupled systems. For this, we return to the overall impact work (105) and study the four summands of which it consists.

The term $\boldsymbol{\Delta}^{\mathrm{T}} \mathbf{G} \boldsymbol{\Delta}$ in the first summand is always greater than or equal to zero, because $\mathbf{G}$ is positive semidefinite by (44). The third summand can be written as a sum, for which we get by the right inequality in (38) that

$$\boldsymbol{\Delta}^{\mathrm{T}} \boldsymbol{\gamma}^{+} = \sum_{i=1}^{n} \boldsymbol{\Delta}_i^{\mathrm{T}} \boldsymbol{\gamma}_i^{+} \leq 0. \tag{109}$$

With $\boldsymbol{\gamma}_i^{\circ} = \boldsymbol{\xi}_i^{\circ}$ from (31) together with the left inequality in (38) and the restriction (108) on the impact coefficients, it holds for the fourth summand that

$$\boldsymbol{\Lambda}^{(-)^{\mathrm{T}}} (\mathbf{I} + \boldsymbol{\epsilon}) \boldsymbol{\gamma}^{\circ} = \sum_{i=1}^{n} (1 + \epsilon_i) \boldsymbol{\Lambda}_i^{(-)^{\mathrm{T}}} \boldsymbol{\gamma}_i^{\circ} \leq 0. \tag{110}$$

In order to ensure energetic consistency $W \leq 0$ in (105) as a whole, it remains to find conditions under which the matrix $(\mathbf{G} - \boldsymbol{\epsilon}\mathbf{G}\boldsymbol{\epsilon})$ in the second summand is at least positive semidefinite, i.e., under which

$$\boldsymbol{\Lambda}^{\mathrm{T}}\mathbf{G}\boldsymbol{\Lambda} - \boldsymbol{\Lambda}^{\mathrm{T}}\boldsymbol{\epsilon}\mathbf{G}\boldsymbol{\epsilon}\boldsymbol{\Lambda} \geq 0 \quad \forall \boldsymbol{\Lambda}. \tag{111}$$

Such conditions have originally been derived by the author's former student Fritz Stöckli in his master thesis [51] for the cases of similar and small impact coefficients ϵ_i as shown in the following.

5.2.1 Similar impact coefficients

We denote by $\epsilon_{\min}$ the smallest and by $\epsilon_{\max}$ the largest of the impact coefficients $\epsilon_i \in [-1, 1]$ and rewrite the second summand in (111) as

$$\boldsymbol{\Lambda}^{\mathrm{T}}\boldsymbol{\epsilon}\mathbf{G}\boldsymbol{\epsilon}\boldsymbol{\Lambda} \equiv \epsilon_{\min}^2\boldsymbol{\Lambda}^{\mathrm{T}}\mathbf{G}\boldsymbol{\Lambda} + \boldsymbol{\Lambda}^{\mathrm{T}}(\boldsymbol{\epsilon} - \epsilon_{\min}\mathbf{I})\mathbf{G}(\boldsymbol{\epsilon} + \epsilon_{\min}\mathbf{I})\boldsymbol{\Lambda}. \tag{112}$$

With it, the condition of positive semidefiniteness (111) becomes

$$\left(1 - \epsilon_{\min}^2\right)\boldsymbol{\Lambda}^{\mathrm{T}}\mathbf{G}\boldsymbol{\Lambda} - \boldsymbol{\Lambda}^{\mathrm{T}}(\boldsymbol{\epsilon} - \epsilon_{\min}\mathbf{I})\mathbf{G}(\boldsymbol{\epsilon} + \epsilon_{\min}\mathbf{I})\boldsymbol{\Lambda} \geq 0 \quad \forall \boldsymbol{\Lambda}. \tag{113}$$

Since $\mathbf{G}$ is symmetric and real, it follows for the first summand in (113) that

$$\left(1 - \epsilon_{\min}^2\right)\boldsymbol{\Lambda}^{\mathrm{T}}\mathbf{G}\boldsymbol{\Lambda} \geq \left(1 - \epsilon_{\min}^2\right)\lambda_{\min}\|\boldsymbol{\Lambda}\|^2, \tag{114}$$

where $\lambda_{\min}$ denotes the smallest (real) eigenvalue of $\mathbf{G}$. For the second summand in (113), it holds that

$$\begin{aligned}\boldsymbol{\Lambda}^{\mathrm{T}}(\boldsymbol{\epsilon} - \epsilon_{\min}\mathbf{I})\mathbf{G}(\boldsymbol{\epsilon} + \epsilon_{\min}\mathbf{I})\boldsymbol{\Lambda} &\leq \|\boldsymbol{\epsilon} - \epsilon_{\min}\mathbf{I}\|\|\mathbf{G}\|\|\boldsymbol{\epsilon} + \epsilon_{\min}\mathbf{I}\|\|\boldsymbol{\Lambda}\|^2 \\ &= (\epsilon_{\max} - \epsilon_{\min})\lambda_{\max}(\epsilon_{\max} + \epsilon_{\min})\|\boldsymbol{\Lambda}\|^2\end{aligned} \tag{115}$$

where $\lambda_{\max}$ is the largest (real) eigenvalue of $\mathbf{G}$, and $\|\mathbf{A}\|$ denotes the matrix norm induced by $\|\mathbf{A}\| := \max_{\mathbf{x}}\{\|\mathbf{A}\mathbf{x}\| \,|\, \|\mathbf{x}\| = 1\}$. By the estimates (114) and (115), we conclude that (111) can be guaranteed if

$$\left(1 - \epsilon_{\min}^2\right)\lambda_{\min}\|\boldsymbol{\Lambda}\|^2 - (\epsilon_{\max} - \epsilon_{\min})\lambda_{\max}(\epsilon_{\max} + \epsilon_{\min})\|\boldsymbol{\Lambda}\|^2 \geq 0 \tag{116}$$

or, after canceling $\boldsymbol{\Lambda}$, that the inequality

$$\frac{\epsilon_{\max}^2 - \epsilon_{\min}^2}{1 - \epsilon_{\min}^2} \leq \frac{\lambda_{\min}}{\lambda_{\max}} \tag{117}$$

is sufficient for the matrix $(\mathbf{G} - \boldsymbol{\epsilon}\mathbf{G}\boldsymbol{\epsilon})$ to be positive semidefinite. We therefore conclude that similar impact coefficients ϵ_i in the sense of (117) provide a sufficient condition for the impact to be energetically consistent, i.e, to fulfill the impact work inequality $W \leq 0$ with W according to (105).

5.2.2 Small impact coefficients

Another sufficient condition for energetic consistency is obtained from (111) by the following estimation: Similarly to (114), we have for the first term in (111)

$$\boldsymbol{\Lambda}^{\mathrm{T}}\mathbf{G}\boldsymbol{\Lambda} \geq \lambda_{\min}\|\boldsymbol{\Lambda}\|^2. \tag{118}$$

For the second term in (111), it holds that

$$\boldsymbol{\Lambda}^{\mathrm{T}}\boldsymbol{\epsilon}\mathbf{G}\boldsymbol{\epsilon}\boldsymbol{\Lambda} \leq \|\boldsymbol{\epsilon}\|\|\mathbf{G}\|\|\boldsymbol{\epsilon}\|\|\boldsymbol{\Lambda}\|^2 = \epsilon_{\max}^2\lambda_{\max}\|\boldsymbol{\Lambda}\|^2. \tag{119}$$

By the estimates (118) and (119), we conclude that (111) can be guaranteed if

$$\lambda_{\min}\|\boldsymbol{\Lambda}\|^2 - \epsilon_{\max}^2\lambda_{\max}\|\boldsymbol{\Lambda}\|^2 \geq 0 \tag{120}$$

or, after canceling $\boldsymbol{\Lambda}$, that the inequality

$$\epsilon_{\max}^2 \leq \frac{\lambda_{\min}}{\lambda_{\max}} \tag{121}$$

is sufficient for $(\mathbf{G} - \boldsymbol{\epsilon}\mathbf{G}\boldsymbol{\epsilon})$ to be positive semidefinite. In other words, impact coefficients that are small in the sense of (121) provide another sufficient condition for the impact to be energetically consistent, i.e., to fulfill the impact work inequality $W \leq 0$ with W according to (105).

Note, however, that the conditions (117) and (121) are not independent, but can be related to each other by the inequality

$$\frac{\epsilon_{\max}^2 - \epsilon_{\min}^2}{1 - \epsilon_{\min}^2} \leq \epsilon_{\max}^2. \tag{122}$$

In order to verify this, we multiply both sides with $(1 - \epsilon_{\min}^2) \geq 0$ to obtain

$$\epsilon_{\max}^2 - \epsilon_{\min}^2 \leq \epsilon_{\max}^2\big(1 - \epsilon_{\min}^2\big) \quad \Rightarrow \quad -\epsilon_{\min}^2 \leq -\epsilon_{\max}^2\epsilon_{\min}^2 \quad \Rightarrow \quad \epsilon_{\max}^2 \leq 1, \tag{123}$$

which is true by (108). *Small impact coefficients* in the sense of (121) are therefore a special case of *similar impact coefficients* in the sense of (117). In other words, impact coefficients that respect inequality (121) do automatically respect inequality (117) because of (122).

5.2.3 Equal impact coefficients

A second special case of *similar impact coefficients* is met when they are all equal to each other with value ϵ,

$$\epsilon := \epsilon_1 = \cdots = \epsilon_n. \tag{124}$$

In this case, we have $\epsilon_{\max} = \epsilon_{\min} = \epsilon$, and (117) reduces to $0 \leq \lambda_{\min}/\lambda_{\max}$, which is always true, because the eigenvalues of the positive semidefinite Delassus matrix $\mathbf{G}$ are all non-negative. Alternatively, energetic consistency may directly be verified on the contact work (105) as done in [46]. With $\boldsymbol{\epsilon} = \epsilon\mathbf{I}$, it reduces to

$$W = -\frac{1}{2}\boldsymbol{\Lambda}^{\mathrm{T}}\mathbf{G}\boldsymbol{\Lambda} - \frac{1}{2}\big(1 - \epsilon^2\big)\boldsymbol{\Lambda}^{(-)^{\mathrm{T}}}\mathbf{G}\boldsymbol{\Lambda}^{(-)} + \boldsymbol{\Lambda}^{\mathrm{T}}\boldsymbol{\gamma}^{+} + (1+\epsilon)\boldsymbol{\Lambda}^{(-)^{\mathrm{T}}}\boldsymbol{\gamma}^{\circ}. \tag{125}$$

The critical matrix $(\mathbf{G} - \boldsymbol{\epsilon}\mathbf{G}\boldsymbol{\epsilon})$ in (105) is now $(1 - \epsilon^2)\mathbf{G}$, and its positive semidefiniteness is guaranteed by (108).

5.2.4 Completely elastic impact

We call an impact to be *completely elastic* iff all impact coefficients are equal to one, i.e., if $\epsilon = 1$ in (124). A completely elastic impact is therefore a special case of *equal impact coefficients* which by itself is a special case of *similar impact coefficients*, and is always energetically consistent. Kinematic unilateral constraints are explicitly allowed for this case, in contrast to Newtonian impacts [27], for which they had to be excluded because of the restrictions on their impact coefficients. Completely elastic impacts may be energy preserving. With $\epsilon = 1$ and $\mathbf{\Delta} = \mathbf{\Lambda}^{(+)} - \mathbf{\Lambda}^{(-)}$ according to (42), the contact work (125) becomes

$$W = -\frac{1}{2}\left(\mathbf{\Lambda}^{(+)} - \mathbf{\Lambda}^{(-)}\right)^{\mathrm{T}}\mathbf{G}\left(\mathbf{\Lambda}^{(+)} - \mathbf{\Lambda}^{(-)}\right) + \left(\mathbf{\Lambda}^{(+)} - \mathbf{\Lambda}^{(-)}\right)^{\mathrm{T}}\boldsymbol{\gamma}^{+} + 2\mathbf{\Lambda}^{(-)\mathrm{T}}\boldsymbol{\gamma}^{\circ}. \tag{126}$$

and may become equal to zero under certain conditions: The products $\mathbf{\Lambda}_i^{(-)\mathrm{T}}\boldsymbol{\gamma}_i^{\circ}$ in the last term are equal to zero for the unilateral and bilateral constraints, which can be seen from the left diagrams in Figs. 3 and 4. For all Coulomb type elements, the terms $\mathbf{\Lambda}_i^{(-)\mathrm{T}}\boldsymbol{\gamma}_i^{\circ}$ can be enforced to be equal to zero if the friction coefficients μ_i are chosen big enough to ensure stick after compression, as seen from the left diagrams in Figs. 5, 7, and 8. The remaining terms in (126) vanish if the compression and decompression impulsive forces are equal, $\mathbf{\Lambda}^{(+)} = \mathbf{\Lambda}^{(-)}$. Because of $\epsilon_i = \epsilon_k = 1$, this applies by the right diagram in Fig. 6, or by Eqs. (78) and (89) for all Coulomb type elements. Remaining are the unilateral and bilateral constraints, for which it might indeed happen that $\mathbf{\Lambda}^{(+)} = \mathbf{\Lambda}^{(-)}$ does *not* apply. This is caused by the inequality formulation of the unilateral constraints and occurs in particular for combinations of impact contacts and sprag clutches, such as in the slide-push mechanism that will be presented in Sect. 9.1. Additional conditions, under which the completely elastic impact indeed leads to energy conservation $W = 0$ will be presented in Sect. 8.3, in which the equivalence of Newtonian and Poisson impacts is addressed.

5.2.5 Completely inelastic impact

We call an impact to be *completely inelastic* iff all impact coefficients are equal to zero, i.e., if $\epsilon = 0$ in (124). A completely inelastic impact is therefore a special case of *equal impact coefficients,* which by itself is a special case of *similar impact coefficients*, and is always energetically consistent. Moreover, a completely inelastic impact is a special case of *small impact coefficients* with $\epsilon_{\max} = 0$, for which (121) always holds true. With $\epsilon = 0$ and $\mathbf{\Delta} = \mathbf{\Lambda}^{(+)}$ according to (42), the contact work (125) becomes

$$W = -\frac{1}{2}\mathbf{\Lambda}^{(+)\mathrm{T}}\mathbf{G}\mathbf{\Lambda}^{(+)} - \frac{1}{2}\mathbf{\Lambda}^{(-)\mathrm{T}}\mathbf{G}\mathbf{\Lambda}^{(-)} + \mathbf{\Lambda}^{(+)\mathrm{T}}\boldsymbol{\gamma}^{+} + \mathbf{\Lambda}^{(-)\mathrm{T}}\boldsymbol{\gamma}^{\circ}. \tag{127}$$

A completely inelastic impact terminates already after the compression phase, which will be shown in Sect. 8.3. As a consequence, the decompression impulsive forces $\mathbf{\Lambda}^{(+)}$ are equal to zero, by which the impact work (127) simplifies to

$$W = -\frac{1}{2}\mathbf{\Lambda}^{(-)\mathrm{T}}\mathbf{G}\mathbf{\Lambda}^{(-)} + \mathbf{\Lambda}^{(-)\mathrm{T}}\boldsymbol{\gamma}^{\circ}. \tag{128}$$

This result is the same as if a Newtonian impact is processed with all of its impact coefficients equal to zero, $\varepsilon_i = 0$, which will formally be verified in Sect. 8.

6 Energetic consistency for frictionless systems

In this section, we prove the energetic consistency of Poisson impacts for frictionless systems under the standard restriction $|\epsilon_i| \leq 1$ on the impact coefficients. Allowed in the system is any number and any combination of frictionless bilateral or unilateral geometric or kinematic constraints, i.e., any combination of the impact elements from Sect. 4.1. The original version [51] of this proof is geometrically driven and covers the two types of unilateral constraints.

In order to proof the above assertion, we need the impact equations for compression and decompression from (40),

$$\mathbf{M}\big(\mathbf{u}^{\circ} - \mathbf{u}^{-}\big) = \mathbf{W}\boldsymbol{\Lambda}^{(-)}, \qquad \mathbf{M}\big(\mathbf{u}^{+} - \mathbf{u}^{\circ}\big) = \mathbf{W}\boldsymbol{\Lambda}^{(+)}, \tag{129}$$

as well as two auxiliary velocities $\mathbf{u}^{\diamond}$ and $\mathbf{u}^{\star}$, which are implicitly defined by

$$\mathbf{M}\big(\mathbf{u}^{\diamond} - \mathbf{u}^{\circ}\big) = \mathbf{W}\boldsymbol{\Lambda}^{(-)}, \qquad \mathbf{M}\big(\mathbf{u}^{\star} - \mathbf{u}^{\circ}\big) = \mathbf{W}\boldsymbol{\epsilon}\boldsymbol{\Lambda}^{(-)}. \tag{130}$$

By looking at (130) as kind of impact equations for decompression, $\mathbf{u}^{\diamond}$ would be the post-impact velocity that would be obtained if the decompression impulse would equal the compression impulse $\boldsymbol{\Lambda}^{(-)}$, and $\mathbf{u}^{\star}$ would be the post-impact velocity obtained by a decompression impulse $\boldsymbol{\epsilon}\boldsymbol{\Lambda}^{(-)}$ equal to the one in the classical Poisson setting.

We will further need that the two velocities $\mathbf{u}^{\diamond}$ and $\mathbf{u}^{-}$ are of equal length in the kinetic metric, $\|\mathbf{u}^{\diamond}\|_{\mathbf{M}} = \|\mathbf{u}^{-}\|_{\mathbf{M}}$ or, in other words that

$$\mathbf{u}^{\diamond\mathrm{T}}\mathbf{M}\mathbf{u}^{\diamond} = \mathbf{u}^{-\mathrm{T}}\mathbf{M}\mathbf{u}^{-}. \tag{131}$$

In order to show (131), we take the left equation in (129) and in (130), and build their sum and their difference,

$$\mathbf{M}\big(\mathbf{u}^{\diamond} - \mathbf{u}^{-}\big) = 2\mathbf{W}\boldsymbol{\Lambda}^{(-)}, \quad \mathbf{u}^{\diamond} + \mathbf{u}^{-} = 2\mathbf{u}^{\circ}. \tag{132}$$

The left equation in (132) is now multiplied with the right equation, which yields

$$\big(\mathbf{u}^{\diamond} + \mathbf{u}^{-}\big)^{\mathrm{T}}\mathbf{M}\big(\mathbf{u}^{\diamond} - \mathbf{u}^{-}\big) = 4\mathbf{u}^{\circ\mathrm{T}}\mathbf{W}\boldsymbol{\Lambda}^{(-)}. \tag{133}$$

With the help of $\boldsymbol{\gamma}^{\circ} = \mathbf{W}^{\mathrm{T}}\mathbf{u}^{\circ}$ from (41), one finally obtains

$$\mathbf{u}^{\diamond\mathrm{T}}\mathbf{M}\mathbf{u}^{\diamond} - \mathbf{u}^{-\mathrm{T}}\mathbf{M}\mathbf{u}^{-} = 4\boldsymbol{\gamma}^{\circ\mathrm{T}}\boldsymbol{\Lambda}^{(-)}. \tag{134}$$

Written as a sum, the right-hand side of (134) consists of terms $\gamma_i^{\circ}\Lambda_i^{(-)}$, which all are equal or less than zero by (38) and $\xi_i^{\circ} = \gamma_i^{\circ}$. For the (frictionless) impact elements in Sect. 4.1, they are even equal to zero, which can be verified by the left diagrams in Figs. 3 and 4. We therefore obtain $\boldsymbol{\gamma}^{\circ\mathrm{T}}\boldsymbol{\Lambda}^{(-)} = 0$ in (134), and the equality (131) is verified.

To prove now the energetic consistency for frictionless systems, the post-impact kinetic energy T^{+} is written by a telescopic expansion as

$$\begin{aligned} 2T^{+} &= \mathbf{u}^{+\mathrm{T}}\mathbf{M}\mathbf{u}^{+} \\ &= \mathbf{u}^{+\mathrm{T}}\mathbf{M}\big(\mathbf{u}^{+} - \mathbf{u}^{\star}\big) + \mathbf{u}^{+\mathrm{T}}\mathbf{M}\mathbf{u}^{\star} \\ &= \mathbf{u}^{+\mathrm{T}}\mathbf{M}\big(\mathbf{u}^{+} - \mathbf{u}^{\star}\big) + \mathbf{u}^{+\mathrm{T}}\mathbf{M}\big(\mathbf{u}^{\star} - \mathbf{u}^{\diamond}\big) + \mathbf{u}^{+\mathrm{T}}\mathbf{M}\mathbf{u}^{\diamond}. \end{aligned} \tag{135}$$

The first summand in the last line is now rewritten with the help of the right equations in (129) and (130) as

$$\mathbf{u}^{+\mathrm{T}}\mathbf{M}\big(\mathbf{u}^{+}-\mathbf{u}^{\star}\big)=\mathbf{u}^{+\mathrm{T}}\mathbf{W}\big(\boldsymbol{\Lambda}^{(+)}-\boldsymbol{\epsilon}\boldsymbol{\Lambda}^{(-)}\big)=\mathbf{u}^{+\mathrm{T}}\mathbf{W}\boldsymbol{\Delta}=\boldsymbol{\gamma}^{+\mathrm{T}}\boldsymbol{\Delta}=0, \tag{136}$$

where we have also used $\boldsymbol{\Delta}=\boldsymbol{\Lambda}^{(+)}-\boldsymbol{\epsilon}\boldsymbol{\Lambda}^{(-)}$ from (42) and $\boldsymbol{\gamma}^{+}=\mathbf{W}^{\mathrm{T}}\mathbf{u}^{+}$ from (41). The last statement, $\boldsymbol{\gamma}^{+\mathrm{T}}\boldsymbol{\Delta}=0$, follows from the right inequality in (38), which holds in our (frictionless) case again as an equality by the right diagrams in Figs. 3 and 4. For the second summand in the last line of (135), we obtain by (130)

$$\mathbf{u}^{+\mathrm{T}}\mathbf{M}\big(\mathbf{u}^{\star}-\mathbf{u}^{\diamond}\big)=\mathbf{u}^{+\mathrm{T}}\mathbf{W}\big(\boldsymbol{\epsilon}\boldsymbol{\Lambda}^{(-)}-\boldsymbol{\Lambda}^{(-)}\big)=\boldsymbol{\gamma}^{+\mathrm{T}}(\boldsymbol{\epsilon}-\mathbf{I})\boldsymbol{\Lambda}^{(-)} \tag{137}$$

where we have again used $\boldsymbol{\gamma}^{+}=\mathbf{W}^{\mathrm{T}}\mathbf{u}^{+}$ from (41). Expanded into a sum, it can be written as

$$\mathbf{u}^{+\mathrm{T}}\mathbf{M}\big(\mathbf{u}^{\star}-\mathbf{u}^{\diamond}\big)=\sum_{i=1}^{n}-(1-\epsilon_i)\gamma_i^{+}\Lambda_i^{(-)}\le 0. \tag{138}$$

The inequality follows from the facts that $(1-\epsilon_i)\ge 0$ by the standard restriction on ϵ_i, and that $\gamma_i^{+}\Lambda_i^{(-)}\ge 0$ for the impact elements considered here: For the unilateral constraints, we have $\Lambda_i^{(-)}\ge 0$ and $\gamma_i^{+}\ge 0$ according to Fig. 3, whereas $\gamma_i^{+}=0$ applies by Fig. 4 for the bilateral constraints.

With the help of (136) and (138), one obtains now from the first and the last line of (135) the relation

$$\mathbf{u}^{+\mathrm{T}}\mathbf{M}\mathbf{u}^{+}\le\mathbf{u}^{+\mathrm{T}}\mathbf{M}\mathbf{u}^{\diamond}, \tag{139}$$

where the second member in (139) can be estimated by the Cauchy–Schwartz inequality as

$$\mathbf{u}^{+\mathrm{T}}\mathbf{M}\mathbf{u}^{\diamond}\le\sqrt{\mathbf{u}^{+\mathrm{T}}\mathbf{M}\mathbf{u}^{+}}\cdot\sqrt{\mathbf{u}^{\diamond\mathrm{T}}\mathbf{M}\mathbf{u}^{\diamond}}. \tag{140}$$

The inequalities (139) and (140), together with (131), finally lead to

$$\mathbf{u}^{+\mathrm{T}}\mathbf{M}\mathbf{u}^{+}\le\sqrt{\mathbf{u}^{+\mathrm{T}}\mathbf{M}\mathbf{u}^{+}}\cdot\sqrt{\mathbf{u}^{-\mathrm{T}}\mathbf{M}\mathbf{u}^{-}}, \tag{141}$$

which shows by (98) energetic consistency in the form

$$T^{+}\le\sqrt{T^{+}}\cdot\sqrt{T^{-}}\quad\Rightarrow\quad T^{+}\le T^{-}. \tag{142}$$

For Newtonian impacts [27], unilateral geometric and kinematic constraints in already the most elementary combination have been shown to generate a disastrous increase in the kinetic energy. In contrast, energetic consistency can be assured by (142) in full generality for frictionless systems when Poisson's impact law is applied. The slide-push mechanism from [27], for which Newton's impact law failed so dramatically, will be reconsidered in Sect. 9.1 to demonstrate energetic consistency under Poisson's law.

7 Energetic consistency for one frictional contact

By the famous example of Kane in [28] and [29], it is known that already one single frictional contact in a multibody system may lead to an energy increase if the collision is processed by Newton's impact law. This is not the case for Poisson's impact law, which we will

prove in this section and later demonstrate on the said example. Allowed in the proof is one geometric unilateral constraint, addressed by the lower index N for "normal," together with one of the friction elements from Sect. 4.2, addressed by the lower index T for "tangential." The proof itself is quite labor-intensive and is therefore split into five steps:

1. All relations which are relevant for the proof are put together in Sect. 7.2. Furthermore, two auxiliary velocities $\mathbf{u}_N$ and $\mathbf{u}_T$ are introduced, on which the following estimations are based.
2. In Sect. 7.3, we will shown that the generalized post-impact velocities fulfill for $\epsilon_T \geq \epsilon_N$ the inequality $\|\mathbf{u}^+\|_{\mathbf{M}} \leq \|\mathbf{u}_T\|_{\mathbf{M}}$.
3. In Sect. 7.4, we will shown that the generalized post-impact velocities fulfill for $\epsilon_T \leq \epsilon_N$ the inequality $\|\mathbf{u}^+\|_{\mathbf{M}} \leq \|\mathbf{u}_N\|_{\mathbf{M}}$, provided that a certain term A is nonpositive.
4. In Sect. 7.5, we will prove the two inequalities $\|\mathbf{u}_T\|_{\mathbf{M}} \leq \|\mathbf{u}^-\|_{\mathbf{M}}$ and $\|\mathbf{u}_N\|_{\mathbf{M}} \leq \|\mathbf{u}^-\|_{\mathbf{M}}$, and will deduce from them energetic consistency $T^+ \leq T^-$.
5. We will prove in Sect. 7.6 that the assumption $A \leq 0$ made in step 3 indeed applies for all the Coulomb-type impact elements from Sect. 4.2. The proof is based on Fenchel's inequality from convex analysis, and requires certain indicator and support functions. Alternatively, one can show the same by case distinction, but only for the one-dimensional Coulomb friction element from Sect. 4.2.1, which is performed in Sect. 7.7.

The material from Sects. 7.3, 7.4, 7.5, and 7.7 is taken from the master thesis [51], in which this proof has originally and for a first time been developed for the one-dimensional friction element. The extension to spatial situations requires Fenchel's inequality, which can be found in detail in [47], and which is briefly summarized in the following, as far as needed. The proof can*not* be extended to general situations, as we will see by the counterexample of Sect. 10.

7.1 Fenchel's inequality

Let $f(\mathbf{x})$ be a proper, lower semi-continuous convex function and $f^\star(\mathbf{x}^\star)$ its conjugate. Between f and $f^\star$ holds *Fenchel's inequality*,

$$\mathbf{x}^{\mathrm{T}}\mathbf{x}^\star \leq f(\mathbf{x}) + f^\star\big(\mathbf{x}^\star\big) \quad \forall \mathbf{x},\ \forall \mathbf{x}^\star. \tag{143}$$

If $\mathbf{x}^\star$ is in addition a subgradient of f at $\mathbf{x}$ or, in other words, an element of the subdifferential $\partial f(\mathbf{x})$, then (143) applies even as an equality,

$$\mathbf{x}^\star \in \partial f(\mathbf{x}) \quad \Leftrightarrow \quad \mathbf{x}^{\mathrm{T}}\mathbf{x}^\star = f(\mathbf{x}) + f^\star\big(\mathbf{x}^\star\big). \tag{144}$$

We choose now $f(\mathbf{x}) = I_{\mathscr{C}}(\mathbf{x})$ in (143), where $I_{\mathscr{C}}(\mathbf{x})$ is the *indicator function* of the closed convex set $\mathscr{C}$, defined by $I_{\mathscr{C}}(\mathbf{x}) = 0$ if $\mathbf{x} \in \mathscr{C}$ and $I_{\mathscr{C}}(\mathbf{x}) = +\infty$ else. After having evaluated the indicator, Fenchel's inequality becomes

$$\mathbf{x}^{\mathrm{T}}\mathbf{x}^\star \leq I^\star_{\mathscr{C}}\big(\mathbf{x}^\star\big) \quad \forall \mathbf{x} \in \mathscr{C},\ \forall \mathbf{x}^\star. \tag{145}$$

The function $I^\star_{\mathscr{C}}(\mathbf{x}^\star)$ in (145) is the conjugate of the indicator and is called the *support function* of $\mathscr{C}$. By knowing that the subdifferential of the indicator equals the normal cone, Fenchel's equality (144) can be written for the case of indicator functions and $\mathbf{x} \in \mathscr{C}$ as

$$\mathbf{x}^\star \in \partial I_{\mathscr{C}}(\mathbf{x}) = \mathscr{N}_{\mathscr{C}}(\mathbf{x}) \quad \Leftrightarrow \quad \mathbf{x}^{\mathrm{T}}\mathbf{x}^\star = I^\star_{\mathscr{C}}\big(\mathbf{x}^\star\big). \tag{146}$$

Relations (145) and (146) will be used in Sect. 7.6 to complete the energy proof for arbitrary Coulomb type sets as introduced in Sect. 4.2.

7.2 Problem setting

For the sake of clarity, the main equations for the proof are collected in this section, and equipped with the special notation for a frictional contact. We denote by Λ_N the impulsive force in the normal direction of the frictional contact, and by $\mathbf{w}_N$ the generalized force direction associated with it. The impact laws for compression (31), (32) and decompression (35), (36) for the unilateral geometric constraint are in this section written as

$$\text{compression:} \qquad \gamma_N^\circ \in \mathcal{N}_{\mathbb{R}_0^-}\big(-\Lambda_N^{(-)}\big), \tag{147}$$

$$\text{decompression:} \qquad \gamma_N^+ \in \mathcal{N}_{\mathbb{R}_0^-}(-\Delta_N), \tag{148}$$

$$\Delta_N = \Lambda_N^{(+)} - \epsilon_N \Lambda_N^{(-)}. \tag{149}$$

Depending on the dimension m of the frictional impact law, the impulsive tangential forces are denoted as $\mathbf{\Lambda}_T = (\Lambda_{1T} \dots \Lambda_{mT})^{\mathrm{T}}$, and their generalized force directions are collected in the matrix $\mathbf{W}_T = (\mathbf{w}_{1T} \dots \mathbf{w}_{mT})$. The impact laws, together with the definition of the sets $\mathscr{C}_T^{(-)}$ and $\mathscr{D}_T$ for Coulomb type sets according to (61) and (65), are written as

$$\text{compression:} \qquad \boldsymbol{\gamma}_T^\circ \in \mathcal{N}_{\mathscr{C}_T^{(-)}}\big(-\mathbf{\Lambda}_T^{(-)}\big), \tag{150}$$

$$\mathscr{C}_T^{(-)} = \Lambda_N^{(-)} \mathscr{A}_T, \tag{151}$$

$$\text{decompression:} \qquad \boldsymbol{\gamma}_T^+ \in \mathcal{N}_{\mathscr{D}_T}(-\mathbf{\Delta}_T), \tag{152}$$

$$\mathscr{D}_T = \big(\Lambda_N^{(+)} - \epsilon_T \Lambda_N^{(-)}\big)\mathscr{A}_T, \tag{153}$$

$$\mathbf{\Delta}_T = \mathbf{\Lambda}_T^{(+)} - \epsilon_T \mathbf{\Lambda}_T^{(-)}. \tag{154}$$

In the following sections, we also will frequently use the inequality

$$\Lambda_N^{(+)} \geq \epsilon_N \Lambda_N^{(-)}, \tag{155}$$

which derives from $\Delta_N \geq 0$ in (149) and (148). We further need the impact equations for compression and decompression from (40), which take for our case of one unilateral geometric constraint and one Coulomb type element the form

$$\mathbf{M}\big(\mathbf{u}^\circ - \mathbf{u}^-\big) = \mathbf{w}_N \Lambda_N^{(-)} + \mathbf{W}_T \mathbf{\Lambda}_T^{(-)}, \tag{156}$$

$$\mathbf{M}\big(\mathbf{u}^+ - \mathbf{u}^\circ\big) = \mathbf{w}_N \Lambda_N^{(+)} + \mathbf{W}_T \mathbf{\Lambda}_T^{(+)}. \tag{157}$$

In addition, two auxiliary velocities $\mathbf{u}_T$ and $\mathbf{u}_N$ will be used, which are implicitly defined as

$$\mathbf{M}\big(\mathbf{u}_T - \mathbf{u}^\circ\big) = \epsilon_T\big(\mathbf{w}_N \Lambda_N^{(-)} + \mathbf{W}_T \mathbf{\Lambda}_T^{(-)}\big), \tag{158}$$

$$\mathbf{M}\big(\mathbf{u}_N - \mathbf{u}^\circ\big) = \epsilon_N\big(\mathbf{w}_N \Lambda_N^{(-)} + \mathbf{W}_T \mathbf{\Lambda}_T^{(-)}\big). \tag{159}$$

The energy proof can be performed already within the standard restriction $|\epsilon_{N,T}| \leq 1$, such that the additional requirement $\epsilon_T \leq \epsilon_N$ from Table 1 is not needed here.

7.3 Show $\|\mathbf{u}^+\|_{\mathbf{M}} \leq \|\mathbf{u}_T\|_{\mathbf{M}}$ for $\epsilon_T \geq \epsilon_N$

In order to show $\|\mathbf{u}^+\|_{\mathbf{M}} \leq \|\mathbf{u}_T\|_{\mathbf{M}}$ for $\epsilon_T \geq \epsilon_N$, some basic manipulations on the double post-impact kinetic energy $\mathbf{u}^{+\mathrm{T}}\mathbf{M}\mathbf{u}^+$ are required to bring it into a suitable form,

$$
\begin{aligned}
\mathbf{u}^{+\mathrm{T}}\mathbf{M}\mathbf{u}^{+} &= \mathbf{u}^{+\mathrm{T}}\mathbf{M}\mathbf{u}_T + \mathbf{u}^{+\mathrm{T}}\mathbf{M}\big(\mathbf{u}^{+} - \mathbf{u}^{\circ}\big) + \mathbf{u}^{+\mathrm{T}}\mathbf{M}\big(\mathbf{u}^{\circ} - \mathbf{u}_T\big) \\
&\overset{(158)}{=} \mathbf{u}^{+\mathrm{T}}\mathbf{M}\mathbf{u}_T + \mathbf{u}^{+\mathrm{T}}\mathbf{M}\big(\mathbf{u}^{+} - \mathbf{u}^{\circ}\big) - \mathbf{u}^{+\mathrm{T}}\big(\epsilon_T \mathbf{w}_N \Lambda_N^{(-)} + \epsilon_T \mathbf{W}_T \boldsymbol{\Lambda}_T^{(-)}\big) \\
&\overset{(157)}{=} \mathbf{u}^{+\mathrm{T}}\mathbf{M}\mathbf{u}_T + \mathbf{u}^{+\mathrm{T}}\big(\mathbf{w}_N \Lambda_N^{(+)} + \mathbf{W}_T \boldsymbol{\Lambda}_T^{(+)} - \epsilon_T \mathbf{w}_N \Lambda_N^{(-)} - \epsilon_T \mathbf{W}_T \boldsymbol{\Lambda}_T^{(-)}\big) \\
&\overset{(154)}{=} \mathbf{u}^{+\mathrm{T}}\mathbf{M}\mathbf{u}_T + \mathbf{u}^{+\mathrm{T}}\big(\mathbf{w}_N \Lambda_N^{(+)} - \epsilon_T \mathbf{w}_N \Lambda_N^{(-)} + \mathbf{W}_T \boldsymbol{\Delta}_T\big) \\
&\overset{(149)}{=} \mathbf{u}^{+\mathrm{T}}\mathbf{M}\mathbf{u}_T + \mathbf{u}^{+\mathrm{T}}\big((\epsilon_N - \epsilon_T)\mathbf{w}_N \Lambda_N^{(-)} + \mathbf{w}_N \Delta_N + \mathbf{W}_T \boldsymbol{\Delta}_T\big) \\
&\overset{(34)}{=} \mathbf{u}^{+\mathrm{T}}\mathbf{M}\mathbf{u}_T + (\epsilon_N - \epsilon_T)\gamma_N^{+} \Lambda_N^{(-)} + \gamma_N^{+} \Delta_N + \boldsymbol{\gamma}_T^{+\mathrm{T}} \boldsymbol{\Delta}_T .
\end{aligned} \tag{160}
$$

For the right three summands in the last line of (160), we have $(\epsilon_N - \epsilon_T) \leq 0$ by assumption, $\gamma_N^{+} \geq 0$ and $\Lambda_N^{(-)} \geq 0$ by Fig. 3, $\gamma_N^{+} \Delta_N = 0$ by (50), and $\boldsymbol{\gamma}_T^{+\mathrm{T}} \boldsymbol{\Delta}_T \leq 0$ by the standard property (38). With all these summands less than or equal to zero, we conclude that

$$
\mathbf{u}^{+\mathrm{T}}\mathbf{M}\mathbf{u}^{+} \leq \mathbf{u}^{+\mathrm{T}}\mathbf{M}\mathbf{u}_T \leq \sqrt{\mathbf{u}^{+\mathrm{T}}\mathbf{M}\mathbf{u}^{+}} \cdot \sqrt{\mathbf{u}_T^{\mathrm{T}}\mathbf{M}\mathbf{u}_T}, \tag{161}
$$

where the second term has in addition been estimated by the Cauchy–Schwartz inequality. We finally obtain from (161) that

$$
\mathbf{u}^{+\mathrm{T}}\mathbf{M}\mathbf{u}^{+} \leq \mathbf{u}_T^{\mathrm{T}}\mathbf{M}\mathbf{u}_T \quad \text{for } \epsilon_T \geq \epsilon_N, \tag{162}
$$

which is the result that has to be proven.

7.4 Show $\|\mathbf{u}^{+}\|_{\mathbf{M}} \leq \|\mathbf{u}_N\|_{\mathbf{M}}$ for $\epsilon_T \leq \epsilon_N$

Basically the same operations are needed as in (160) to bring $\mathbf{u}^{+\mathrm{T}}\mathbf{M}\mathbf{u}^{+}$ for $\epsilon_T \leq \epsilon_N$ into a form suitable for further analysis. The only difference is that (159) is used instead of (158),

$$
\begin{aligned}
\mathbf{u}^{+\mathrm{T}}\mathbf{M}\mathbf{u}^{+} &= \mathbf{u}^{+\mathrm{T}}\mathbf{M}\mathbf{u}_N + \mathbf{u}^{+\mathrm{T}}\mathbf{M}\big(\mathbf{u}^{+} - \mathbf{u}^{\circ}\big) + \mathbf{u}^{+\mathrm{T}}\mathbf{M}\big(\mathbf{u}^{\circ} - \mathbf{u}_N\big) \\
&\overset{(159)}{=} \mathbf{u}^{+\mathrm{T}}\mathbf{M}\mathbf{u}_N + \mathbf{u}^{+\mathrm{T}}\mathbf{M}\big(\mathbf{u}^{+} - \mathbf{u}^{\circ}\big) - \mathbf{u}^{+\mathrm{T}}\big(\epsilon_N \mathbf{w}_N \Lambda_N^{(-)} + \epsilon_N \mathbf{W}_T \boldsymbol{\Lambda}_T^{(-)}\big) \\
&\overset{(157)}{=} \mathbf{u}^{+\mathrm{T}}\mathbf{M}\mathbf{u}_N + \mathbf{u}^{+\mathrm{T}}\big(\mathbf{w}_N \Lambda_N^{(+)} + \mathbf{W}_T \boldsymbol{\Lambda}_T^{(+)} - \epsilon_N \mathbf{w}_N \Lambda_N^{(-)} - \epsilon_N \mathbf{W}_T \boldsymbol{\Lambda}_T^{(-)}\big) \\
&\overset{(149)}{=} \mathbf{u}^{+\mathrm{T}}\mathbf{M}\mathbf{u}_N + \mathbf{u}^{+\mathrm{T}}\big(\mathbf{w}_N \Delta_N + \mathbf{W}_T \boldsymbol{\Lambda}_T^{(+)} - \epsilon_N \mathbf{W}_T \boldsymbol{\Lambda}_T^{(-)}\big) \\
&\overset{(154)}{=} \mathbf{u}^{+\mathrm{T}}\mathbf{M}\mathbf{u}_N + \mathbf{u}^{+\mathrm{T}}\big(\mathbf{w}_N \Delta_N + \mathbf{W}_T \boldsymbol{\Delta}_T - (\epsilon_N - \epsilon_T)\mathbf{W}_T \boldsymbol{\Lambda}_T^{(-)}\big) \\
&\overset{(34)}{=} \mathbf{u}^{+\mathrm{T}}\mathbf{M}\mathbf{u}_N + \gamma_N^{+} \Delta_N + \boldsymbol{\gamma}_T^{+\mathrm{T}} \boldsymbol{\Delta}_T - (\epsilon_N - \epsilon_T)\boldsymbol{\gamma}_T^{+\mathrm{T}} \boldsymbol{\Lambda}_T^{(-)} .
\end{aligned} \tag{163}
$$

Again, the right three summands in the last line are checked for nonpositiveness. As in (160), we have $\gamma_N^{+} \Delta_N = 0$. For the remaining terms,

$$
A := \boldsymbol{\gamma}_T^{+\mathrm{T}} \boldsymbol{\Delta}_T - (\epsilon_N - \epsilon_T)\boldsymbol{\gamma}_T^{+\mathrm{T}} \boldsymbol{\Lambda}_T^{(-)} \quad \text{with } \epsilon_T \leq \epsilon_N, \tag{164}
$$

however, we cannot immediately deduce that they are less than or equal to zero. We will leave this to Sect. 7.6, in which we will show that $A \leq 0$ indeed holds true. By anticipating this result, we now conclude that

$$
\mathbf{u}^{+\mathrm{T}}\mathbf{M}\mathbf{u}^{+} \leq \mathbf{u}^{+\mathrm{T}}\mathbf{M}\mathbf{u}_N \leq \sqrt{\mathbf{u}^{+\mathrm{T}}\mathbf{M}\mathbf{u}^{+}} \cdot \sqrt{\mathbf{u}_N^{\mathrm{T}}\mathbf{M}\mathbf{u}_N}, \tag{165}
$$

where we have again used the Cauchy–Schwartz inequality to relate the left to the right expression. We finally obtain

$$\mathbf{u}^{+\mathrm{T}}\mathbf{M}\mathbf{u}^{+} \le \mathbf{u}_N^{\mathrm{T}}\mathbf{M}\mathbf{u}_N \quad \text{for } \epsilon_T \le \epsilon_N, \tag{166}$$

which completes this part of the proof.

7.5 Show $\|\mathbf{u}_N\|_{\mathbf{M}} \le \|\mathbf{u}^-\|_{\mathbf{M}}$ and $\|\mathbf{u}_T\|_{\mathbf{M}} \le \|\mathbf{u}^-\|_{\mathbf{M}}$

We first show that $\|\mathbf{u}_N\|_{\mathbf{M}} \le \|\mathbf{u}^-\|_{\mathbf{M}}$. By performing some basic operations on the quadratic difference of the two terms involved, we obtain

$$\begin{aligned}
\mathbf{u}_N^{\mathrm{T}}\mathbf{M}\mathbf{u}_N - \mathbf{u}^{-\mathrm{T}}\mathbf{M}\mathbf{u}^- &= \big(\mathbf{u}_N + \mathbf{u}^-\big)^{\mathrm{T}}\mathbf{M}\big(\mathbf{u}_N - \mathbf{u}^-\big) \\
&= \big(\mathbf{u}_N + \mathbf{u}^-\big)^{\mathrm{T}}\big(\mathbf{M}\big(\mathbf{u}_N - \mathbf{u}^\circ\big) + \mathbf{M}\big(\mathbf{u}^\circ - \mathbf{u}^-\big)\big) \\
&\overset{(156)}{=} \big(\mathbf{u}_N + \mathbf{u}^-\big)^{\mathrm{T}}\big(\mathbf{M}\big(\mathbf{u}_N - \mathbf{u}^\circ\big) + \big(\mathbf{w}_N \Lambda_N^{(-)} + \mathbf{W}_T \mathbf{\Lambda}_T^{(-)}\big)\big) \\
&\overset{(159)}{=} \big(\mathbf{u}_N + \mathbf{u}^-\big)^{\mathrm{T}}\big((1+\epsilon_N)\big(\mathbf{w}_N \Lambda_N^{(-)} + \mathbf{W}_T \mathbf{\Lambda}_T^{(-)}\big)\big) \\
&= (1+\epsilon_N)\big(\mathbf{u}_N + \mathbf{u}^-\big)^{\mathrm{T}}\mathbf{W}\mathbf{\Lambda}^{(-)},
\end{aligned} \tag{167}$$

where we have used in the last line the abbreviations

$$\mathbf{W} := \begin{pmatrix}\mathbf{w}_N & \mathbf{W}_T\end{pmatrix}, \qquad \mathbf{\Lambda}^{(-)} := \begin{pmatrix}\Lambda_N^{(-)} \\ \mathbf{\Lambda}_T^{(-)}\end{pmatrix}. \tag{168}$$

We eliminate now the term $(\mathbf{u}_N + \mathbf{u}^-)$ from the last line of (167). For this, we take $\mathbf{u}_N$ from (159) and $\mathbf{u}^-$ from (156), both equipped with the abbreviation (168),

$$\mathbf{u}_N = \mathbf{u}^\circ + \epsilon_N \mathbf{M}^{-1}\mathbf{W}\mathbf{\Lambda}^{(-)}, \qquad \mathbf{u}^- = \mathbf{u}^\circ - \mathbf{M}^{-1}\mathbf{W}\mathbf{\Lambda}^{(-)} \tag{169}$$

and build their sum as

$$\mathbf{u}_N + \mathbf{u}^- = 2\mathbf{u}^\circ - (1-\epsilon_N)\mathbf{M}^{-1}\mathbf{W}\mathbf{\Lambda}^{(-)}. \tag{170}$$

By substituting (170) into the last line of (167) and again performing some basic manipulations on the resulting term, we get

$$\begin{aligned}
\mathbf{u}_N^{\mathrm{T}}\mathbf{M}\mathbf{u}_N - \mathbf{u}^{-\mathrm{T}}\mathbf{M}\mathbf{u}^- &= (1+\epsilon_N)\big(2\mathbf{u}^\circ - (1-\epsilon_N)\mathbf{M}^{-1}\mathbf{W}\mathbf{\Lambda}^{(-)}\big)^{\mathrm{T}}\mathbf{W}\mathbf{\Lambda}^{(-)} \\
&= 2(1+\epsilon_N)\mathbf{u}^{\circ\mathrm{T}}\mathbf{W}\mathbf{\Lambda}^{(-)} - \big(1-\epsilon_N^2\big)\mathbf{\Lambda}^{(-)\mathrm{T}}\mathbf{W}^{\mathrm{T}}\mathbf{M}^{-1}\mathbf{W}\mathbf{\Lambda}^{(-)} \\
&\overset{(44)}{=} 2(1+\epsilon_N)\mathbf{u}^{\circ\mathrm{T}}\mathbf{W}\mathbf{\Lambda}^{(-)} - \big(1-\epsilon_N^2\big)\mathbf{\Lambda}^{(-)\mathrm{T}}\mathbf{G}\mathbf{\Lambda}^{(-)} \\
&\overset{(168)}{=} 2(1+\epsilon_N)\big(\mathbf{u}^{\circ\mathrm{T}}\mathbf{w}_N \Lambda_N^{(-)} + \mathbf{u}^{\circ\mathrm{T}}\mathbf{W}_T \mathbf{\Lambda}_T^{(-)}\big) - \big(1-\epsilon_N^2\big)\mathbf{\Lambda}^{(-)\mathrm{T}}\mathbf{G}\mathbf{\Lambda}^{(-)} \\
&\overset{(34)}{=} 2(1+\epsilon_N)\big(\gamma_N^\circ \Lambda_N^{(-)} + \boldsymbol{\gamma}_T^{\circ\,\mathrm{T}}\mathbf{\Lambda}_T^{(-)}\big) - \big(1-\epsilon_N^2\big)\mathbf{\Lambda}^{(-)\mathrm{T}}\mathbf{G}\mathbf{\Lambda}^{(-)}.
\end{aligned} \tag{171}$$

For the summands in the last line of (171), we have $\gamma_N^\circ \Lambda_N^{(-)} = 0$ by the left diagram in Fig. 3, $\boldsymbol{\gamma}_T^{\circ\,\mathrm{T}}\mathbf{\Lambda}_T^{(-)} \le 0$ by the standard property (38) for compression, where $\boldsymbol{\gamma}_T^\circ = \boldsymbol{\xi}_T^\circ$, and

$\boldsymbol{\Lambda}^{(-)\mathrm{T}}\mathbf{G}\boldsymbol{\Lambda}^{(-)} \geq 0$ because $\mathbf{G}$ is positive semidefinite. With $|\epsilon_N| \leq 1$, the whole right-hand side of (171) is less than or equal to zero, and we can deduce that

$$\mathbf{u}_N^{\mathrm{T}}\mathbf{M}\mathbf{u}_N \leq \mathbf{u}^{-\mathrm{T}}\mathbf{M}\mathbf{u}^{-}. \tag{172}$$

In order to show the second assertion,

$$\mathbf{u}_T^{\mathrm{T}}\mathbf{M}\mathbf{u}_T \leq \mathbf{u}^{-\mathrm{T}}\mathbf{M}\mathbf{u}^{-}, \tag{173}$$

precisely the same steps as in (167)–(171) have to be performed, but with $(\mathbf{u}_T, \epsilon_T)$ instead of $(\mathbf{u}_N, \epsilon_N)$, and with (158) in (167) instead of (159).

Finally, we combine the two inequalities (162) and (173), and in the same way the two inequalities (166) and (172), to obtain

$$\begin{aligned} \mathbf{u}^{+\mathrm{T}}\mathbf{M}\mathbf{u}^{+} &\leq \mathbf{u}_T^{\mathrm{T}}\mathbf{M}\mathbf{u}_T \leq \mathbf{u}^{-\mathrm{T}}\mathbf{M}\mathbf{u}^{-} \quad \text{for } \epsilon_T \geq \epsilon_N, \\ \mathbf{u}^{+\mathrm{T}}\mathbf{M}\mathbf{u}^{+} &\leq \mathbf{u}_N^{\mathrm{T}}\mathbf{M}\mathbf{u}_N \leq \mathbf{u}^{-\mathrm{T}}\mathbf{M}\mathbf{u}^{-} \quad \text{for } \epsilon_T \leq \epsilon_N. \end{aligned} \tag{174}$$

By the inequalities between the utmost left and right terms in (174), we see that energetic consistency applies,

$$T^{+} \leq T^{-}, \tag{175}$$

independent of whether $\epsilon_T \geq \epsilon_N$ or the reverse. We therefore have shown that one frictional contact within an arbitrary multibody system is always energetically consistent under the standard restriction $|\epsilon_{N,T}| \leq 1$ when processed with Poisson's inequality impact law.

7.6 Prove that $A \leq 0$ for general Coulomb type sets

To complete the proof, it remains to show that A in (164) is indeed less than or equal to zero. The term A consists of a difference,

$$A = \boldsymbol{\Delta}_T^{\mathrm{T}}\boldsymbol{\gamma}_T^{+} - (\epsilon_N - \epsilon_T)\boldsymbol{\Lambda}_T^{(-)\mathrm{T}}\boldsymbol{\gamma}_T^{+} \quad \text{with } \epsilon_T \leq \epsilon_N, \tag{176}$$

formed by two duality pairings with one of the vectors in each pairing being $\boldsymbol{\gamma}_T^{+}$. The other vectors are $-\boldsymbol{\Delta}_T$ and $-(\epsilon_N - \epsilon_T)\boldsymbol{\Lambda}_T^{(-)}$, respectively. By (152), we have implicitly that

$$-\boldsymbol{\Delta}_T \in \mathscr{D}_T. \tag{177}$$

Furthermore, (152) relates $\boldsymbol{\gamma}_T^{+}$ and $-\boldsymbol{\Delta}_T$ by a normal cone inclusion, which may equivalently be stated by the associated support function as

$$\boldsymbol{\gamma}_T^{+} \in \mathscr{N}_{\mathscr{D}_T}(-\boldsymbol{\Delta}_T) = \partial I_{\mathscr{D}_T}(-\boldsymbol{\Delta}_T) \quad \Leftrightarrow \quad -\boldsymbol{\Delta}_T^{\mathrm{T}}\boldsymbol{\gamma}_T^{+} = I_{\mathscr{D}_T}^{\star}\big(\boldsymbol{\gamma}_T^{+}\big), \tag{178}$$

thanks to Fenchel's equality (146). If we can now show that

$$-(\epsilon_N - \epsilon_T)\boldsymbol{\Lambda}_T^{(-)} \in \mathscr{D}_T, \tag{179}$$

we may afterward apply Fenchel's inequality (145) on the pairing $-(\epsilon_N - \epsilon_T)\boldsymbol{\Lambda}_T^{(-)\mathrm{T}}\boldsymbol{\gamma}_T^{+}$, relate the resulting expression to (178), and deduce from them $A \leq 0$. In order to show (179), we start with $-\boldsymbol{\Lambda}_T^{(-)} \in \mathscr{C}_T^{(-)}$ from (150), and apply (151),

$$-\boldsymbol{\Lambda}_T^{(-)} \in \mathscr{C}_T^{(-)} \overset{(151)}{=} \Lambda_N^{(-)}\mathscr{A}_T. \tag{180}$$

Both sides of (180) are now multiplied with the nonnegative number $(\epsilon_N - \epsilon_T)$, and further processed with the inequality (155) and the definition of $\mathscr{D}_T$ in (153),

$$\begin{aligned} -(\epsilon_N - \epsilon_T)\mathbf{\Lambda}_T^{(-)} &\in (\epsilon_N - \epsilon_T)\Lambda_N^{(-)}\mathscr{A}_T \\ &= \big(\epsilon_N \Lambda_N^{(-)} - \epsilon_T \Lambda_N^{(-)}\big)\mathscr{A}_T \\ &\overset{(155)}{\subseteq} \big(\Lambda_N^{(+)} - \epsilon_T \Lambda_N^{(-)}\big)\mathscr{A}_T \\ &\overset{(153)}{=} \mathscr{D}_T, \end{aligned} \tag{181}$$

which already yields the desired result (179). As a consequence, Fenchel's inequality (145) applies in the form

$$-(\epsilon_N - \epsilon_T)\mathbf{\Lambda}_T^{(-)^{\mathrm{T}}}\boldsymbol{\gamma}_T^+ \le I^\star_{\mathscr{D}_T}\big(\boldsymbol{\gamma}_T^+\big). \tag{182}$$

We take now Eq. (182) and subtract from it the right equation in (178) to obtain

$$-(\epsilon_N - \epsilon_T)\mathbf{\Lambda}_T^{(-)^{\mathrm{T}}}\boldsymbol{\gamma}_T^+ + \mathbf{\Delta}_T^{\mathrm{T}}\boldsymbol{\gamma}_T^+ \le I^\star_{\mathscr{D}_T}\big(\boldsymbol{\gamma}_T^+\big) - I^\star_{\mathscr{D}_T}\big(\boldsymbol{\gamma}_T^+\big) = 0. \tag{183}$$

By comparing this expression with (176), we see that

$$A \le 0, \tag{184}$$

which is the desired result that we were going to prove.

7.7 Prove that $A \le 0$ for one-dimensional friction

The kinematic step constraint of Coulomb type from Sect. 4.2.1 is the simplest special case of the frictional impact elements presented in Sect. 4.2. As a one-dimensional impact element, the inequality (184) can easily be derived by case distinction as done in [51], and the more involved approach via the support functions as necessary for the two-dimensional friction laws can be avoided: According to (73), the set $\mathscr{D}_T$ needed in the impact law is

$$\mathscr{D}_T = \mu\big(\Lambda_N^{(+)} - \epsilon_T \Lambda_N^{(-)}\big)[-1, 1], \tag{185}$$

and A from (176) reduces for this case to

$$A = \Delta_T \gamma_T^+ - (\epsilon_N - \epsilon_T)\Lambda_T^{(-)}\gamma_T^+. \tag{186}$$

In order to prove now $A \le 0$, we start with the case $\gamma_T^+ = 0$, which immediately yields

$$\gamma_T^+ = 0 \quad \Rightarrow \quad A = 0. \tag{187}$$

For $\gamma_T^+ \neq 0$, we see from (75) that Δ_T is either one of the two boundary points of $\mathscr{D}_T$,

$$|\Delta_T| = \mu\big(\Lambda_N^{(+)} - \epsilon_T \Lambda_N^{(-)}\big), \tag{188}$$

which leads with $\Lambda_N^{(+)} \ge \epsilon_N \Lambda_N^{(-)}$ from (155) to the inequality

$$|\Delta_T| \ge \mu\big(\epsilon_N \Lambda_N^{(-)} - \epsilon_T \Lambda_N^{(-)}\big). \tag{189}$$

Furthermore, we see from the left diagram in Fig. 5 that $\mu\Lambda_N^{(-)} \geq |\Lambda_T^{(-)}|$, such that (189) can now be estimated as

$$|\Delta_T| \geq (\epsilon_N - \epsilon_T)\big|\Lambda_T^{(-)}\big|. \tag{190}$$

In a next step, we multiply both sides of (190) with $|\gamma_T^+|$,

$$|\Delta_T|\big|\gamma_T^+\big| \geq (\epsilon_N - \epsilon_T)\big|\Lambda_T^{(-)}\big|\big|\gamma_T^+\big|, \tag{191}$$

and take into account that $|a||b| = |ab|$,

$$\big|\Delta_T\gamma_T^+\big| \geq (\epsilon_N - \epsilon_T)\big|\Lambda_T^{(-)}\gamma_T^+\big|. \tag{192}$$

We further see by (75) that $\Delta_T\gamma_T^+ \leq 0$. As a consequence, $|\Delta_T\gamma_T^+| = -\Delta_T\gamma_T^+$, which turns (192) into

$$-\Delta_T\gamma_T^+ \geq (\epsilon_N - \epsilon_T)\big|\Lambda_T^{(-)}\gamma_T^+\big|. \tag{193}$$

We eliminate now $\Delta_T\gamma_T^+$ with the help of (186) to get

$$-A - (\epsilon_N - \epsilon_T)\Lambda_T^{(-)}\gamma_T^+ \geq (\epsilon_N - \epsilon_T)\big|\Lambda_T^{(-)}\gamma_T^+\big| \tag{194}$$

or, after having brought everything except of A to the right-hand side,

$$A \leq -(\epsilon_N - \epsilon_T)\big(\Lambda_T^{(-)}\gamma_T^+ + \big|\Lambda_T^{(-)}\gamma_T^+\big|\big). \tag{195}$$

The last term on the right is of the form $x + |x| \geq 0$. We further have by (166) that $\epsilon_T \leq \epsilon_N$, hence $A \leq 0$. By summarizing the steps (189)–(100), we have therefore shown that

$$\gamma_T^+ \neq 0 \quad \Rightarrow \quad A \leq 0, \tag{196}$$

which, together with (188), completes the proof.

8 On the equivalence of Newton's and Poisson's impact law

For coupled problems with more than one impact element, Newton's and Poisson's impact law may behave essentially different. There is, however, at least one case for which both impact laws can be related to each other, namely if their impact coefficients are all the same. For systems with only geometric unilateral constraints, the equivalence of Newton's and Poisson's impact law has already been shown in [24] by a geometrically inspired proof. In the following, we generalize this idea to arbitrary impact elements as presented in Sect. 4. Let therefore be

$$\epsilon := \epsilon_1 = \cdots = \epsilon_n = \varepsilon_1 = \cdots = \varepsilon_n, \tag{197}$$

where ϵ_i denotes the Poisson impact coefficients in (35), and ε_i the Newtonian impact coefficients in (14). For the Newtonian impact, we need (14) and (15) together with the impact equation in local coordinates,

$$\boldsymbol{\gamma}_N^+ - \boldsymbol{\gamma}^- = \mathbf{G}\boldsymbol{\Lambda}, \qquad \boldsymbol{\xi} = \boldsymbol{\gamma}_N^+ + \epsilon\boldsymbol{\gamma}^-, \qquad \boldsymbol{\xi}_i \in \mathscr{N}_{\mathscr{C}_i}(-\boldsymbol{\Lambda}_i). \tag{198}$$

where the left equation in (198) results from (12) together with (13) as shown in [27]. Furthermore, we have equipped the Newtonian post-impact relative velocities $\boldsymbol{\gamma}_N^+$ with a lower

index N to distinguish them from the Poisson post-impact relative velocities, which will henceforth be denoted by $\boldsymbol{\gamma}_P^+$. For the Poisson impact, we need (43) and (42), as well as the impact laws (32) and (36),

$$\boldsymbol{\gamma}^\circ - \boldsymbol{\gamma}^- = \mathbf{G}\boldsymbol{\Lambda}^{(-)}, \qquad \boldsymbol{\xi}^\circ = \boldsymbol{\gamma}^\circ, \qquad \boldsymbol{\xi}_i^\circ \in \mathscr{N}_{\mathscr{C}_i^{(-)}}\big(-\boldsymbol{\Lambda}_i^{(-)}\big), \tag{199}$$

$$\boldsymbol{\gamma}_P^+ - \boldsymbol{\gamma}^\circ = \mathbf{G}\boldsymbol{\Lambda}^{(+)}, \qquad \boldsymbol{\Lambda} = \boldsymbol{\Lambda}^{(+)} - \epsilon\boldsymbol{\Lambda}^{(-)}, \qquad \boldsymbol{\gamma}_{Pi}^+ \in \mathscr{N}_{\mathscr{D}_i}(-\boldsymbol{\Delta}_i). \tag{200}$$

Note that we already have used (197) to express in (198) and (200) the various impact coefficients by their common one, ϵ. In the following, we derive some conditions under which (198) is equivalent to (199) and (200) in the sense that both impact problems terminate with the same post-impact relative velocities $\boldsymbol{\gamma}_N^+ = \boldsymbol{\gamma}_P^+$ under the same overall impulsive forces $\boldsymbol{\Lambda} = \boldsymbol{\Lambda}^{(-)} + \boldsymbol{\Lambda}^{(+)}$. The proof is done in accordance with the energetic restrictions of the Newtonian impact coefficients $-1 < \epsilon \leq 1$, which have been derived in [27].

8.1 Compression

In this section, we relate Poisson's compression phase (199) to the Newtonian impact (198). We assume that all magnitudes in (198) are known and set

$$\boldsymbol{\Lambda}^{(-)} := \frac{1}{1+\epsilon}\boldsymbol{\Lambda} \quad \text{and} \quad \boldsymbol{\xi}^\circ := \frac{1}{1+\epsilon}\boldsymbol{\xi} \tag{201}$$

for the terms in Poisson compression phase (199). We show now that $(\boldsymbol{\Lambda}^{(-)}, \boldsymbol{\xi}^\circ)$ according to (201) is a indeed solution of (199), if (198) holds.

We start by verifying the first two equations in (199). To do this, the relative velocity $\boldsymbol{\gamma}_N^+$ is eliminated from the first equation in (198) with the help of the second equation, which gives

$$\boldsymbol{\xi} - (1+\epsilon)\boldsymbol{\gamma}^- = \mathbf{G}\boldsymbol{\Lambda}. \tag{202}$$

We divide now both sides of (202) by $(1+\epsilon)$,

$$\frac{1}{1+\epsilon}\boldsymbol{\xi} - \boldsymbol{\gamma}^- = \frac{1}{1+\epsilon}\mathbf{G}\boldsymbol{\Lambda}, \tag{203}$$

and rewrite the resulting expression together with (201) as

$$\boldsymbol{\xi}^\circ - \boldsymbol{\gamma}^- = \mathbf{G}\boldsymbol{\Lambda}^{(-)}, \tag{204}$$

which already proves the first two equations in (199).

It remains to show that Poisson's impact law for compression, i.e., the inclusion to the right of (199), follows from Newton's impact law in (198) if (201) applies. The object $\mathscr{N}_{\mathscr{C}_i}(-\boldsymbol{\Lambda}_i)$ in Newton's impact law is the normal cone to $\mathscr{C}_i$ at $-\boldsymbol{\Lambda}_i$, i.e., a cone $\mathscr{K}$, fulfilling $\alpha\mathbf{x} \in \mathscr{K}$ whenever $\mathbf{x} \in \mathscr{K}$ and $\alpha > 0$ by definition. We therefore may multiply $\boldsymbol{\xi}_i$ in the normal cone inclusion (198) by any positive number and state Newton's impact law equivalently as

$$\frac{1}{1+\epsilon}\boldsymbol{\xi}_i \in \mathscr{N}_{\mathscr{C}_i}(-\boldsymbol{\Lambda}_i). \tag{205}$$

In the next step, we use that the normal cone remains invariant under positive scaling $\alpha > 0$ of the associated convex set and its elements, $\mathscr{N}_{\mathscr{C}}(\mathbf{x}) = \mathscr{N}_{\alpha\mathscr{C}}(\alpha\mathbf{x})$, which immediately

follows from its definition. We scale now both the set $\mathscr{C}_i$ and the argument $-\mathbf{\Lambda}_i$ in (205) by again the same positive number and obtain

$$\frac{1}{1+\epsilon}\boldsymbol{\xi}_i \in \mathscr{N}_{\frac{1}{1+\epsilon}\mathscr{C}_i}\left(-\frac{1}{1+\epsilon}\mathbf{\Lambda}_i\right). \tag{206}$$

By using (201), this inclusion can now be written as

$$\boldsymbol{\xi}_i^{\circ} \in \mathscr{N}_{\frac{1}{1+\epsilon}\mathscr{C}_i}\left(-\mathbf{\Lambda}_i^{(-)}\right), \tag{207}$$

which is Poisson's impact law for compression in (199), *provided* that $\frac{1}{1+\epsilon}\mathscr{C}_i \equiv \mathscr{C}_i^{(-)}$. The latter condition has to be shown for the two types of impact elements from Sect. 4. These are the closed convex cones from Sect. 4.1, for which it immediately applies by the first paragraph of the said section, and the Coulomb type sets from Sect. 4.2. For them, we have by (61) that $\mathscr{C}_i^{(-)} = \Lambda_k^{(-)}\mathscr{A}_i$, where $\Lambda_k^{(-)} = \frac{1}{1+\epsilon}\Lambda_k$ by (201). As a consequence, we obtain that $\mathscr{C}_i^{(-)} = \frac{1}{1+\epsilon}\Lambda_k\mathscr{A}_i$, which gives together with $\Lambda_k\mathscr{A}_i = \mathscr{C}_i$ from (58) the desired equality.

By summarizing the result of the above proof, we have shown that $(\boldsymbol{\xi}^{\circ}, \mathbf{\Lambda}^{(-)}) = \frac{1}{1+\epsilon}(\boldsymbol{\xi}, \mathbf{\Lambda})$ solves Poisson's phase of compression (199), if $(\boldsymbol{\xi}, \mathbf{\Lambda})$ is a solution of Newton's impact problem (198) and vice versa, since all steps in the proof can be reversed.

8.2 Decompression

For the second part of the proof, we assume that both the Newtonian impact problem (198) and Poisson's compression phase (199) are satisfied under the relations (201). For the decompression impulsive force, we set

$$\mathbf{\Lambda}^{(+)} := \frac{\epsilon}{1+\epsilon}\mathbf{\Lambda}, \tag{208}$$

and derive now the conditions under which it solves the Poisson decompression phase (200).

We first determine the value of $\boldsymbol{\gamma}_P^+$ in the left equation of (200). For this, we add the left equations in (199) and (200), substitute $\mathbf{\Lambda}^{(-)}$ and $\mathbf{\Lambda}^{(+)}$ from (201) and (208), and compare the result with the left equation in (198),

$$\boldsymbol{\gamma}_P^+ - \boldsymbol{\gamma}^- = \mathbf{G}\left(\mathbf{\Lambda}^{(-)} + \mathbf{\Lambda}^{(+)}\right) = \mathbf{G}\left(\frac{1}{1+\epsilon}\mathbf{\Lambda} + \frac{\epsilon}{1+\epsilon}\mathbf{\Lambda}\right) = \mathbf{G}\mathbf{\Lambda} = \boldsymbol{\gamma}_N^+ - \boldsymbol{\gamma}^-. \tag{209}$$

We obtain

$$\boldsymbol{\gamma}_P^+ = \boldsymbol{\gamma}_N^+ =: \boldsymbol{\gamma}^+, \tag{210}$$

i.e., that the Newtonian and Poisson post-impact relative velocities are equal to each other, which we denote in the sequel by $\boldsymbol{\gamma}^+$.

In a final step, we have to make sure that the decompression impulsive force (208) that was shown to provide equal post-impact velocities (210) does not conflict with Poisson's impact law for decompression in the right expression of (200). For this, we calculate $\mathbf{\Delta}$ from the second equation in (200) as

$$\mathbf{\Delta} = \frac{\epsilon}{1+\epsilon}\mathbf{\Lambda} - \frac{\epsilon}{1+\epsilon}\mathbf{\Lambda} = 0, \tag{211}$$

where we have again used (201) and (208). With the help of the second equation in (198) and (211), Newton's and Poisson's impact laws from the right expression of (198) and (200) may now be written as

$$\boldsymbol{\gamma}_i^+ \in \mathscr{N}_{\mathscr{C}_i}(-\boldsymbol{\Lambda}_i) - \epsilon\boldsymbol{\gamma}_i^-, \qquad \boldsymbol{\gamma}_i^+ \in \mathscr{N}_{\mathscr{D}_i}(0). \tag{212}$$

The assumed decompression impulse $\boldsymbol{\Lambda}^{(+)}$ from (208) is compatible with Poisson's impact law if the resulting set $\mathscr{N}_{\mathscr{D}_i}(0)$ does not further restrict the set $\mathscr{N}_{\mathscr{C}_i}(-\boldsymbol{\Lambda}_i) - \epsilon\boldsymbol{\gamma}_i^-$ from Newton's impact law, to which $\boldsymbol{\gamma}_i^+$ belongs. We therefore have to investigate the conditions under which

$$\mathscr{N}_{\mathscr{C}_i}(-\boldsymbol{\Lambda}_i) - \epsilon\boldsymbol{\gamma}_i^- \subseteq \mathscr{N}_{\mathscr{D}_i}(0) \tag{213}$$

holds true for every type of impact elements, which we are going to check now.

For the *unilateral constraints*, we have by (48) and (49) that $\mathscr{C}_i = \mathscr{D}_i = \mathbb{R}_0^-$. With $\mathscr{N}_{\mathbb{R}_0^-}(0) = \mathbb{R}_0^+$, inclusion (213) takes the form $\mathscr{N}_{\mathbb{R}_0^-}(-\Lambda_i) - \epsilon\gamma_i^- \subseteq \mathbb{R}_0^+$. We further have that $\mathscr{N}_{\mathbb{R}_0^-}(-\Lambda_i) \subseteq \mathbb{R}_0^+$ for any $\Lambda_i \geq 0$, with $\mathscr{N}_{\mathbb{R}_0^-}(-\Lambda_i) = \mathbb{R}_0^+$ as the most restrictive case for the above inclusion. From $\mathbb{R}_0^+ - \epsilon\gamma_i^- \subseteq \mathbb{R}_0^+$, we deduce that

$$\epsilon\gamma_i^- \leq 0 \tag{214}$$

is a sufficient condition for (213) to hold. For the *bilateral constraints*, we have by (53) and (54) that $\mathscr{C}_i = \mathscr{D}_i = \mathbb{R}$. With $\mathscr{N}_{\mathbb{R}}(\cdot) \equiv \{0\}$ independent on the argument, inclusion (213) becomes $\{0\} - \epsilon\gamma_i^- \subseteq \{0\}$ and apparently holds only true if

$$\epsilon\gamma_i^- = 0. \tag{215}$$

For all *Coulomb type elements*, we have by (201) and (208) that $\Lambda_k^{(+)} = \epsilon\Lambda_k^{(-)}$ for the associated geometric unilateral constraints. As a consequence, we obtain $\mathscr{D}_i = \{0\}$ by (66), and the inclusion (213) becomes $\mathscr{N}_{\mathscr{C}_i}(-\boldsymbol{\Lambda}_i) - \epsilon\boldsymbol{\gamma}_i^- \subseteq \mathscr{N}_{\{0\}}(0)$. For one-dimensional friction, $\{0\}$ has to be considered as a subset of $\mathbb{R}$, which yields $\mathscr{N}_{\{0\}}(0) = \mathbb{R}$ and $\mathscr{N}_{\mathscr{C}_i}(-\Lambda_i) - \epsilon\gamma_i^- \subseteq \mathbb{R}$, which is always true. For the two-dimensional cases of isotropic and orthotropic friction, $\{0\}$ has to be considered as a subset of $\mathbb{R}^2$, which yields $\mathscr{N}_{\{0\}}(0) = \mathbb{R}^2$, with again no restrictions on the values of $\epsilon\boldsymbol{\gamma}_i^-$ in (213).

8.3 Summary

We have shown the equivalence of Newton's and Poisson's impact law for equal impact coefficients if the conditions (214) and (215) on the preimpact relative velocities γ_i^- of the unilateral and bilateral constraints are met. In particular, we can draw the following conclusions:

1. Completely inelastic impact $\epsilon = 0$: For this case, conditions (214) and (215) always apply, and the two impact laws are therefore always equivalent. Moreover, we see from (208) that $\boldsymbol{\Lambda}^{(+)} = 0$, which means by the first equation of (200) that $\boldsymbol{\gamma}^+ = \boldsymbol{\gamma}^\circ$. In other words, the Poisson impact terminates already after the phase of compression, and the phase of decompression leaves all the compression magnitudes unchanged by $\boldsymbol{\Lambda}^{(+)} = 0$.
2. Impacts with $\epsilon \neq 0$ under kinematic and kinetic consistency: In order to comply with (215), all geometric and kinematic bilateral constraints have to provide kinematically admissible pre-impact relative velocities $\gamma_i^- = 0$. The situation is more involved for the

unilateral constraints. According to Table 1, the values of their impact coefficients are restricted to $0 \leq \epsilon \leq 1$ for Poisson's impact law. For Newton's impact law, kinematic consistency requires $0 \leq \varepsilon \leq 1$ for the *geometric* unilateral constraints, and $-1 < \varepsilon \leq 0$ for the *kinematic* unilateral constraints, as seen from Table 1 in [27]. As a consequence, the Poisson and the Newtonian impact coefficient of the *kinematic* unilateral constraints can never be set equal to each other, because their admissible ranges do not provide any common values except of zero. For the *geometric* unilateral constraints, we have $0 \leq \varepsilon \leq 1$ for both impact models, from which kinematically admissible preimpact relative velocities $\gamma_i^- \leq 0$ follow in (214). We conclude that Newton's and Poisson's impact law are equivalent for equal restitution coefficients $\epsilon \neq 0$ under kinematic and kinetic consistency, if all bilateral and all geometric unilateral constraints are initialized with kinematically admissible preimpact relative velocities, and if no *kinematic* unilateral constraints are present.

3. Completely elastic impact $\epsilon = 1$: As a special case of the above, *kinematic* unilateral constraints have again to be excluded. Furthermore, we see from (201) and (208) that $\mathbf{\Lambda}^{(-)} = \mathbf{\Lambda}^{(+)} = \frac{1}{2}\mathbf{\Lambda}$, by which the first two summands in (126) vanish. Together with the results from Sect. 5.2.4, we may now summarize the conditions under which a Poisson impact is sufficiently energy preserving: Allowed are arbitrary combinations of all the impact elements from Sect. 4, with the only exception of the kinematic unilateral constraint. All impact coefficients have to be equal to one. All geometric and kinematic bilateral constraints, as well as all geometric unilateral constraints have to be initialized with kinematically admissible preimpact relative velocities. In addition, the friction coefficients of all Coulomb-type elements have to be chosen big enough, such that the Poisson impact terminates in the stick regime. Under these conditions, we obtain conservation of kinetic energy $W = 0$ in (126), and the post-impact state is the same as for Newton's impact law.

The fact that kinematic unilateral constraints have to be excluded for $\epsilon \neq 0$ in the above proof is very natural and is caused by the superiority of Poisson's impact law. As it has been shown in [27], Newton's impact law may dramatically fail in the presence of kinematic unilateral constraints. Supposed that Poisson's law does a better job, the resulting post-impact state can not be the same as the one obtained by Newton's law. Conservation of energy for $\epsilon = 1$ in the presence of kinematic unilateral constraints is in general not possible. This will be shown by the slide-push mechanism in Sect. 9.1.

9 Examples

In this section, three different examples are discussed. For all of them, the concept of Newtonian impacts fails, whereas Poisson's approach does at least not lead to obvious contradictions with the expected results. Throughout all the examples, the concept of an appropriate "ansatz" is used, which merely means that a particular state of the impact law is anticipated and afterward verified by doing the necessary calculations. Sometimes, the ansatz in the examples is physically reasoned, sometimes it appears just out of the sky. We do not check whether another ansatz might lead to a solution as well, which is left for the reader. In other words, we do not touch in this article the question of uniqueness of solutions. We know, however, about the uniqueness of the post-impact generalized velocities for the examples without Coulomb type friction, because the underlying mathematical structure is that of a strictly convex quadratic program.

9.1 The slide-push mechanism

The slide-push mechanism has been introduced in [27] to demonstrate that energetic inconsistency for Newtonian impacts already may occur in the presence of one geometric and one kinematic unilateral constraint. As depicted in Fig. 9, the mechanism consists of two bodies with mass m, a hard contact between body 1 and the environment, and a sprag clutch between body 1 and body 2. The sprag clutch is arranged such that the two bodies can move away from each other, but not approach each other. The restitution coefficient of the hard contact is $\epsilon_A = 1$, whereas the impact parameter of the sprag clutch is left open within the formerly derived restrictions $0 \le \epsilon_B \le 1$. The inertial positions of the masses are denoted by x_1 and x_2, and the relative velocities in the impact elements by γ_A and γ_B. Furthermore, we set $u_1 := \dot{x}_1$ and $u_2 := \dot{x}_2$ for the generalized velocities.

In contrast to [27], the system is now treated with Poisson's impact law, for which it has to be formulated according to (40)–(42). We set up the generalized velocities $\mathbf{u}$, the relative velocities $\boldsymbol{\gamma}$, and the impulsive forces $\boldsymbol{\Lambda}$ as in [27], and introduce the auxiliary variables $\boldsymbol{\Delta}$ accordingly,

$$\mathbf{u} = \begin{pmatrix} u_1 \\ u_2 \end{pmatrix}, \qquad \boldsymbol{\gamma} = \begin{pmatrix} \gamma_A \\ \gamma_B \end{pmatrix}, \qquad \boldsymbol{\Lambda} = \begin{pmatrix} \Lambda_A \\ \Lambda_B \end{pmatrix}, \qquad \boldsymbol{\Delta} = \begin{pmatrix} \Delta_A \\ \Delta_B \end{pmatrix}. \tag{216}$$

By this setting, we obtain from the impact equations in [27] the same expressions for the mass matrix $\mathbf{M}$, the generalized force directions $\mathbf{W}$, and the Delassus operator $\mathbf{G} = \mathbf{W}^{\mathrm{T}}\mathbf{M}^{-1}\mathbf{W}$. Together with the impact coefficient matrix $\boldsymbol{\epsilon}$ in (42), they are

$$\mathbf{M} = \begin{pmatrix} m & 0 \\ 0 & m \end{pmatrix}, \qquad \mathbf{W} = \begin{pmatrix} 1 & -1 \\ 0 & 1 \end{pmatrix}, \qquad \mathbf{G} = \frac{1}{m}\begin{pmatrix} 1 & -1 \\ -1 & 2 \end{pmatrix}, \qquad \boldsymbol{\epsilon} = \begin{pmatrix} 1 & 0 \\ 0 & \epsilon_B \end{pmatrix}, \tag{217}$$

which completes the mathematical description of the problem, up to the impact laws. The kinetic energy T of the system is

$$T = \frac{1}{2}mu_1^2 + \frac{1}{2}mu_2^2. \tag{218}$$

It will later be used to check the impact for energetic consistency when it is processed by Poisson's law.

For the preimpact configuration, we assume as in [27] that body 1 is moving with velocity v towards the wall, whereas body 2 is at rest, causing the sprag clutch to work in its unconstrained direction. The preimpact generalized and relative velocities therefore are

$$\mathbf{u}^- = \begin{pmatrix} -v \\ 0 \end{pmatrix}, \qquad \boldsymbol{\gamma}^- = \begin{pmatrix} -v \\ v \end{pmatrix}, \tag{219}$$

which can directly be verified from Fig. 9. In order to solve the compression phase, the associated impact laws have to be evaluated together with the left equation in (45). The

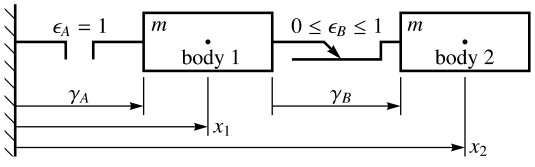

Fig. 9 The slide-push mechanism, consisting of one geometric unilateral constraint and one kinematic unilateral constraint

latter is $\boldsymbol{\gamma}^\circ = \mathbf{G}\boldsymbol{\Lambda}^{(-)} + \boldsymbol{\gamma}^-$ and can be brought with the help of (217) and (219) to the explicit form

$$\begin{pmatrix} \gamma_A^\circ \\ \gamma_B^\circ \end{pmatrix} = \frac{1}{m} \begin{pmatrix} 1 & -1 \\ -1 & 2 \end{pmatrix} \begin{pmatrix} \Lambda_A^{(-)} \\ \Lambda_B^{(-)} \end{pmatrix} + \begin{pmatrix} -v \\ v \end{pmatrix}. \tag{220}$$

Driven by the maximum dissipation property of the compression phase, we take $\boldsymbol{\gamma}^\circ = 0$ as an ansatz, solve with it (220) for $\boldsymbol{\Lambda}^{(-)}$,

$$\boldsymbol{\gamma}^\circ = \begin{pmatrix} 0 \\ 0 \end{pmatrix}, \qquad \boldsymbol{\Lambda}^{(-)} = \begin{pmatrix} mv \\ 0 \end{pmatrix}, \tag{221}$$

and verify afterward that this result is in accordance with the compression impact law from the left diagram in Fig. 3. The latter may mathematically be expressed by the inequality-complementarity conditions $\gamma_i^\circ \geq 0$, $\Lambda_i^{(-)} \geq 0$, and $\gamma_i^\circ \Lambda_i^{(-)} = 0$, which are indeed satisfied by each pair of components in (221). As a result, the system is in standstill after compression, realized by only the impulsive force $\Lambda_A^{(-)} = mv$ between body 1 and the environment, whereas the impulsive force in the sprag clutch is equal to zero, $\Lambda_B^{(-)} = 0$.

The decompression phase is driven by $\boldsymbol{\gamma}^+ = \mathbf{G}\boldsymbol{\Delta} + (\mathbf{G}\boldsymbol{\epsilon}\boldsymbol{\Lambda}^{(-)} + \boldsymbol{\gamma}^\circ)$ from the right equation in (45), which gives together with (217) and (221)

$$\begin{pmatrix} \gamma_A^+ \\ \gamma_B^+ \end{pmatrix} = \frac{1}{m} \begin{pmatrix} 1 & -1 \\ -1 & 2 \end{pmatrix} \begin{pmatrix} \Delta_A \\ \Delta_B \end{pmatrix} + \begin{pmatrix} v \\ -v \end{pmatrix}. \tag{222}$$

Note that the impact coefficient ϵ_B from the sprag clutch does *not at all* enter these equations, which is caused by the vanishing compression impulsive force $\Lambda_B^{(-)} = 0$. For decompression, we expect body 1 to bounce back from the wall under a Poisson decompression impulsive force $\Lambda_A^{(+)}$ following the first line in (52) and leading to $\Delta_A = 0$. In contrast, the sprag clutch will be pushed to the right, which requires a nonvanishing impulsive decompression force $\Lambda_B^{(+)} > 0$. Since we had $\Lambda_B^{(-)} = 0$, only the second line in (52) can apply. We therefore take $\Delta_A = 0$ and $\gamma_B^+ = 0$ as an ansatz, and solve with it (222) for the remaining unknowns Δ_B and γ_A^+. The result

$$\boldsymbol{\gamma}^+ = \begin{pmatrix} \frac{1}{2}v \\ 0 \end{pmatrix}, \qquad \boldsymbol{\Delta} = \begin{pmatrix} 0 \\ \frac{1}{2}mv \end{pmatrix} \tag{223}$$

is by pairs in accordance with the inequality-complementarity conditions (50) for decompression, and is therefore the solution of the impact problem. In a final step, the decompression impulsive forces $\boldsymbol{\Lambda}^{(+)}$ and post-impact generalized velocities $\mathbf{u}^+$ are calculated as

$$\boldsymbol{\Lambda}^{(+)} = \begin{pmatrix} mv \\ \frac{1}{2}mv \end{pmatrix}, \qquad \mathbf{u}^+ = \begin{pmatrix} \frac{1}{2}v \\ \frac{1}{2}v \end{pmatrix} \tag{224}$$

where we have used $\boldsymbol{\Lambda}^{(+)} = \boldsymbol{\Delta} + \boldsymbol{\epsilon}\boldsymbol{\Lambda}^{(-)}$ from (42) together with the particular values in (217), (221), and (223). As recognized from $\mathbf{u}^+$, both bodies are moving after the impact with the same velocity $\frac{1}{2}v$ to the right.

With the help of (218) and the results for $\mathbf{u}^-$ and $\mathbf{u}^+$ from (219) and (224), the pre and post-impact kinetic energy, as well as the energy difference can be calculated as

$$T^- = \frac{1}{2}mv^2, \qquad T^+ = \frac{1}{4}mv^2, \qquad W = T^+ - T^- = -\frac{1}{4}mv^2. \tag{225}$$

We see by the negative value of the impact work W that the impact process is energetically consistent, which supports our theoretical result from Sect. 6. Note, however, that conservation of energy under the standard restriction $0 \leq \epsilon_A \leq 1$ can never be achieved in this example, because the second impact parameter ϵ_B fully drops out from the decompression phase. Such behavior seems to be typical for systems with sprag clutches.

9.2 Frictional impact at a double pendulum

The most prominent example of an energetically inconsistent impact is Kane's double pendulum [28], which strikes the environment by a frictional collision under Newton's impact law. Two cases are reported in [29], for which an increase in the kinetic energy has been observed. These results have been confirmed and discussed in many works on the same or on very similar systems; see, e.g., [7, 13, 16, 18, 34, 54, 55]. In some of these contributions, the system has also been processed by certain variants of Poisson's impact law, which always have produced energetically consistent results in the sense that the overall kinetic energy is not increased by the impact. In order to support these findings, we apply now our inequality setting of Poisson impacts on the two critical cases of the original system [29], and compare the results with those formerly obtained for the very same system by Newton's impact law [27].

The double pendulum is depicted in Fig. 10 and consists of two identical uniform rods with mass m and length l. Its upper endpoint O is hinged at the origin of the inertial frame $(\mathbf{e}_x^I, \mathbf{e}_y^I, \mathbf{e}_z^I)$, whereas its lower endpoint C strikes a horizontal surface by a frictional impact. The contact is modeled in the normal direction by a geometric unilateral constraint according to Sect. 4.1.1, and in the tangential direction by the one-dimensional Coulomb friction element from Sect. 4.2.1. The double pendulum therefore constitutes a mechanical system with one frictional contact, for which Poisson's impact law has been proven in Sect. 7 to be energetically consistent. All data in the following semianalytical approach are kept in accordance with those of the original example in [29], and all numerical values are rounded to four digits. As in [27], the system is parameterized by the generalized coordinates $\mathbf{q} = (\varphi_1 \varphi_2)^{\mathrm{T}}$, which measure the absolute angles of the two rods. The contact angles and the preimpact

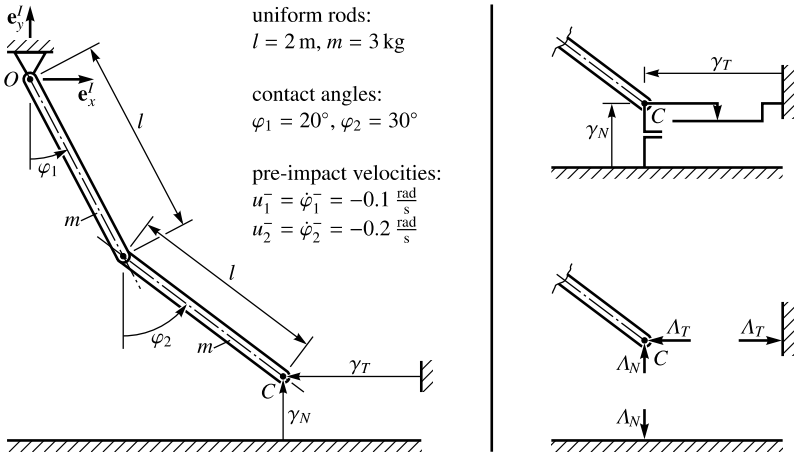

Fig. 10 Double pendulum striking the environment by a frictional impact according to [29]. Mechanical model with impact data, contact elements, and impulsive forces acting on the contact point C

generalized velocities are as specified in Fig. 10. By setting

$$\mathbf{q} = \begin{pmatrix} \varphi_1 \\ \varphi_2 \end{pmatrix}, \qquad \dot{\mathbf{q}} =: \mathbf{u} = \begin{pmatrix} u_1 \\ u_2 \end{pmatrix}, \qquad \boldsymbol{\gamma} = \begin{pmatrix} \gamma_N \\ \gamma_T \end{pmatrix}, \qquad \boldsymbol{\Lambda} = \begin{pmatrix} \Lambda_N \\ \Lambda_T \end{pmatrix}, \qquad \boldsymbol{\Delta} = \begin{pmatrix} \Delta_N \\ \Delta_T \end{pmatrix}, \tag{226}$$

we obtain the same mathematical representation of the system as in [27]. In particular, the mass matrix $\mathbf{M}$ and the matrix of the generalized force directions $\mathbf{W} = (\mathbf{w}_N \mathbf{w}_T)$ have been computed in [27] to be

$$\mathbf{M} = \begin{pmatrix} 16.0 & 5.9088 \\ 5.9088 & 4.0 \end{pmatrix} \text{kg m}^2, \qquad \mathbf{W} = \begin{pmatrix} 0.6840 & -1.8794 \\ 1.0 & -1.7321 \end{pmatrix} \text{m}. \tag{227}$$

Furthermore, the Delassus operator $\mathbf{G} = \mathbf{W}^{\mathrm{T}} \mathbf{M}^{-1} \mathbf{W}$ together with the Poisson impact coefficient matrix $\boldsymbol{\epsilon}$ is needed,

$$\mathbf{G} = \begin{pmatrix} 0.3365 & -0.5071 \\ -0.5071 & 0.8134 \end{pmatrix} \text{kg}^{-1}, \qquad \boldsymbol{\epsilon} = \begin{pmatrix} \epsilon_N & 0 \\ 0 & 0 \end{pmatrix}, \tag{228}$$

where the values of $\mathbf{G}$ have again been taken from [27], and the tangential restitution coefficient has been chosen as $\epsilon_T = 0$, as for the Newtonian impact in [27]. Finally,

$$T = \frac{1}{2} \mathbf{u}^{\mathrm{T}} \mathbf{M} \mathbf{u} \tag{229}$$

denotes the kinetic energy of the system, used to demonstrate that the Poisson impact for this example is indeed dissipative.

The kinetic energy before the impact T^- can be derived by (229) from the preimpact generalized velocities $\mathbf{u}^-$ and the mass matrix $\mathbf{M}$ in (227), and gives

$$\mathbf{u}^- = \begin{pmatrix} -0.1 \\ -0.2 \end{pmatrix} \frac{\text{rad}}{\text{s}}, \qquad T^- = 0.2782 \text{ J}. \tag{230}$$

The preimpact relative velocities $\boldsymbol{\gamma}^-$ in the normal and the tangential direction are obtained from (41) with $\mathbf{W}$ and $\mathbf{u}^-$ according to (227) and (230),

$$\boldsymbol{\gamma}^- = \begin{pmatrix} -0.2684 \\ 0.5343 \end{pmatrix} \frac{\text{m}}{\text{s}}. \tag{231}$$

All these values can already be found in [27] and are shown here just for completeness. The pre-impact velocities $\mathbf{u}^-$ are such that both rods turn clockwise, which makes the endpoint C of the lower pendulum to move downward to the left, as seen by the values of $\boldsymbol{\gamma}^-$ and Fig. 10.

The two critical cases in Kane's example require the two restitution coefficients $\varepsilon_N = 0.5$ and $\varepsilon_N = 0.7$, but a common friction coefficient $\mu = 0.5$. Since the restitution coefficients are not needed until the decompression phase, the equations for compression (29)–(32) apply with

$$\mu = 0.5 \tag{232}$$

in the same form for both cases. The compression phase is fully determined by the left equation in (45), i.e., $\boldsymbol{\gamma}^\circ = \mathbf{G} \boldsymbol{\Lambda}^{(-)} + \boldsymbol{\gamma}^-$ with $\mathbf{G}$ and $\boldsymbol{\gamma}^-$ according to (228) and (231), together with the associated impact laws. To solve these two equations for the four unknowns $(\gamma_N^\circ, \gamma_T^\circ)$ and

$(\Lambda_N^{(-)}, \Lambda_T^{(-)})$, we take as an ansatz for two of the four variables $\gamma_N^\circ = 0$ and $\Lambda_T^{(-)} = -\mu\Lambda_N^{(-)}$, which leads to the solution

$$\boldsymbol{\gamma}^\circ = \begin{pmatrix} 0 \\ 0.1187 \end{pmatrix} \frac{\mathrm{m}}{\mathrm{s}}, \qquad \boldsymbol{\Lambda}^{(-)} = \begin{pmatrix} 0.4549 \\ -0.2274 \end{pmatrix} \mathrm{N\,s}. \tag{233}$$

In a final step, the ansatz has to be checked for consistency with respect to the compression impact laws from the left diagrams of Figs. 3 and 5. With $\Lambda_N^{(-)} \geq 0$ associated with $\gamma_N^\circ = 0$ and $\gamma_T^\circ \geq 0$ associated with $\Lambda_T^{(-)} = -\mu\Lambda_N^{(-)}$, the compression impact laws are indeed fulfilled, and (233) is the solution of the compression phase. By substituting $\boldsymbol{\Lambda}^{(-)}$ into the left equation of (40), the generalized velocities $\mathbf{u}^\circ$ after compression can be computed, and from them the associated kinetic energy T° by (229),

$$\mathbf{u}^\circ = \begin{pmatrix} -0.1709 \\ 0.1169 \end{pmatrix} \frac{\mathrm{rad}}{\mathrm{s}}, \qquad T^\circ = 0.1429\ \mathrm{J}. \tag{234}$$

After compression, the upper rod still turns clockwise but with an increased angular velocity, the lower rod turns anticlockwise, and the endpoint C still slides to the left by maintaining contact. The normal component $\Lambda_N^{(-)}$ of the impulsive compression force acts on the pendulum point C in upward direction. The tangential component $\Lambda_T^{(-)}$ acts on C to the right, opposing the sliding direction.

We solve now Poisson's decompression phase for the first critical case in Kane's example, which has shown an energy increase for a Newtonian restitution coefficient of $\varepsilon_N = 0.5$ with stick at the end of the impact. We choose the Poisson restitution coefficient to be

$$\epsilon_N = 0.5, \tag{235}$$

and solve the right equation in (45), i.e., $\boldsymbol{\gamma}^+ = \mathbf{G}\boldsymbol{\Delta} + (\mathbf{G}\boldsymbol{\epsilon}\boldsymbol{\Lambda}^{(-)} + \boldsymbol{\gamma}^\circ)$, together with the decompression impact laws (50), (51) and (75), (76). The four unknowns are $\boldsymbol{\gamma}^+$ and $\boldsymbol{\Delta}$, whereas $\mathbf{G}$, $\boldsymbol{\epsilon}$, $\boldsymbol{\Lambda}^{(-)}$ and $\boldsymbol{\gamma}^\circ$ can be taken from (228) and (233). For the ansatz, we expect a normal impulsive force according to Poisson's original law, which is $\Lambda_N^{(+)} = \epsilon_N \Lambda_N^{(-)}$, and hence $\Delta_N = 0$ by (76), and we try stick $\gamma_T^+ = 0$ in the tangential direction. This yields

$$\boldsymbol{\gamma}^+ = \begin{pmatrix} 0.0786 \\ 0 \end{pmatrix} \frac{\mathrm{m}}{\mathrm{s}}, \qquad \boldsymbol{\Delta} = \begin{pmatrix} 0 \\ -0.0041 \end{pmatrix} \mathrm{N\,s}, \qquad \boldsymbol{\Lambda}^{(+)} = \begin{pmatrix} 0.2274 \\ -0.0041 \end{pmatrix} \mathrm{N\,s}, \tag{236}$$

and is in accordance with the decompression impact laws, because $\gamma_N^+ \geq 0$ associated with $\Delta_N = 0$ fulfills (50), and $|\Lambda_T^{(+)}| \leq \mu\Lambda_N^{(+)}$ associated with $\gamma_T^+ = 0$ fulfills (75), since we have $\Delta_T = \Lambda_T^{(+)}$ by (76) due to $\epsilon_T = 0$. Upon substitution of $\boldsymbol{\Lambda}^{(+)}$ into the right equation of (40), one gets the post-impact generalized velocities $\mathbf{u}^+$, and from them the post-impact kinetic energy T^+ by (229),

$$\mathbf{u}^+ = \begin{pmatrix} -0.1961 \\ 0.2127 \end{pmatrix} \frac{\mathrm{rad}}{\mathrm{s}}, \qquad T^+ = 0.1516\ \mathrm{J}. \tag{237}$$

This yields, together with (230), the contact work

$$W = T^+ - T^- = -0.1266\ \mathrm{J} \tag{238}$$

and shows that the impact is indeed dissipative, in contrast to the result when Newton's impact law is used. By the values in (236) and (237), one observes the following post-impact

motion: The upper rod turns clockwise with an even more increased angular velocity, the lower rod turns anticlockwise with an increased angular velocity compared to compression, and the endpoint C lifts off the ground without any tangential velocity. The normal component $\Lambda_N^{(+)}$ of the impulsive compression force acts on the pendulum point C in upward direction. The tangential component $\Lambda_T^{(+)}$ acts on C to the right, which is the same direction as for compression.

The second critical case in [29], which showed slip reversal under Newton's impact law, requires a restitution coefficient

$$\epsilon_N = 0.7. \tag{239}$$

In order to evaluate Poisson's decompression phase, we proceed precisely as for the first critical case by solving $\boldsymbol{\gamma}^+ = \mathbf{G}\boldsymbol{\Delta} + (\mathbf{G}\boldsymbol{\epsilon}\boldsymbol{\Lambda}^{(-)} + \boldsymbol{\gamma}^\circ)$ together with the impact laws. The same ansatz as above, i.e., $\Delta_N = 0$ and $\gamma_T^+ = 0$, leads to the solution

$$\boldsymbol{\gamma}^+ = \begin{pmatrix} 0.0805 \\ 0 \end{pmatrix} \frac{\mathrm{m}}{\mathrm{s}}, \qquad \boldsymbol{\Delta} = \begin{pmatrix} 0 \\ 0.0526 \end{pmatrix} \mathrm{N\,s}, \qquad \boldsymbol{\Lambda}^{(+)} = \begin{pmatrix} 0.3184 \\ 0.0526 \end{pmatrix} \mathrm{N\,s}, \tag{240}$$

which is again in accordance with the impact laws because of $\gamma_N^+ \geq 0$ and $|\Lambda_T^{(+)}| \leq \mu \Lambda_N^{(+)}$. The generalized post-impact velocities $\mathbf{u}^+$ and the associated kinetic energy T^+ are obtained as

$$\mathbf{u}^+ = \begin{pmatrix} -0.2007 \\ 0.2178 \end{pmatrix} \frac{\mathrm{rad}}{\mathrm{s}}, \qquad T^+ = 0.1588\ \mathrm{J}, \tag{241}$$

and the contact work W becomes

$$W = T^+ - T^- = -0.1194\ \mathrm{J}. \tag{242}$$

Again, the impact behaves dissipative as expected by the energy proof of Sect. 7. The post-impact motion is topologically the same as for the first case, with the only difference that

Table 2 Comparison of the results obtained by Poisson's and Newton's impact law for the frictional impact at the double pendulum. The impact has been initialized with the preimpact relative velocities $\gamma_N^- = -0.2684 \frac{\mathrm{m}}{\mathrm{s}}$ and $\gamma_T^- = 0.5343 \frac{\mathrm{m}}{\mathrm{s}}$, and has been processed with a friction coefficient $\mu = 0.5$. Displayed are the normal and tangential post-impact relative velocities $\gamma_{N,T}^+$, the associated impulsive forces $\Lambda_{N,T}$ with $\Lambda_{N,T} = \Lambda_{N,T}^{(-)} + \Lambda_{N,T}^{(+)}$ in the case of Poisson, the generalized post-impact velocities $u_{1,2}^+$, the impact work W, and the tangential post-impact state

	Newton $\varepsilon_N = 0.5$	Poisson $\epsilon_N = 0.5$	Newton $\varepsilon_N = 0.7$	Poisson $\epsilon_N = 0.7$
γ_N^+ [$\frac{\mathrm{m}}{\mathrm{s}}$]	0.1342	0.0786	0.1879	0.0805
γ_T^+ [$\frac{\mathrm{m}}{\mathrm{s}}$]	0	0	−0.0177	0
Λ_N [N s]	3.4079	0.6823	5.4995	0.7733
Λ_T [N s]	1.4676	−0.2315	2.7498	−0.1748
u_1^+ [$\frac{\mathrm{rad}}{\mathrm{s}}$]	−0.3346	−0.1961	−0.4430	−0.2007
u_2^+ [$\frac{\mathrm{rad}}{\mathrm{s}}$]	0.3631	0.2127	0.4909	0.2178
W [J]	0.1634	−0.1266	0.4889	−0.1194
state	stick	stick	slip	stick

the tangential decompression impulsive force $\Lambda_T^{(+)}$ on the lower endpoint C acts now to the left to ensure the stick condition.

Table 2 shows the results obtained by Poisson's and Newton's impact law [27] for the two critical cases of Kane's example. By comparing the associated values, one observes that the two impact laws behave *entirely different*. In particular, the tangential impulsive forces differ from each other not only in their values, *but even* in their directions.

9.3 Newton's cradle with three balls

Newton's cradle consists of a linear chain of equal balls. In the idealized standard experiment, all but the first ball are initially at rest, slightly touching each other. The first ball is then shot against its neighbor with a velocity v. By the occurring impact, a process is initiated in which the linear momentum of the first ball is sequentially transferred by the deformability of the bodies to the last ball in the chain, which then detaches with the same velocity v. In the following, we propose two different mechanical interpretations on how to deal with this behavior within a rigid body framework. In both approaches, all contacts are closed, forming a problem with multiple contacts at the same time. If the balls in Newton's cradle are represented by rigid bodies *and* the contacts between them are assumed to be hard, nearly all of the physics responsible for the experimental result has been eliminated from the mechanical model. Nevertheless, we still are able to reproduce the observed behavior.

In our first interpretation, we assume the impacts to be successive. The resulting impact sequence can be solved by applying either Newton's or Poisson's impact law in the following way: In order to keep the sequential momentum transfer in the model, one breaks down the overall impact event into four subevents, in which the currently moving ball hands over its linear momentum to its right neighbor by a completely elastic single collision. This impact sequence may be *visualized* by tiny gaps between the balls, as depicted in the left part of Fig. 11.

An even coarser model is obtained when the overall impact process is considered as instantaneous, without any timing or sequencing of subevents. In such a setting, the only possible and remaining mechanical interpretation is an instantaneous momentum transfer from the first to the last contact, which is sketched on the right of Fig. 11. As demonstrated in [26], this kind of momentum transfer can not be handled by the standard Newtonian impact laws [27] with just diagonal entries in the restitution coefficient matrix, but would require certain extensions as done in [9, 42]. The cleanest way to treat such problems is in the author's opinion the concept of far distant interaction that allows nonneighboring bodies to directly communicate with each other via artificial, nonmaterial contacts; see, e.g., [2]. However, although not designed for this purpose, Poisson's impact law allows for reproducing the result in Newton's cradle. In order to realize the instantaneous momentum transfer, the initial collision between the two leftmost balls has to be as dissipative that the contact stays closed after the entire impact event, whereas the rightmost balls have to

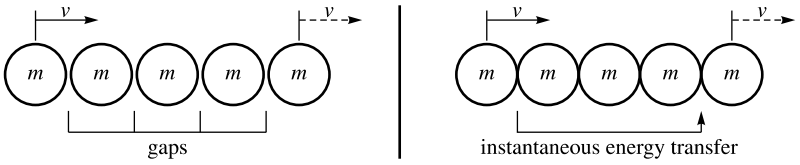

Fig. 11 Newton's cradle: Model with four successive impacts to the *left*, model with one instantaneous impact to the *right*. The latter requires an instantaneous energy transfer from the first to the last contact

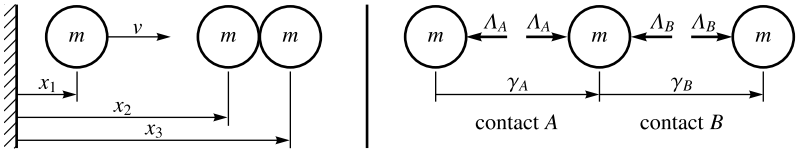

Fig. 12 Newton's cradle with three balls: Mechanical system and parameterization to the *left*, free body diagram with impulsive forces and relative velocities to the *right*

actively bounce away from each other like in a pinball machine, thereby gaining the same amount of energy as dissipated in the other contact, and requiring a local Poisson restitution coefficient *greater* than 1 as a necessary consequence.

We now demonstrate the above on Newton's cradle with three balls (Fig. 12) and determine the values of the two restitution coefficients ϵ_A and ϵ_B such that the right ball detaches with the same velocity v as the left ball has approached. The positions of the three balls are denoted by x_1, x_2, x_3, and the two contacts between them are labeled by A and B. For the parameterization of the system, we set

$$\mathbf{q} = \begin{pmatrix} x_1 \\ x_2 \\ x_3 \end{pmatrix}, \qquad \dot{\mathbf{q}} =: \mathbf{u} = \begin{pmatrix} u_1 \\ u_2 \\ u_3 \end{pmatrix}, \qquad \boldsymbol{\gamma} = \begin{pmatrix} \gamma_A \\ \gamma_B \end{pmatrix}, \qquad \boldsymbol{\Lambda} = \begin{pmatrix} \Lambda_A \\ \Lambda_B \end{pmatrix}, \qquad \boldsymbol{\Delta} = \begin{pmatrix} \Delta_A \\ \Delta_B \end{pmatrix} \tag{243}$$

and obtain for the mass matrix $\mathbf{M}$, the generalized force directions $\mathbf{W} = (\mathbf{w}_A \mathbf{w}_B)$, the Delassus operator $\mathbf{G} = \mathbf{W}^{\mathrm{T}} \mathbf{M}^{-1} \mathbf{W}$, and the Poisson restitution coefficient matrix $\boldsymbol{\epsilon}$

$$\mathbf{M} = \begin{pmatrix} m & 0 & 0 \\ 0 & m & 0 \\ 0 & 0 & m \end{pmatrix}, \qquad \mathbf{W} = \begin{pmatrix} -1 & 0 \\ 1 & -1 \\ 0 & 1 \end{pmatrix}, \qquad \mathbf{G} = \frac{1}{m} \begin{pmatrix} 2 & -1 \\ -1 & 2 \end{pmatrix}, \tag{244}$$

$$\boldsymbol{\epsilon} = \begin{pmatrix} \epsilon_A & 0 \\ 0 & \epsilon_B \end{pmatrix},$$

where $\mathbf{w}_A$ and $\mathbf{w}_B$ have been obtained from the relative velocities $\gamma_A = u_2 - u_1$ and $\gamma_B = u_3 - u_2$. We assume for the preimpact configuration that the left ball approaches with velocity v, whereas the other two balls are at standstill. The generalized and relative preimpact velocities are therefore obtained as

$$\mathbf{u}^- = \begin{pmatrix} v \\ 0 \\ 0 \end{pmatrix}, \qquad \boldsymbol{\gamma}^- = \begin{pmatrix} -v \\ 0 \end{pmatrix}. \tag{245}$$

For compression, we solve $\boldsymbol{\gamma}^\circ = \mathbf{G}\boldsymbol{\Lambda}^{(-)} + \boldsymbol{\gamma}^-$ in (45) with the maximum dissipation ansatz $\boldsymbol{\gamma}^\circ = 0$, which leads with (244) and (245) to

$$0 = \frac{1}{m} \begin{pmatrix} 2 & -1 \\ -1 & 2 \end{pmatrix} \begin{pmatrix} \Lambda_A^{(-)} \\ \Lambda_B^{(-)} \end{pmatrix} + \begin{pmatrix} -v \\ 0 \end{pmatrix}, \tag{246}$$

and hence to the solution

$$\boldsymbol{\gamma}^\circ = \begin{pmatrix} 0 \\ 0 \end{pmatrix}, \qquad \boldsymbol{\Lambda}^{(-)} = \frac{1}{3} m v \begin{pmatrix} 2 \\ 1 \end{pmatrix}, \tag{247}$$

which indeed fulfills the inequality-complementarity conditions shown in the left graph of Fig. 3. The generalized velocities $\mathbf{u}^\circ$ are then computed from $\mathbf{u}^\circ = \mathbf{u}^- + \mathbf{M}^{-1}\mathbf{W}\boldsymbol{\Lambda}^{(-)}$ in (40), where (244), (245), and (247) have to be used to obtain

$$\mathbf{u}^\circ = \begin{pmatrix} v \\ 0 \\ 0 \end{pmatrix} + \frac{1}{3}v \begin{pmatrix} -1 & 0 \\ 1 & -1 \\ 0 & 1 \end{pmatrix} \begin{pmatrix} 2 \\ 1 \end{pmatrix} = \frac{1}{3}v \begin{pmatrix} 1 \\ 1 \\ 1 \end{pmatrix}. \tag{248}$$

The values of $\mathbf{u}^\circ$ reveal that all three balls are moving after compression with a common velocity to the right, which is one third of the initial velocity of the left ball.

The decompression phase is driven by the equation $\boldsymbol{\gamma}^+ = \mathbf{G}\boldsymbol{\Delta} + (\mathbf{G}\boldsymbol{\epsilon}\boldsymbol{\Lambda}^{(-)} + \boldsymbol{\gamma}^\circ)$ from (45), from which we now determine the values of the restitution coefficients ϵ_A and ϵ_B such that the typical behavior of Newton's cradle applies. After the impact, we want the left two balls to stick together and, therefore, set $\gamma_A^+ = 0$. The right ball should leave the others with velocity v, which requires $\gamma_B^+ = v$ and $\Delta_B = 0$ as a necessary consequence on the impact law (50). With these values, we obtain together with (244) and (247)

$$\begin{pmatrix} 0 \\ v \end{pmatrix} = \frac{1}{m} \begin{pmatrix} 2 & -1 \\ -1 & 2 \end{pmatrix} \begin{pmatrix} \Delta_A \\ 0 \end{pmatrix} + \frac{1}{3}v \begin{pmatrix} 2 & -1 \\ -1 & 2 \end{pmatrix} \begin{pmatrix} 2\epsilon_A \\ \epsilon_B \end{pmatrix}, \tag{249}$$

and after multiplication with m and expansion of the matrix-vector products

$$\begin{pmatrix} 0 \\ mv \end{pmatrix} = \begin{pmatrix} 2\Delta_A \\ -\Delta_A \end{pmatrix} + \frac{1}{3}mv \begin{pmatrix} 4\epsilon_A - \epsilon_B \\ 2\epsilon_B - 2\epsilon_A \end{pmatrix}. \tag{250}$$

Multiplication of the first line by 3 and of the second line by 6 yields the two equations

$$6\Delta_A = mv(\epsilon_B - 4\epsilon_A) \quad \text{and} \quad 6\Delta_A = mv(4\epsilon_B - 4\epsilon_A - 6), \tag{251}$$

from which the impact coefficient in the right contact can be determined as

$$\epsilon_B = 2. \tag{252}$$

The value of ϵ_A can not be derived from (251). Instead, the inequality $\Delta_A \geq 0$ from (50) has to apply, which restricts by (251) and (252) the possible values of ϵ_A to

$$\epsilon_A \leq \frac{1}{2}. \tag{253}$$

This condition ensures that Poisson's decompression law is kept in the exceptional case for contact A according to the second line in (52), and does prevent the contact to open as it would happen for larger values of ϵ_A. According to our ansatz and Eqs. (251) and (252), the solution of the decompression phase can now be summarized as

$$\boldsymbol{\gamma}^+ = \begin{pmatrix} 0 \\ v \end{pmatrix}, \qquad \boldsymbol{\Delta} = \frac{1}{3}mv \begin{pmatrix} 1 - 2\epsilon_A \\ 0 \end{pmatrix}. \tag{254}$$

The decompression impulsive forces $\boldsymbol{\Lambda}^{(+)}$ then follow from (42) by $\boldsymbol{\Lambda}^{(+)} = \boldsymbol{\Delta} + \boldsymbol{\epsilon}\boldsymbol{\Lambda}^{(-)}$, which gives together with (244), (247), (252), and (254)

$$\boldsymbol{\Lambda}^{(+)} = \frac{1}{3}mv \begin{pmatrix} 1 - 2\epsilon_A \\ 0 \end{pmatrix} + \frac{1}{3}mv \begin{pmatrix} 2\epsilon_A \\ 2 \end{pmatrix} = \frac{1}{3}mv \begin{pmatrix} 1 \\ 2 \end{pmatrix}. \tag{255}$$

Note that the undetermined impact coefficient ϵ_A drops out by this operation, and that the components of $\mathbf{\Lambda}^{(-)}$ from (247) and $\mathbf{\Lambda}^{(+)}$ from (255) are the same but just interchanged, which had to be expected by the symmetry of the system. In a final step, the post-impact generalized velocities $\mathbf{u}^+$ are computed from (40) as $\mathbf{u}^+ = \mathbf{u}^\circ + \mathbf{M}^{-1}\mathbf{W}\mathbf{\Lambda}^{(+)}$. With the help of (244), (248), (255), this gives

$$\mathbf{u}^+ = \frac{1}{3}v\begin{pmatrix}1\\1\\1\end{pmatrix} + \frac{1}{3}v\begin{pmatrix}-1 & 0\\1 & -1\\0 & 1\end{pmatrix}\begin{pmatrix}1\\2\end{pmatrix} = \begin{pmatrix}0\\0\\v\end{pmatrix}. \tag{256}$$

After the impact, the left two balls are indeed at rest, and the right ball leaves with velocity v as expected.

10 Energetic inconsistency at Poisson impacts

In this section, we present an example for which Poisson's impact law becomes energetically inconsistent under the standard restrictions of the impact coefficients $0 \le \epsilon_i \le 1$. Needed is at least one frictional contact together with at least one other unilateral constraint. Otherwise, the consistency results of Sects. 6 and 7 would apply. Energetic inconsistency has to be understood in the sense that the *overall* kinetic energy of the system is increased by the impact, but not just an energy portion related to one of the impact elements as, e.g., in the right contact of Newton's cradle in Sect. 9.3. Up to our knowledge, the example presented here is the first and the only so far that is able to show an energy increase in Poisson impacts. It has been invented in the master thesis [51], together with the calculations necessary to demonstrate the energy gain.

The energy increase in the following example is caused by the simple fact that the *same* impulsive force applied to masses of *different* size leads to *different* kinetic energies: Suppose a point mass M moving with velocity v. In order to bring it to standstill, an impulsive force $\mathscr{F} = Mv$ is needed. After standstill, decrease the mass to m and apply the same impulsive force $\mathscr{F}$ again. This brings the now smaller mass to the new velocity $\frac{M}{m}v$. The difference in kinetic energy is $T^+ - T^- = \frac{1}{2}Mv^2(\frac{M}{m} - 1)$ and is greater than zero for $M > m$.

For our example, an inhomogeneous rigid bar is needed, which we set up according to Fig. 13. It consists of a homogeneous rigid bar (length $2l$, center of mass S, mass m_1, moment of inertia Θ_S with respect to S), and an additional point mass m_2 attached to S. We choose m_2 as

$$m_2 = \frac{\alpha - 3}{3}m_1 \quad (\alpha \ge 3) \tag{257}$$

to independently adjust the overall mass of the body and the moment of inertia relative to each other by the values of α. The overall mass of the body is $m := m_1 + m_2$, which gives with the help of (257)

$$m = \frac{\alpha}{3}m_1. \tag{258}$$

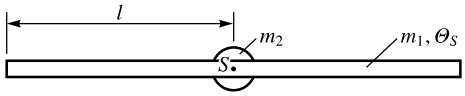

Fig. 13 Rigid body, consisting of a rigid bar and an additional point mass attached to its center of mass S

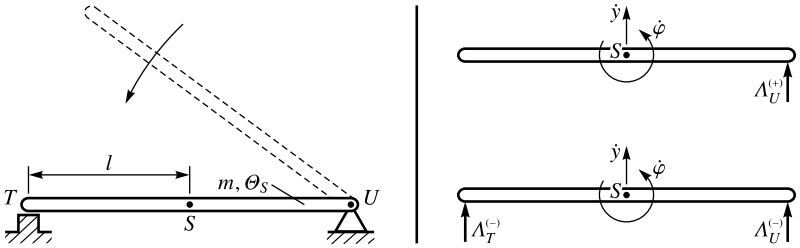

Fig. 14 Two-stage impact process on an inhomogeneous bar: Impact configuration for the first stage to the *left*, free body diagrams for the first and the second stage to the *right*

The moment of inertia of the overall body with respect to its center of mass S is $\Theta_S = \frac{1}{3} m_1 l^2$ and can be written by (258) as

$$\Theta_S = \frac{m l^2}{\alpha}. \tag{259}$$

The following analysis on the impact dynamics of the body from Fig. 13 is split into two parts. In the first part, the mechanism leading to the energy increase is explained by means of a simplified two-stage model. It turns out that a change in the constraint configuration by passing from the first to the second stage is responsible for the energy gain. These two stages can be identified with the compression and decompression phase of a frictional Poisson impact, which is demonstrated on the final model in the second part. In both parts, the rigid body from Fig. 13 is used, and its inertia terms are henceforth addressed by (m, Θ_S) with Θ_S according to (259).

10.1 Energy gain under changing constraint configurations

We investigate now a sequence of two impacts that act on the body from Fig. 13 under different constraint configurations, in order to demonstrate that the kinetic energy is increased at the end. The first stage of this process will in the final example correspond with the phase of compression, and the second stage with the phase of decompression.

The constraint configuration of the body for the first stage is shown on the left of Fig. 14. The body is hinged at its right endpoint U, and initially turns anticlockwise, to hit a rigid support with its left endpoint T. The free body diagram for this impact configuration is depicted on the lower right of Fig. 14. We assume the preimpact velocities to be

$$\dot{y}^- = -v, \qquad \dot{\varphi}^- = \frac{v}{l}, \tag{260}$$

and want to determine the two impulsive forces $\Lambda_T^{(-)}$ and $\Lambda_U^{(-)}$ such that the body is at rest after this impact,

$$\dot{y}^\circ = 0, \qquad \dot{\varphi}^\circ = 0. \tag{261}$$

From the linear and angular momentum theorem for impacts,

$$m\left(\dot{y}^\circ - \dot{y}^-\right) = \Lambda_U^{(-)} + \Lambda_T^{(-)}, \qquad \Theta_S\left(\dot{\varphi}^\circ - \dot{\varphi}^-\right) = l\Lambda_U^{(-)} - l\Lambda_T^{(-)}, \tag{262}$$

we obtain for the current impact configuration (260), (261) together with (259) the two equations

$$mv = \Lambda_U^{(-)} + \Lambda_T^{(-)}, \qquad -\frac{mv}{\alpha} = \Lambda_U^{(-)} - \Lambda_T^{(-)}, \tag{263}$$

which can be solved for $\Lambda_T^{(-)}$ and $\Lambda_U^{(-)}$ to give

$$\Lambda_T^{(-)} = \frac{1}{2\alpha} mv(\alpha+1), \qquad \Lambda_U^{(-)} = \frac{1}{2\alpha} mv(\alpha-1). \tag{264}$$

The kinetic energy E^- before the impact is

$$\begin{aligned} E^- &= \frac{1}{2} m \dot{y}^{-2} + \frac{1}{2} \Theta_S \dot{\varphi}^{-2} \\ &= \frac{1}{2} m v^2 + \frac{1}{2} \frac{ml^2}{\alpha} \frac{v^2}{l^2} \\ &= \frac{1}{2\alpha^2} m v^2 \alpha(\alpha+1), \end{aligned} \tag{265}$$

where (259) and (260) have been used to bring it to its final form.

For the second stage, we remove from the system the hinge and the rigid support at points U and T, and apply an external impulsive force $\Lambda_U^{(+)}$ at the right endpoint U of the rod, as depicted in the upper right of Fig. 14. We further assume the size of $\Lambda_U^{(+)}$ to be

$$\Lambda_U^{(+)} = \Lambda_U^{(-)}, \tag{266}$$

in order to determine from the linear and angular momentum theorems

$$m\big(\dot{y}^+ - \dot{y}^\circ\big) = \Lambda_U^{(+)}, \qquad \Theta_S\big(\dot{\varphi}^+ - \dot{\varphi}^\circ\big) = l\Lambda_U^{(+)} \tag{267}$$

the post-impact velocities $(\dot{y}^+, \dot{\varphi}^+)$ for the current configuration. With Θ_S from (259), the initial velocities $(\dot{y}^\circ, \dot{\varphi}^\circ)$ from (261), and the applied impulsive force $\Lambda_U^{(+)}$ from (266) and (264), one obtains

$$m\dot{y}^+ = \frac{1}{2\alpha} mv(\alpha-1), \qquad \frac{ml^2}{\alpha}\dot{\varphi}^+ = \frac{1}{2\alpha} mlv(\alpha-1), \tag{268}$$

and hence the result

$$\dot{y}^+ = \frac{1}{2\alpha} v(\alpha-1), \qquad \dot{\varphi}^+ = \frac{1}{2l} v(\alpha-1). \tag{269}$$

With it, the kinetic energy E^+ is computed as

$$\begin{aligned} E^+ &= \frac{1}{2} m \dot{y}^{+2} + \frac{1}{2} \Theta_S \dot{\varphi}^{+2} \\ &= \frac{1}{8\alpha^2} mv^2(\alpha-1)^2 + \frac{1}{8\alpha} mv^2(\alpha-1)^2 \\ &= \frac{1}{8\alpha^2} mv^2(\alpha-1)^2(\alpha+1), \end{aligned} \tag{270}$$

where again (259) has been used. The energy difference for the overall impact process is now obtained from (265) and (270) as

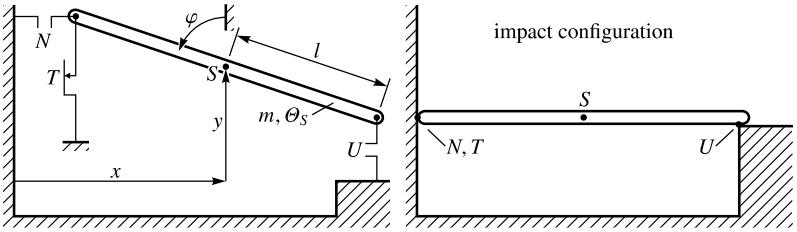

Fig. 15 Frictional multicontact problem of an inhomogeneous rod. *Left*: Mechanical system with impact elements. *Right*: Configuration at which the rod impacts against the environment

$$E^+ - E^- = \frac{1}{8\alpha^2} m v^2 \big((\alpha-1)^2(\alpha+1) - 4\alpha(\alpha+1)\big)$$
$$= \frac{1}{8\alpha^2} m v^2 (\alpha+1)\big((\alpha-1)^2 - 4\alpha\big) \tag{271}$$

and turns out to be positive under the restriction $\alpha \geq 3$ from (257), if

$$\alpha > 3 + 2\sqrt{2} \approx 5.828. \tag{272}$$

In this case, the kinetic energy is increased by the considered impact process, caused by a reduction of the effective mass at U due to the constraint removal at T. In the next section, we will discuss the same but slightly extended example to show that the deletion of the hinge and the rigid support can be performed by Poisson impact elements.

10.2 Energy gain by a frictional Poisson multi-impact

The final example, on which we demonstrate that Poisson impacts may become energetically inconsistent, is depicted in Fig. 15. It consists of the same inhomogeneous rigid bar as before, but is equipped with an additional degree of freedom x, which allows the left end of the rod to horizontally impact against a vertical wall by the geometric unilateral constraint N. Furthermore, the rigid support T has been replaced by a Coulomb friction element T, and the hinge U by a geometric unilateral constraint U, constituting a frictionless contact with the horizontal environment. The task of the unilateral geometric constraint U is to represent the hinge during compression, to realize its deletion for decompression, and to provide the decompression impulsive force $\Lambda_U^{(+)}$ according to (266) by a restitution coefficient $\epsilon_U = 1$. The task of the Coulomb friction element T is to realize the rigid support by large friction coefficient μ, which brings the left end of the rod to stop after compression. The task of the unilateral geometric constraint N is to switch off the Coulomb friction element T, and hence to remove the rigid support after compression, which is done by a restitution coefficient $\epsilon_N = 0$. With $\epsilon_T \leq \epsilon_N$ according to (70), the three impact coefficients are therefore chosen as

$$\epsilon_N = 0, \qquad \epsilon_T = 0, \qquad \epsilon_U = 1, \tag{273}$$

and the former constraint deletion is now realized by the specific values of these impact coefficients. In other words, Poisson impact elements can be (mis)used to a certain extent as switches, to change the constraint configuration after compression.

We are now going to put this system into our framework for Poisson impacts and to process it in the same way as all the examples before. For the parameterization of the system,

we set

$$\mathbf{q}=\begin{pmatrix}x\\y\\\varphi\end{pmatrix},\qquad \mathbf{u}:=\dot{\mathbf{q}}=\begin{pmatrix}\dot{x}\\\dot{y}\\\dot{\varphi}\end{pmatrix},\qquad \boldsymbol{\gamma}=\begin{pmatrix}\gamma_N\\\gamma_T\\\gamma_U\end{pmatrix},\qquad \boldsymbol{\Lambda}=\begin{pmatrix}\Lambda_N\\\Lambda_T\\\Lambda_U\end{pmatrix},\qquad \boldsymbol{\Delta}=\begin{pmatrix}\Delta_N\\\Delta_T\\\Delta_U\end{pmatrix}. \tag{274}$$

The impact configuration $\mathbf{q}_0$ is depicted in the right part of Fig. 15 and is addressed by the coordinates $\mathbf{q}_0=(x_0,y_0,\varphi_0)^{\mathrm{T}}=(l,0,\frac{\pi}{2})^{\mathrm{T}}$. The linear and angular momentum theorems for this impact configuration are

$$m\big(\dot{x}^+-\dot{x}^-\big)=\Lambda_N,\qquad m\big(\dot{y}^+-\dot{y}^-\big)=\Lambda_U+\Lambda_T,\qquad \Theta_S\big(\dot{\varphi}^+-\dot{\varphi}^-\big)=l\Lambda_U-l\Lambda_T, \tag{275}$$

where the points of application and the directions of the impulsive forces Λ_U and Λ_T are as in the free body diagrams of Fig. 14, and Λ_N acts on the left end of the body horizontally to the right. The relative velocities associated with the three impact elements for the given impact configuration are

$$\gamma_N=\dot{x},\qquad \gamma_T=\dot{y}-l\dot{\varphi},\qquad \gamma_U=\dot{y}+l\dot{\varphi}. \tag{276}$$

From (275), (276), and (273), the mass matrix $\mathbf{M}$, the matrix of the generalized force directions $\mathbf{W}$, and the impact coefficient matrix $\boldsymbol{\epsilon}$ are identified to be

$$\mathbf{M}=\begin{pmatrix}m&0&0\\0&m&0\\0&0&\Theta_S\end{pmatrix},\qquad \mathbf{W}=\begin{pmatrix}1&0&0\\0&1&1\\0&-l&l\end{pmatrix},\qquad \boldsymbol{\epsilon}=\begin{pmatrix}0&0&0\\0&0&0\\0&0&1\end{pmatrix}, \tag{277}$$

according to the parameterization (274). The Delassus operator $\mathbf{G}$ is then calculated as

$$\mathbf{G}=\mathbf{W}^{\mathrm{T}}\mathbf{M}^{-1}\mathbf{W}=\begin{pmatrix}\frac{1}{m}&0&0\\0&\frac{1}{m}+\frac{l^2}{\Theta_S}&\frac{1}{m}-\frac{l^2}{\Theta_S}\\0&\frac{1}{m}-\frac{l^2}{\Theta_S}&\frac{1}{m}+\frac{l^2}{\Theta_S}\end{pmatrix}=\frac{1}{m}\begin{pmatrix}1&0&0\\0&1+\alpha&1-\alpha\\0&1-\alpha&1+\alpha\end{pmatrix}, \tag{278}$$

where Θ_S from (259) has been used for its final representation.

The preimpact velocities are chosen such that the bar is turning anticlockwise around its right endpoint, which itself is sliding on the ground to the left. With $u>0$ and $v>0$, this is realized by

$$\dot{x}^-=-u,\qquad \dot{y}^-=-v,\qquad \dot{\varphi}^-=\frac{v}{l}, \tag{279}$$

where $\dot{y}^-$ and $\dot{\varphi}^-$ are precisely as in (260). The associated relative velocities can now be computed from (276) and are

$$\gamma_N^-=-u,\qquad \gamma_T^-=-2v,\qquad \gamma_U^-=0. \tag{280}$$

For compression, we solve $\boldsymbol{\gamma}^\circ=\mathbf{G}\boldsymbol{\Lambda}^{(-)}+\boldsymbol{\gamma}^-$ from (45) with the ansatz

$$\gamma_N^\circ=0,\qquad \gamma_T^\circ=0,\qquad \gamma_U^\circ=0, \tag{281}$$

to obtain the same velocities ($\dot{y}^\circ = 0, \dot{\varphi}^\circ = 0$) as in (261). This yields the linear system of equations

$$0 = \frac{1}{m}\begin{pmatrix} 1 & 0 & 0 \\ 0 & 1+\alpha & 1-\alpha \\ 0 & 1-\alpha & 1+\alpha \end{pmatrix}\begin{pmatrix} \Lambda_N^{(-)} \\ \Lambda_T^{(-)} \\ \Lambda_U^{(-)} \end{pmatrix} + \begin{pmatrix} -u \\ -2v \\ 0 \end{pmatrix}, \tag{282}$$

from which the impulsive forces for compression can be calculated as

$$\Lambda_N^{(-)} = mu, \qquad \Lambda_T^{(-)} = \frac{1}{2\alpha} mv(\alpha+1), \qquad \Lambda_U^{(-)} = \frac{1}{2\alpha} mv(\alpha-1). \tag{283}$$

Note that the values of $\Lambda_U^{(-)}$ and $\Lambda_T^{(-)}$ are by (264) the same as in the previous example. In order to verify the ansatz, the impact laws for compression have to be checked against violation. With $\gamma_N^\circ = 0$ and $\gamma_U^\circ = 0$, the associated impulsive forces have to obey the inequalities $\Lambda_N^{(-)} \geq 0$ and $\Lambda_U^{(-)} \geq 0$, as required by the left diagram in Fig. 3. This clearly holds true for $\Lambda_N^{(-)}$, but also for $\Lambda_U^{(-)}$ since $\alpha \geq 3$ by (257). For the friction element, we have $\gamma_T^\circ = 0$. This causes by the left diagram in Fig. 5 the stick condition $|\Lambda_T^{(-)}| \leq \mu \Lambda_N^{(-)}$, which can be evaluated with the help of (283) to obtain a lower bound of the friction coefficient as

$$\mu \geq \frac{\alpha+1}{2\alpha}\frac{v}{u}. \tag{284}$$

To summarize the results of the compression phase, we conclude that the unilateral constraint U and the frictional contact N, T are indeed able to represent the action of the hinge and the rigid support on the rod by the very same impulsive forces.

In order to process the decompression phase, we have to solve the right equation in (45), i.e. $\boldsymbol{\gamma}^+ = \mathbf{G}\boldsymbol{\Delta} + (\mathbf{G}\boldsymbol{\epsilon}\boldsymbol{\Lambda}^{(-)} + \boldsymbol{\gamma}^\circ)$. With the ansatz

$$\Delta_N = 0, \qquad \Delta_T = 0, \qquad \Delta_U = 0 \tag{285}$$

and the values in (281), it reduces to $\boldsymbol{\gamma}^+ = \mathbf{G}\boldsymbol{\epsilon}\boldsymbol{\Lambda}^{(-)}$ and can be written as

$$\begin{pmatrix} \gamma_N^+ \\ \gamma_T^+ \\ \gamma_U^+ \end{pmatrix} = \frac{1}{m}\begin{pmatrix} 1 & 0 & 0 \\ 0 & 1+\alpha & 1-\alpha \\ 0 & 1-\alpha & 1+\alpha \end{pmatrix}\begin{pmatrix} 0 & 0 & 0 \\ 0 & 0 & 0 \\ 0 & 0 & 1 \end{pmatrix}\begin{pmatrix} \Lambda_N^{(-)} \\ \Lambda_T^{(-)} \\ \Lambda_U^{(-)} \end{pmatrix}. \tag{286}$$

Substitution of (283) into (286) yields the post-impact relative velocities as

$$\gamma_N^+ = 0, \qquad \gamma_T^+ = \frac{-1}{2\alpha} v(\alpha-1)^2, \qquad \gamma_U^+ = \frac{1}{2\alpha} v\big(\alpha^2 - 1\big). \tag{287}$$

The decompression impulsive forces are calculated from (42) by $\boldsymbol{\Lambda}^{(+)} = \boldsymbol{\Delta} + \boldsymbol{\epsilon}\boldsymbol{\Lambda}^{(-)}$, which reduces to $\boldsymbol{\Lambda}^{(+)} = \boldsymbol{\epsilon}\boldsymbol{\Lambda}^{(-)}$ because of (285). With $\epsilon_U = 1$ as the only nonzero entry in the restitution matrix $\boldsymbol{\epsilon}$ from (277), we obtain $\Lambda_U^{(+)} = \Lambda_U^{(-)}$ as in (266), and all together with (283)

$$\Lambda_N^{(+)} = 0, \qquad \Lambda_T^{(+)} = 0, \qquad \Lambda_U^{(+)} = \frac{1}{2\alpha} mv(\alpha-1). \tag{288}$$

With $\Delta_N = 0$ together with $\gamma_N^+ = 0$, and $\Delta_U = 0$ together with $\gamma_U^+ > 0$, the ansatz is apparently in accordance with the impact law (50) for the impact elements N and U. For the

impact element T, the conditions in (75) have to be checked. With $\epsilon_T = 0$ and $\Lambda_N^{(+)} = 0$, we obtain in (75) for the driving term $\mu(\Lambda_N^{(+)} - \epsilon_T \Lambda_N^{(-)}) \equiv 0$ and deduce that any value for γ_T^+ is allowed. Finally, note that $\Lambda_T^{(+)} = 0$ in (288) realizes the deletion of the rigid support T in our previous example, which is accomplished by the normal restitution coefficient $\epsilon_N = 0$. The latter makes the normal decompression impulsive force $\Lambda_N^{(+)}$ to disappear, and with it the associated tangential component $\Lambda_T^{(+)}$ thanks to Coulomb's law.

By knowing $\mathbf{u}^-$, $\mathbf{\Lambda}^{(-)}$ and $\mathbf{\Lambda}^{(+)}$ from (279), (283) and (288), the post-impact generalized velocities $\mathbf{u}^+$ can now be computed by $\mathbf{M}(\mathbf{u}^+ - \mathbf{u}^-) = \mathbf{W}(\mathbf{\Lambda}^{(-)} + \mathbf{\Lambda}^{(+)})$ from the two equations in (40). In a first step, this yields

$$\begin{pmatrix} m & 0 & 0 \\ 0 & m & 0 \\ 0 & 0 & \Theta_S \end{pmatrix} \begin{pmatrix} \dot{x}^+ + u \\ \dot{y}^+ + v \\ \dot{\varphi}^+ - \frac{v}{l} \end{pmatrix} = \begin{pmatrix} 1 & 0 & 0 \\ 0 & 1 & 1 \\ 0 & -l & l \end{pmatrix} \begin{pmatrix} mu \\ \frac{1}{2\alpha} mv(\alpha + 1) \\ \frac{1}{\alpha} mv(\alpha - 1) \end{pmatrix}, \tag{289}$$

and after expanding the matrix vector products,

$$\begin{pmatrix} m(\dot{x}^+ + u) \\ m(\dot{y}^+ + v) \\ \Theta_S(\dot{\varphi}^+ - \frac{v}{l}) \end{pmatrix} = \begin{pmatrix} mu \\ \frac{1}{2\alpha} mv(3\alpha - 1) \\ \frac{1}{2\alpha} mlv(\alpha - 3) \end{pmatrix}. \tag{290}$$

With Θ_S from (259), we get the final result

$$\dot{x}^+ = 0, \qquad \dot{y}^+ = \frac{1}{2\alpha} v(\alpha - 1), \qquad \dot{\varphi}^+ = \frac{1}{2l} v(\alpha - 1), \tag{291}$$

in which the post-impact velocities $\dot{y}^+$ and $\dot{\varphi}^+$ again coincide with those from (269). The kinetic energy of the system is

$$T = \frac{1}{2} m\dot{x}^2 + \frac{1}{2} m\dot{y}^2 + \frac{1}{2} \Theta_S \dot{\varphi}^2, \tag{292}$$

from which the impact work can be computed. By taking into account that the pre and post-impact velocities for $\dot{y}$ and $\dot{\varphi}$ are the same as in the previous example, we can take the former result (271) and express the energy difference as

$$T^+ - T^- = E^+ - E^- - \frac{1}{2} mu^2. \tag{293}$$

Note that the completely inelastic collision against the vertical wall adds to the dissipation of the overall impact by $\frac{1}{2} mu^2$. However, an energy increase is still possible and easy to realize. For this, choose some α according to the inequality (272), adjust afterward u such that $T^+ - T^- > 0$ holds, and determine finally from (284) the friction coefficient μ necessary to achieve the stick state at the end of compression.

As an energy increase is possible in this example, the two conditions (117) and (121) for small and similar impact coefficients that sufficiently ensure energetic consistency, cannot be expected to hold. To demonstrate this, the eigenvalues of the Delassus operator $\mathbf{G}$ from (278) have to be determined. They apparently are

$$\lambda_1 = \frac{1}{m}, \qquad \lambda_2 = \frac{2}{m}, \qquad \lambda_3 = \frac{2\alpha}{m}, \tag{294}$$

with λ_1 being the smallest and λ_3 the largest. This leads to the reciprocal condition number

$$\frac{\lambda_{\min}}{\lambda_{\max}} = \frac{1}{2\alpha} \leq \frac{1}{6}, \tag{295}$$

revealing that neither (117) nor (121) can be met with $\epsilon_{\max} = 1$ and $\epsilon_{\min} = 0$, as it is in our example by (273).

11 Conclusion

In this paper, we have presented a full account of Poisson's impact law in inequality form. Various impact elements, which all are equipped with a restitution coefficient, have been set into a common mathematical framework. This allows for an arbitrary combination of impact elements within a multibody system or, even more general, within any finite-dimensional Lagrangian system. Multicontact configurations can be accessed in this way by a very structured approach. In the author's opinion, Poisson's impact law is superior to Newton's impact law for most application problems, which is supported by the various examples and energetic consistency proofs in the paper. The overall better behavior of Poisson impacts results from the impulse-based approach instead of the kinematic restitution law, together with the splitting of the impact event into two subphases. However, even Poisson's impact law in integrated form, as treated in this paper, is far from being perfect.

The first fundamental problem is that the friction law for impact-free motion, i.e., the friction force as a function of the tangential relative velocity, can*not* be brought in closed form by integration to the impulse-velocity level. Although this problem is slightly disarmed for Poisson impacts by the bisection of the impact event, it is still present and leads to questionable results if slip reversal or transitions from stick to slip take place *within* one of the two subphases. The second fundamental problem lies in the assumption that the compression phase, and also the decompression phase, and thus the impact itself, terminates simultaneously in all impact elements. Systems that require sequential impacts can in general *not* be solved by our approach. The only possibility to resolve both of the above problems is a further subsequencing of the impact event in the sense of Routh or Keller. This, however, leads to a dramatically increasing number of possible solutions, as already pointed out in [14]. At the end, one of these solution has to be singled out, which can*not* be done by the mechanical model alone, but requires additional physical arguments to identify the true impact sequence.

The problem of sequential impacts is often caused by an insufficient spatial discretization of the system, by which too much of the underlying physics has been eliminated. Instead of the subsequencing technique, we recommend for such cases a refinement of the model by, e.g., adding elasticity, in order to dynamically decouple the impacting contacts from each other, which becomes manifested in additional zeros in the off-diagonal terms of the Delassus operator. Our particular approach is to put the elasticity *in* the bodies to which it physically belongs, but to leave the contacts *hard* and to still process them with the methods as described. In our opinion, an impact model can be regarded as robust, as soon as a parameterization of the overall system has been found, such that the impact process is well approximated by nearly inelastic behavior. Models involving big restitution coefficients have to be taken with utmost care.

Appendix

For completeness, we verify that Poisson's impact law for compression (32) indeed maximizes the losses in kinetic energy under the constraints that the impact equations (29) and the restrictions $-\boldsymbol{\Lambda}_i^{(-)} \in \mathscr{C}_i^{(-)}$ on the impulsive forces are met. This fact is so well known in the community that it has—to the best of our knowledge—never been formally derived in one place, maybe due to its obviousness; see, e.g., [42]. Actually, everything about this optimality property can be found in [39] and roots even back to [38]. What we do is to condense the information provided on the various places in [39] to the desired formulation. We consider the convex optimization problem

$$\text{minimize} \quad T^{\circ}\big(\mathbf{u}^{\circ}\big) = \frac{1}{2}\mathbf{u}^{\circ\mathrm{T}}\mathbf{M}\mathbf{u}^{\circ} \tag{296}$$

$$\text{subject to} \quad \mathbf{M}\big(\mathbf{u}^{\circ} - \mathbf{u}^{-}\big) = \sum_{i=1}^{n} \mathbf{W}_i \boldsymbol{\Lambda}_i^{(-)} \tag{297}$$

$$\text{and} \quad -\boldsymbol{\Lambda}_i^{(-)} \in \mathscr{C}_i^{(-)}, \tag{298}$$

where T° is the kinetic energy of the system at the end of compression. We will show that Poisson's impact law for compression (32) provides the optimality conditions of the above minimization problem. For doing this proof, we rigorously use matrix notation by setting $\mathbf{W} := (\mathbf{W}_1, \ldots, \mathbf{W}_n)$, $\boldsymbol{\Lambda}^{(-)} := (\boldsymbol{\Lambda}_1^{(-)\mathrm{T}}, \ldots, \boldsymbol{\Lambda}_n^{(-)\mathrm{T}})^{\mathrm{T}}$, $\mathscr{C}^{(-)} := \mathscr{C}_1^{(-)} \times \cdots \times \mathscr{C}_n^{(-)}$ in (297), (298), and later $\boldsymbol{\gamma} := (\boldsymbol{\gamma}_1^{\mathrm{T}}, \ldots, \boldsymbol{\gamma}_n^{\mathrm{T}})^{\mathrm{T}}$. We further change the cost function (296) to an equivalent one by subtracting the constant T^{-} from it, which is the preimpact kinetic energy. The new cost function therefore is $T^{\circ}(\mathbf{u}^{\circ}) - T^{-} =: W^{(-)}(\mathbf{u}^{\circ})$, i.e., the contact work for compression according to (99). With it, the optimization problem (296)–(298) can now be stated as

$$\text{minimize} \quad W^{(-)}\big(\mathbf{u}^{\circ}\big) = \frac{1}{2}\mathbf{u}^{\circ\mathrm{T}}\mathbf{M}\mathbf{u}^{\circ} - \frac{1}{2}\mathbf{u}^{-\mathrm{T}}\mathbf{M}\mathbf{u}^{-} \tag{299}$$

$$\text{subject to} \quad \mathbf{M}\big(\mathbf{u}^{\circ} - \mathbf{u}^{-}\big) = \mathbf{W}\boldsymbol{\Lambda}^{(-)} \tag{300}$$

$$\text{and} \quad -\boldsymbol{\Lambda}^{(-)} \in \mathscr{C}^{(-)}. \tag{301}$$

The equality constraint (300) can now be eliminated from the cost function (299) by performing the very same steps as in (99), where the abbreviations (41) for the terms $\mathbf{W}^{\mathrm{T}}\mathbf{u}^{\circ} =: \boldsymbol{\gamma}^{\circ}$ and $\mathbf{W}^{\mathrm{T}}\mathbf{u}^{-} =: \boldsymbol{\gamma}^{-}$ have also been used. In addition, we need the left equation in (43), which has formerly been derived by again using only (41) and (300). Together, this gives

$$W^{(-)} = \frac{1}{2}\big(\boldsymbol{\gamma}^{\circ} + \boldsymbol{\gamma}^{-}\big)^{\mathrm{T}}\boldsymbol{\Lambda}^{(-)} \quad \text{and} \quad \boldsymbol{\gamma}^{\circ} - \boldsymbol{\gamma}^{-} = \mathbf{G}\boldsymbol{\Lambda}^{(-)}, \tag{302}$$

and allows us to finally eliminate $\boldsymbol{\gamma}^{\circ}$ from the cost function $W^{(-)}$. The resulting optimization problem

$$\text{minimize} \quad W^{(-)}\big(\boldsymbol{\Lambda}^{(-)}\big) = \frac{1}{2}\boldsymbol{\Lambda}^{(-)\mathrm{T}}\mathbf{G}\boldsymbol{\Lambda}^{(-)} + \boldsymbol{\gamma}^{-\mathrm{T}}\boldsymbol{\Lambda}^{(-)} \tag{303}$$

$$\text{subject to} \quad -\boldsymbol{\Lambda}^{(-)} \in \mathscr{C}^{(-)} \tag{304}$$

is now exclusively stated in terms of the compression impulsive forces $\boldsymbol{\Lambda}^{(-)}$. With the help of the indicator function $I_{\mathscr{C}^{(-)}}$, the constraints (304) can equivalently be taken into account

in the extended cost function $W_\star^{(-)}$, which yields the unconstrained problem

$$\text{minimize} \quad W_\star^{(-)}\big(\mathbf{\Lambda}^{(-)}\big) = \frac{1}{2}\mathbf{\Lambda}^{(-)^{\mathrm{T}}}\mathbf{G}\mathbf{\Lambda}^{(-)} + \boldsymbol{\gamma}^{-^{\mathrm{T}}}\mathbf{\Lambda}^{(-)} + I_{\mathscr{C}^{(-)}}\big(-\mathbf{\Lambda}^{(-)}\big). \tag{305}$$

By taking the subdifferential of (305), we obtain the optimality conditions $0 \in \partial W_\star^{(-)}(\mathbf{\Lambda}^{(-)})$, which explicitly gives

$$0 \in \mathbf{G}\mathbf{\Lambda}^{(-)} + \boldsymbol{\gamma}^{-} - \partial I_{\mathscr{C}^{(-)}}\big(-\mathbf{\Lambda}^{(-)}\big). \tag{306}$$

We finally substitute in (306) the right equation from (302) and replace the subdifferential of the indicator by the normal cone. The resulting expression

$$\boldsymbol{\gamma}^{\circ} \in \mathscr{N}_{\mathscr{C}^{(-)}}\big(-\mathbf{\Lambda}^{(-)}\big) \tag{307}$$

is Poisson's impact law for compression (31)–(32) or, equivalently, Newton's law (14)–(15) for a completely inelastic impact $\varepsilon = 0$.

References

1. Acary, V., Brogliato, B.: Numerical Methods for Nonsmooth Dynamical Systems. Applications in Mechanics and Electronics. Lecture Notes in Applied and Computational Mechanics, vol. 35. Springer, Berlin (2008)
2. Aeberhard, U.: Geometrische Behandlung idealer Stösse. Diss. ETH No. 17695, Zurich (2008)
3. Aoustin, Y., Chevallereau, C., Formalsky, A.: Numerical and experimental study of the virtual quadrupedal walking robot-semiquad. Multibody Syst. Dyn. **16**, 1–20 (2006)
4. Asano, F.: High-speed dynamic gait generation for limit cycle walkers based on forward-tilting impact posture. Multibody Syst. Dyn. (2012). doi:10.1007/s11044-012-9326-7
5. Asano, F.: Robust pseudo virtual passive dynamic walking with control of swing-leg retraction. Multibody Syst. Dyn. (2012). doi:10.1007/s11044-012-9338-3
6. Beitelschmidt, M.: Reibstöße in Mehrkörpersystemen. VDI-Fortschrittberichte Schwingungstechnik, Reihe 11, vol. 275. VDI-Verlag, Düsseldorf (1999)
7. Bowling, A., Flickinger, D.M., Harmeyer, S.: Energetically consistent simulation of simultaneous impacts and contacts in multibody systems with friction. Multibody Syst. Dyn. **22**, 27–45 (2009)
8. Brogliato, B.: Internal couplings between unilateral and bilateral holonomic constraints in frictionless Lagrangian systems. Multibody Syst. Dyn. (2012). doi:10.1007/s11044-012-9317-8
9. Brogliato, B., Zhang, H., Liu, C.: Analysis of a generalized kinematic impact law for multibody-multicontact systems, with application to the planar rocking block and chains of balls. Multibody Syst. Dyn. **27**, 351–382 (2012)
10. Cataldo, E., Sampaio, R.: A brief review and a new treatment for rigid bodies collision models. J. Braz. Soc. Mech. Sci. **23**(1), 63–78 (2001)
11. Chang, C.C., Peng, S.T.: Impulsive motion of multibody systems. Multibody Syst. Dyn. **17**, 47–70 (2007)
12. Chang, C.C., Liu, C.Q., Huston, R.L.: Dynamics of multibody systems subjected to impulsive constraints. Multibody Syst. Dyn. **8**, 161–184 (2002)
13. Djerassi, S.: Collision with friction, part A: Newton's hypothesis. Multibody Syst. Dyn. **21**, 37–54 (2009)
14. Djerassi, S.: Collision with friction, part b: Poisson's and Stronge's hypotheses. Multibody Syst. Dyn. **21**, 55–70 (2009)
15. Djerassi, S.: Reply by the author to Stronge, W.J. Multibody Syst. Dyn. **24**, 129–131 (2010)
16. Djerassi, S.: Stronge's hypothesis-based solution to the planar collision-with-friction problem. Multibody Syst. Dyn. **24**, 493–515 (2010)
17. Djerassi, S.: Three-dimensional, one-point collision with friction. Multibody Syst. Dyn. **27**, 173–195 (2012)
18. Flickinger, D.M., Bowling, A.: Simultaneous oblique impacts and contacts in multibody systems with friction. Multibody Syst. Dyn. **23**, 249–261 (2010)

19. Font-Llagunes, J.M., Barjau, A., Pàmies-Vilà, R., Kövecses, J.: Dynamic analysis of impact in swing-through crutch gait using impulsive and continuous contact models. Multibody Syst. Dyn. **28**, 257–282 (2012)
20. Förg, M., Pfeiffer, F., Ulbrich, H.: Simulation of unilateral constrained systems with many bodies. Multibody Syst. Dyn. **14**, 137–154 (2005)
21. García Orden, J.C., Goicolea, J.M.: Conserving properties in constrained dynamics of flexible multibody systems. Multibody Syst. Dyn. **4**, 225–244 (2000)
22. Glocker, Ch.: Multiple impacts with friction in rigid multibody systems. Nonlinear Dyn. **7**, 471–497 (1995)
23. Glocker, Ch.: Dynamik von Starrkörpersystemen mit Reibung und Stößen. VDI-Fortschrittberichte Mechanik/Bruchmechanik, Reihe 18, vol. 182. VDI-Verlag, Düsseldorf (1995)
24. Glocker, Ch.: Newton's and Poisson's impact law for the non-convex case of re-entrant corners. In: Gao, D.Y. (ed.) Complementarity, Duality and Symmetry in Nonlinear Mechanics. Advances in Mechanics and Mathematics, vol. 6, pp. 101–125. Kluwer, Dordrecht (2004)
25. Glocker, Ch.: Models of non-smooth switches in electrical systems. Int. J. Circuit Theory Appl. **33**, 205–234 (2005)
26. Glocker, Ch.: An introduction to impacts. In: Haslinger, J., Stavroulakis, G. (eds.) Nonsmooth Mechanics of Solids. CISM Courses and Lectures, vol. 485, pp. 45–102. Springer, Wien (2006)
27. Glocker, Ch.: Energetic consistency conditions for standard impacts, part I: Newton-type inequality impact laws and Kane's example. Multibody Syst. Dyn. **13**, 447–463 (2012)
28. Kane, T.R.: A dynamics puzzle. Stanford Mechanics Alumni Club Newsletter **6** (1983)
29. Kane, T.R., Levinson, D.A.: Dynamics: Theory and Applications. McGraw Hill, New York (1985)
30. Khulief, Y.A.: Spatial formulation of elastic multibody systems with impulsive constraints. Multibody Syst. Dyn. **4**, 383–406 (2000)
31. Klisch, T.: Contact mechanics in multibody systems. Multibody Syst. Dyn. **2**, 335–354 (1998)
32. Kokkevis, E., Metaxas, D.: Efficient dynamic constraints for animating articulated figures. Multibody Syst. Dyn. **2**, 89–114 (1998)
33. Kövecses, J., Cleghorn, W.L., Fenton, R.G.: Dynamic modeling and analysis of a robot manipulator intercepting and capturing a moving object, with the consideration of structural flexibility. Multibody Syst. Dyn. **3**, 137–162 (1999)
34. Lankarani, H.M., Pereira, M.S.: Treatment of impact with friction in planar multibody mechanical systems. Multibody Syst. Dyn. **6**, 203–227 (2001)
35. Lens, E.V., Cardona, A., Géradin, M.: Energy preserving time integration for constrained multibody systems. Multibody Syst. Dyn. **11**, 41–61 (2004)
36. Modarres, N., Kövecses, J., Angeles, J.: Impacts in multibody systems: modeling and experiments. Multibody Syst. Dyn. **20**, 163–176 (2008)
37. Möller, M.: Consistent integrators for non-smooth dynamical systems. Diss. ETH No. 19715, Zurich (2011)
38. Moreau, J.J.: Sur les lois de frottement, de plasticité et de viscosité. Acad. Sci. Paris, Sér. A **271**, 608–611 (1970)
39. Moreau, J.J.: Unilateral contact and dry friction in finite freedom dynamics. In: Moreau, J.J., Panagiotopoulos, P.D. (eds.) Non-Smooth Mechanics and Applications. CISM Courses and Lectures, vol. 302, pp. 1–82. Springer, Wien (1988)
40. Muraro, A., Chevallereau, C., Aoustin, Y.: Optimal trajectories for a quadruped robot with trot, amble and curvet gaits for two energetic criteria. Multibody Syst. Dyn. **9**, 39–62 (2003)
41. Negrut, D., Tasora, A., Mazhar, H., Heyn, T., Hahn, P.: Leveraging parallel computing in multibody dynamics. Multibody Syst. Dyn. **27**, 95–117 (2012)
42. Paoli, L., Schatzman, M.: Penalty approximation for dynamical systems submitted to multiple non-smooth constraints. Multibody Syst. Dyn. **8**, 347–366 (2002)
43. Pfeiffer, F.: Mechanical System Dynamics. Lecture Notes in Applied and Computational Mechanics, vol. 40. Springer, Berlin (2005)
44. Pfeiffer, F.: Energy losses of impacts with friction. In: Proc. of the ASME 2009 IDETC/CIE Conferences, San Diego, USA, vol. 4, pp. 407–410 (2009)
45. Pfeiffer, F.: Energy considerations for frictional impacts. Arch. Appl. Mech. **80**(1), 47–56 (2010)
46. Pfeiffer, F., Glocker, C.: Multibody Dynamics with Unilateral Contacts. Wiley, New York (1996)
47. Rockafellar, R.T.: Convex Analysis. Princeton Univ. Press, Princeton (1972)
48. Rockafellar, R.T.: Marginal values and second-order necessary conditions for optimality. Math. Program. **26**, 245–286 (1983)
49. Rodriguez, A., Bowling, A.: Solution to indeterminate multipoint impact with frictional contact using constraints. Multibody Syst. Dyn. **28**, 313–330 (2012)

50. Schulz, M., Mücke, R., Walser, H.P.: Optimisation of mechanisms with collisions and unilateral constraints. Multibody Syst. Dyn. **1**, 223–240 (1997)
51. Stöckli, F.: Stossgesetze und energetische Konsistenz. Master thesis, Center of Mechanics, ETH, Zürich, Zürich (2008)
52. Stronge, W.J.: Rigid body collision with friction. Proc. R. Soc. Lond. A **431**, 169–181 (1990)
53. Stronge, W.J.: Impact Mechanics. Cambridge University Press, Cambridge (2000)
54. Stronge, W.J.: Generalized impulse and momentum applied to multibody impact with friction. Mech. Struct. Mach. **29**(2), 239–260 (2001)
55. Stronge, W.J.: Comment: collision with friction, part B: Poisson's and Stronge's hypotheses. Multibody Syst. Dyn. **27**, 123–127 (2010)
56. Vukobratovic, M., Potkonjak, V., Babkovic, K., Borovac, B.: Simulation model of general human and humanoid motion. Multibody Syst. Dyn. **17**, 71–96 (2007)
57. Zhen, Z., Liu, C.: The analysis and simulation for three-dimensional impact with friction. Multibody Syst. Dyn. **18**, 511–530 (2007)
58. Zhen, Z., Liu, C., Chen, B.: The Painlevé paradox studied at a 3D slender rod. Multibody Syst. Dyn. **19**, 323–343 (2008)